TABLE OF CONTENTS

LIST OF FIGURES

LIST OF TABLES

GLOSSARY OF NOTATIONS

CA, θ	Contact angle on flat surfaces (degree)
θ'	Contact angle of the composite surface in Cassie-Baxter model (degree)
θ^*	Apparent contact angle on a rough surface in Wenzel model (degree)
θ_A	Advancing contact angle (degree)
θ_R	Receding contact angle (degree)
CAH	Contact angle hysteresis (degree)
θ_T	Tilt angle (degree)
γ	Surface tension of a liquid (mN/m)
γ_{SV}	Surface tension of solid-vapor interface (mN/m)
γ_{SL}	Surface tension of solid-liquid interface (mN/m)
γ_{LV}	Surface tension of liquid-vapor interface (mN/m)
f	Fraction of solid surface area wet by the liquid
W_A	Work of adhesion (mN/m)
R	Roughness factor in Wenzel equation (unit-less)
τ	Shear stress of ice detachment (Pa)
ARF	Adhesion reduction factor (unit-less)
F	Centrifugal force equal to adhesion force (N)
r	Beam radius (m)
ω	Rotation speed of the beam (or) angular acceleration (m/s^2)
A	Apparent de-iced area of the sample surface (m^2)
m	Mass of accumulated ice on Al surfaces (g)
γ_c	Critical surface tension (mJ/m^2)
EG	Ethylene glycol

PG	Propylene glycol
BTSE	Bis-1, 2-(triethoxysilyl) ethane
SA	Stearic acid
FAS	Fluoroalkyl-silane
ODTMS	Octadecyltrimethoxysilane
OTS	Octadecyltrichlorosilane
DLC	Diamond-like carbon
AA	Aluminium alloy
SAM	Self assembled monolayer
MeOH	Methanol
CC	Conversion coating
CCCs	Chromate conversion coatings
PCCs	Permanganate conversion coatings
rms	Root-mean-square
IAS	Ice adhesion strength
TEOS	Tetraethyl orthosilicate
PTFE	Polytetrafluoroethylene
CVD	Chemical vapor deposition
PECVD	Plasma-enhanced chemical vapor deposition
PVD	Physical vapor deposition
AFM	Atomic Force Microscopy
SEM	Scanning Electron Microscopy
RTV	Room-temperature-vulcanized
XPS	X-ray Photoelectron Spectroscopy
EDS	Energy-Dispersive X-ray Spectroscopy

CHAPTER 1

INTRODUCTION

1.1 Background

Atmospheric ice assumes a wide range of fascinating forms, each type beautiful in its own way although many pose severe risks to the security of overhead networks for electric power, communications and other related systems [1]. Ice and wet-snow adhesion can seriously impair the operation of electric power lines, helicopters, other aircraft, transportation, telecommunication networks, antennae, shipping and superstructures, and so forth, in countries where a cold climate prevails in winter. Ice adhesion causes a significant amount of damage and, consequently financial losses may ensue in numerous sectors of the economy. Prevention of or facilitating the removal of icing requires reducing its adhesive strength. Therefore, various de-icing and anti-icing techniques were developed over the last several decades. While most of the techniques currently in use are the active de-icing methods, all of them are employed where accumulations are substantial. Passive approaches to the problem are gaining in popularity; amongst these is the developing of anti-icing or icephobic coatings [2]. Even though there is, as yet, no material which is completely capable of preventing ice and snow build-up on its surface [3], certain coatings are believed to bring about reduced adhesion. This is expected to result in lower ice or wet-snow accumulation on such surfaces. Thus far, such coatings have not been proposed as "*ready to use*", although some candidate coatings have been tested by several groups. With regard to the subject of this project, which deals with reduction of ice accumulation on aluminium alloys (AA) surfaces, it should be remembered that corrosion is always a serious issue when it comes to using AAs outdoors. Aluminium alloys with their wide range of properties are used extensively in

many industrial sectors due to their strength, ductility, formability, workability, and corrosion resistance. In view of the fact that all modern AAs use other metal additives to improve the strength values of the material, this inevitably leads to the increased susceptibility of such alloys to electrochemical corrosion. Thus, while developing durable anti-icing coatings on Al surfaces, their anticorrosive resistance should necessarily be kept in mind as an important issue regarding coating durability and stability.

1.2 Description of the Icing Problem

Ice accumulation on exposed surfaces may lead to severe damage and consequences involving the interrupted operation or integrity of outdoor civilian, industrial or military structures, transmission line cables, naval craft, fishing vessels and ice breakers in cold climate countries subjected to extreme weather conditions. Atmospheric icing occurs when the surfaces of exposed structures come into contact with supercooled water droplets or snow particles. Each year, numerous failures due to ice or snow accumulation are reported from Canada, the United States, Russia, Iceland, Japan and Norway. Therefore, various de-icing and anti-icing techniques have been developing for several decades [3]. In the specific case of power transmission lines, ice or wet snow can cause serious damages due to their high adherence to both metallic and insulator surfaces resulting in cable sagging and short circuits which are caused by static ice overloads on towers and cables (Fig.1.1).

Figure 1.1. Wires collapsed under weight of ice accumulation.

Aerodynamically unstable ice also increases the amplitude of wind-induced dynamic oscillations, galloping, while decreasing the damping rate, which leads to the high mechanical stress on conductors, insulating supports, cables and towers. In addition, when the accumulated ice suddenly drops off from a conductor, excessive mechanical tensions are generated. All these factors cause high amplitude movements of cables, increasing the possibility of little or no clearance between the adjacent cables or between cables and towers [4]. Failure to protect high voltage power lines and conductors from the accumulation of ice may result in tremendous damage and can even lead to the mechanical failure of the cables or to load shedding events, as was the case during the 1998 or 2007 ice storms in Eastern Canada and certain of the U.S.A states [5]. Similarly, ice accretion, together with superimposed contamination, often causes a decrease in the flashover threshold voltage of outdoor insulators, resulting in occasional outages [6]. The need for reliable transmission and distribution networks under the most severe icing conditions highlights the importance of ice adhesion studies. The characteristics of ice vary depending on environmental conditions, such as air temperature, wind velocity, water droplet size, and liquid water content. Atmospheric ice results from a variety of conditions, including hoarfrost caused by condensation of vapor, in-cloud icing involving the freezing of supercooled water droplets in clouds or fog, and finally, precipitation icing resulting from freezing rain, drizzle, wet snow, or dry snow. Several groups [7-9] classified ice into three basic categories: hard rime, soft rime, and glaze. Of most economical concern are glaze, hard rime, wet snow and mixtures. Previous studies show it is possible to distinguish between them using temperature measurement [10].

1.3 Current solutions

Preventing ice build-up has long been a technological challenge. Ice, with its broad range from snow to glaze, generally accretes during periods of sub-zero temperatures through the impact of supercooled water droplets and can stick to everything. Many attempts have been made

to reduce ice adhesion and accretion. The main contributors to ice adhesion on surfaces are: hydrogen bonds, Van der Waals forces, and non-polar covalent bonds [11-13]. The two main strategies for dealing with the icing problem are: active de-icing methods including thermal, electrical, chemical or mechanical techniques; and passive methods which do not need external energy for de-icing or for preventing ice accretion. While active methods are used widely, passive approaches have few industrial applications. They are environmentally friendly compared to de-icing fluids and are cheaper than active methods which are energy-consuming and expensive to operate [5]. Traditional approaches rely on the mechanical breaking up of the accreted ice or using chemicals to melt it, which are all impermanent solutions. There are a number of effective methods involving electrolysis, which is one of the "elegant" de-icing techniques, it is not, however, a practical method and it requires the presence of a layer of ice in order to remove it [11]. Heating the surface to melt the ice by applying the Joule effect or a high frequency current is another effective approach which unfortunately requires a large supply of energy. Numerous types of anti-icing fluids such as ethylene glycol (EG) and propylene glycol (PG) are used to prevent ice build-up on aircraft, however, they need frequent application in large quantities [15] thereby making their use both time-consuming and expensive. Furthermore, such de-icers are often toxic and environmentally unsafe [16, 17]. Passive approaches to the problem, among which is the development of icephobic coatings, imply that such coatings must necessarily fulfill both of the following requirements: to provide a considerable reduction in snow and ice adhesion, and to ensure a reasonably long service-life in the form of reliable durability. Although the current methods are efficient, they consume a great deal of energy, while at the same time necessitating elaborate infrastructures and maintenance [14]. The ideal solution to these problems would be the application of a solid, durable, easy to apply, and inexpensive material which reduces adhesion to such an extent that ice falls off under the pull of gravity. [14]. In fact, few studies have focused on understanding the basic mechanisms of ice adhesion to find a substitute way of preventing ice accretion from a fundamental standpoint [18]. Such a way would be to

produce a durable solid anti-icing coating with a view to inhibiting ice accumulation rather than eliminating it after its accretion. Such coatings are called ***anti-icing*** or ***icephobic*** materials [2].

1.4 Principal Objectives of the Research

The main purpose of this study is to reduce ice accumulation on aluminium surfaces using various low surface energy coatings; it will also endeavor to study the stability and anticorrosive performance of these same coatings. The specific objectives of the research are the following:

1. Preparing and characterizing several types of coating as candidates for upper layers using different low surface energy materials, namely, alkylsilane and fluoroalkylsilane-based layers. Also included is the preparation of multi-layer organosilane-based layers where the first layer contributes mainly for its anti-corrosive qualities.

2. Preparing and characterizing a variety of coating types as candidates for under-layers which would provide satisfactory density and anticorrosive performance; these might include, some inorganic conversion coatings and organosilane-based layers and sol-gel based layers.

3. Morphological and compositional characterization of the prepared coatings.

4. Study of ice adhesion on such prepared samples including their evaluation in terms of hydrophobic and icephobic properties.

5. Investigation of coating durability and stability.

1.5 Methodology

Taking into consideration the definition of the project objectives, the following experiments were carried out on polished coated AA2024 and AA6061 using different anticorrosive and anti-icing layers as well as applying various experimental parameters and different pre/post treatments. The methodology used will be found summarized in the following subsections:

1.5.1 Coating Preparation

1. Preparation of Anticorrosive Coatings on AA Substrates

A few candidate materials have already been tested as anticorrosive underlayers. More specifically, inorganic conversion coatings based on permanganate treatment and organosilane-based layers were prepared and applied to the surface of Al alloys. It would be useful to mention here that organosilane coupling agents followed by a self-assembled monolayer (SAM) coating process seem to be an interesting alternative system for replacing the toxic chromates, namely the bis-1, 2-(triethoxysilyl) ethane (BTSE) thin layers [19]. Curing of the silane layer has the potential for improving the barrier properties of the film. Greater detail concerning organosilane coupling agents will be provided further on in the text.

2. Preparation of Icephobic Coatings on Al Alloy Surfaces

In parallel, materials providing low-surface energy were also tested as candidates for top layer application. Alkylsilane-based and fluoroalkylsilane-based layers were chosen for this purpose. The influence of various parameters on the formation and properties of such layers was analyzed in order to optimize the coating process. Such coatings were formed and tested both singly on Al substrates, and in combination on the abovementioned anticorrosive under-layers. Alkylsilane layers were previously proposed as potentially icephobic and anticorrosive coatings, however, no extensive follow-up investigation ensued. The hydrophobic properties of the coatings, and their surface characteristics were measured in order to study their influence on the adhesion of ice. Lastly, ice adhesion was tested on these coatings in order to find out the parameters governing this property of the coating system.

1.5.2 Characterization Methods

The analytical technique and equipments used are listed below:

- **Contact angle goniometer:** To evaluate surface wetting behavior (contact angle, CA) and wetting hysteresis (contact angle hysteresis, CAH).

- **Wind tunnel for ice accretion:** The ice accumulated on coated samples was a glaze type prepared by spraying supercooled water droplets in a wind tunnel at subzero temperatures, thereby simulating those of natural outdoor atmospheric icing in order to study the mechanism of ice growth on coated surfaces.

- **Ice adhesion tests using a centrifuge adhesion testing machine:** For testing the strength of ice adhesion to the surfaces under study in order to discover what parameters govern these properties.

Experimental and analytical facilities used in this research:

- Atomic Force Microscope (AFM) for imaging surface topography.
- Cold Climatic Chamber to conduct experiments at subzero temperatures.
- Scanning Electron Microscope (SEM) for surface imaging.
- Energy-Dispersive X-ray Spectroscopy (EDS) for chemical analysis of surface.
- Spin-Coater to prepare coatings.
- X-ray Photoelectron Spectroscopy (XPS) to determine chemical composition of surfaces.
- Optical Microscope for sample surface imaging.

1.6 Originality and Significance of Research

As stated earlier, this project intends to examine study and develop various low surface energy coatings to reduce ice and wet-snow accumulation on outdoor structures made of Al

alloys. Alkyl-terminated coatings were previously proposed as potentially ice-releasing coatings, while a reduction in ice adhesion by a factor of ~2 [2, 8, 9] compared to bare Al has been reported. Such coatings were not studied extensively, however, and no systematic work has been carried out to date. For the purposes of this thesis, different organic coatings terminated with alkyl groups were prepared; both the stability of the coatings in water and their ice-repellent performance over time were carefully studied by means of facilities provided at the CIGELE* and the INGIVRE**. Alternatively, corrosion should be taken into account seriously considering that such alloys are known to be subjected to humid and aggressive environments. Anticorrosive properties and the performance of the coating were thus also assessed, more specifically those which may be deemed environmentally friendly alternatives to the currently prevailing chromate-based treatments. There is an increasing demand in the area urging towards the development of new environmentally friendly, inexpensive and easy-to-apply protective chemicals for various Al alloys. A judicious combination of both low-surface energy and satisfactory anticorrosive performance was also evaluated. Their imperviousness to water, evaluated ice adhesion, together with the effect of all possible conditions on coating durability was investigated. Of the enterprises involved, at least two major companies in this province may potentially benefit from these research results. Principally, Hydro Quebec, which is traditionally involved in developing anti-icing techniques and preparing coatings with reduced ice accumulation on the metal surfaces, and Alcan, another big representative of industry, for whom improved corrosive resistance of the Al alloy surface has been of constant interest for several decades now.

1.7 Overview of the Thesis

This thesis consists of eight chapters which may be itemized as follows:

---

* The Industrial Chair on Atmospheric Icing of Power Network Equipment.

** The Canada Research Chair on Engineering of Power Network Atmospheric Icing.

- Chapter **1** is the basic introduction to this thesis, and provides a summary of the background to the research including the issues and problems involved in the icing, research objectives, and the methodology applied. The motivation for this work is also discussed.

- Chapters **2** and **3** present a fundamental statement followed by a current review of the literature available in the field pertaining to the topics of this research, namely, atmospheric icing, hydrophobic properties, superhydrophobicity, icephobicity, and corrosion phenomena. These make it possible for this thesis to follow the test principles and processes required, together with, the results obtained, and the reasons for selecting the applied coatings for this particular project. These reviews will contribute to helping the reader understand the choice of experimental parameters.

- Chapter **4** provides an overview of the coating-preparation processes, the facilities used, and the methodology followed for this purpose in relation to the objectives introduced in Chapter **1**. This chapter covers the details of the facilities, the techniques, and the instruments used in the study, *i.e.* a Contact Angle Goniometer, a cold room, a Spin Coater, Energy-Dispersive X-ray Spectroscopy (EDS) and others. Subsequently, details are provided of the methods applied, the one layer approach and the multi-layer approach.

- Chapter **5** provides descriptions of the experimental results and the issues faced throughout the experimental process. The hydrophobic properties, stability, corrosion investigation and the surface characteristics of coated flat AA surfaces using various technique and methods were taken into consideration and discussed.

- Chapter **6** will discuss in detail the experimental results obtained for nano-rough coated Al surfaces in terms of hydrophobic properties and stability, based on hydrophobicity tests and morphological analyses of surface, also including all the possible permutations between the parameters tested.

- Chapter **7** will discuss the ice releasing performance of flat and rough-coated Al surfaces as well as the possible effects of ice detachment on coating properties.

- Chapter **8** states the conclusions and recommendations drawn from the work; the results obtained and discussions of the results reported in the previous chapters. The conclusions emerging from this thesis make it possible to illustrate the assessment of our contribution to the progress of this field.

- The references cited in this thesis are presented at the end, after the final chapter.

CHAPTER 2

REVIEW OF THE LITERATURE

2.1 Introduction

Broadly speaking, icing occurs when freezing water is deposited on surfaces at or below the freezing point. This natural phenomenon may result from freezing rain, sleet, wet snow, cold fog, supercooled clouds or vapour, or even from spray or splashing water. Occasionally, above-freezing wet snow may, in some instances, stick to certain surfaces. As the activities of humankind have broadened and become more sophisticated, icing has become increasingly (more) troublesome and intrusive. It is especially hazardous to various aircraft, notably when it builds up on helicopter blades. It also affects power and communications lines, antennae, and pavements, either directly or from trees destroyed by the weight of the ice. Where icing cannot be tolerated, costly means are required to prevent its formation or to remove it entirely. Controlling ice-formation by means of its physical removal, whether by heating or through the application of the appropriate chemicals, might be possible. However, it would prove to be an expensive proposition and not broadly practicable.

The main objective of this chapter is to introduce the occurrence of icing in nature and its consequences; also to learn what causes ice adhesion and how to minimize it by drawing on studies concerning adhesion, wettability and interface chemistry. On this basis and from the specialized literature available on ice adhesion, ice testing, and acquired experiments in ice countermeasures, ways and means have been hereby sought for to reduce the adhesion of ice to various textures so that it will either undergo self-shedding or be otherwise easier to remove mechanically.

2.2 Icing in Nature and the 1998 Ice Storm

Ice and wet snow accretion on structures is a significant problem faced by design engineers in cold climate countries, such as Canada and the United States. Icing is especially difficult for transmission line design because these lines typically go through large, sparsely populated areas where observational data is scarce. Tall communication tower designs face similar problems [20]. Atmospheric icing is defined by the International Standards Organization *(ISO)* and the International Council on Large Electric Systems as any process of ice or snow accumulation on objects exposed to the atmosphere in contact with supercooled water drops or snow particles [21]. Atmospheric icing is further classified into types of ice, based upon the method of deposition and the characteristics of the deposits. These include glaze from the precipitation of freezing rain or freezing drizzle, snow, rime ice resulting from supercooled cloud or fog droplets, and hoar frost resulting from the deposition of water vapour directly as ice crystals [22]. Sleet, a form of freezing precipitation, and superstructure ice resulting from sea spray, are traditionally not classified as atmospheric icing, but they are similar in the processes of their formation. Ice build-up on high voltage power and distribution lines may lead to the mechanical failure of the cables or even lead to loss of insulation [23-27] and electric arcs or insulator flashovers between power lines and metallic supports, the latter being at ground potential entailing power outages and often incurring major costs. Ice or wet snow can cause serious problems which are due to their high adherence to both metallic and insulator surfaces over the entire area exposed. Ice accumulation on high voltage power lines can lead to mechanical failure resulting from the static load of accreted ice, or from the dynamic stresses of ice shedding. On average, the shedding rate is higher for freezing rain and wet snow, compared to in-cloud icing [10] or wind-induced galloping events, as was made evident from the January 1998 ice storm. For six days in January of 1998, freezing rain coated parts of Ontario, Québec, and New Brunswick with 7-11 cm of ice (see Figure 2.1, left) causing widespread long-term power outages. Due to the collapse of power lines

and supporting structures as a result of ice accumulation, over 4.7 million people in Canada lost power during the storm, along with another 500,000 in the United States. The Canadian utility company Hydro-Québec was particularly hard hit, with over 1,850 miles of power network suffering the impact of the storm with ~130 power transmission towers destroyed, as shown in Figure 2.1, right. Extensive and long-term power outages, some of them lasting for as long as a month, were caused by the overwhelming accumulation of ice on power lines, as may be seen in the figure, as well as by trees falling on power lines and transmission towers, bringing them down.

Figure 2.1. Icing (left); and destruction of power transmission line post and pylon caused by accumulated ice (right). (Ice Storm, Québec, January 1998.) [6, 28].

The widespread power outages and lengthy repair delays created significant political pressure, and also directed much public hostility towards Hydro-Québec. According to the National Climatic Data Center (1999), this ice storm was the most expensive natural disaster in North America for which the total economic loss at the time was estimated at approximately US$4.4 billion, with US$3.0 billion in Canada alone [6, 28]. Atmospheric icing is one of the major factors to be considered in power line design and reliability. The most dangerous ice accretions are glaze, hard rime, wet snow, and mixtures of these. Previous results show that it is possible to distinguish between them using temperature measurement facilities, together with the comparative analysis of data recorded by an icing rate meter a heated rain and snow gauge. Over the past decades, researchers have tried to improve methods of reducing or eliminating the adhesion of ice to a surface. In this research work, which is based on the literature available on

ice formation and the adhesion of ice to surfaces, we prepared and tested a number of coatings aimed at reducing the adhesion of ice to Al surfaces so that it will be easier to remove and thus cut down on any concomitant harmful effects of ice adhesion.

2.3 Different Types of Atmospheric Ice in Nature (Generic Definitions and Meteorological Conditions)

According to the *ISO-12494* standard [29], ice accretion may be defined as any process of ice build-up or snow accretion on the surface of an object exposed to the atmosphere. Ice is generally accreted during periods of sub-zero temperature through the impact of supercooled droplets of water on the surface. According to results obtained from Levene's test, water drops can be cooled down far below the freezing point of bulk water (0°C) [30] on which tiny water drops may remain in liquid state below the freezing point. For a supercooled droplet, the liquid state is thermodynamically unstable and indeed the most stable state for a super-cooled droplet is the solid state. The freezing process may be accelerated by the presence of any substance, such as a freezing nucleus, which makes the growth of an ice crystal about itself possible [31]. Previous studies, however, have shown that the ice nucleating ability of a particle is influenced by several physical and chemical factors while also being size-dependent and slow processes [32]. It should be noted that smaller droplets have less possibility of containing nuclei [30]. The best nucleus for ice is a small piece of ice because such a nucleus has a crystal structure similar to that of ice itself which allows water to crystallize by repeating its structure; this is the reason for which supercooled water droplets tend to join the ice layers covering outdoor structures rapidly.

Atmospheric Icing Types: Atmospheric icing is further classified by the type of ice produced, based upon methods of deposition and the characteristics of the deposits. According

to the meteorological conditions *(ISO-12494 standard),* atmospheric icing is traditionally classified based on two different formation processes:

A) Precipitation icing, including freezing precipitation and wet snow, forms when a warm layer of air (above 0°C) is trapped between two layers of cold air (below 0°C) during the precipitation of freezing rain, occurring wherever appropriate conditions prevail, regardless of altitude. Precipitation starts falling in the form of snow and, upon reaching the warm air, the snow particles melt to become water and finally, they encounter the low-level cold air and become supercooled water droplets [33].

B) In-cloud icing occurs when the supercooled water droplets in a cloud come into contact with an exposed structure; generally, in-cloud icing relates to aircraft flying through clouds or equipment installed at a high altitude [34]. Ice types are determined by wind speed, supercooled droplet size, air temperature, and the properties of objects being hit by droplets [35]. A classification may be based on other parameters, however, as shown in tables 2.1 and 2.2. The physical properties and the appearance of the accreted ice will vary widely according to the variations of the meteorological conditions prevailing during the ice growth [22].

Table 2.1. Typical properties of accreted atmospheric ice [22].

Type of ice	Density [kg/m^3]	Adhesion & Cohesion	General Appearance	
			Colour	Shape
Glaze	900	strong	transparent	evenly distributed/ icicles
Wet snow	300-600	weak (forming) strong (frozen)	white	evenly distributed/ eccentric
Hard rime	600-900	strong	opaque	eccentric, pointing windward
Soft rime	200-600	low to medium	white	eccentric pointing windward

Besides the properties mentioned in Table 2.1, other parameters may be used to describe the nature of accreted ice including compressive strength measured in relation to yield and crushing, as well as shear strength. The maximum amount of accreted ice will depend on several

factors, the most important being humidity, temperature, and the length of the ice accretion period.

Table 2.2. Meteorological parameters controlling atmospheric ice accretion [22].

Type of ice	Air temperature [°C]	Wind speed [m/s]	Droplet size	Water content in air	Typical event duration
Precipitation icing					
Glaze (freezing rain or drizzle)	$-10 < t_a < 0$	any	large	medium	hours
Wet snow	$0 < t_a < +3$	any	flakes	very high	hours
In-cloud icing					
Glaze	see fig. 1	see fig. 1	medium	high	hours
Hard rime	see fig. 1	see fig. 1	medium	medium	days
Soft rime	see fig. 1	see fig. 1	small	low	days

However, a main precondition for significant ice accretion remains the dimensions of the object exposed and its orientation to the direction of the icing wind. Table 2.2 gives a schematic outline of the major meteorological parameters controlling ice accretion. A cloud or fog consists of small water droplets or ice crystals. Even if the temperature is below the freezing point of water, the droplets may remain in the liquid state. Such supercooled droplets freeze immediately on impact with objects in the airflow. When the flux of water droplets towards the object is less than the freezing rate, each droplet freezes before the next droplet impinges on the same spot, and the ice growth is said to be dry. When the water flux increases, the ice growth will tend to be wet, because the droplets do not have the required time to freeze, before the next one impinges. In general, dry icing results in different types of rime containing air bubbles, while wet icing always forms glaze, whether solid and clear. Figure 2.2 gives an indication of the parameters controlling the major types of ice formation. The density of accreted ice varies widely from low (soft rime) to medium (hard rime) to high (glaze).

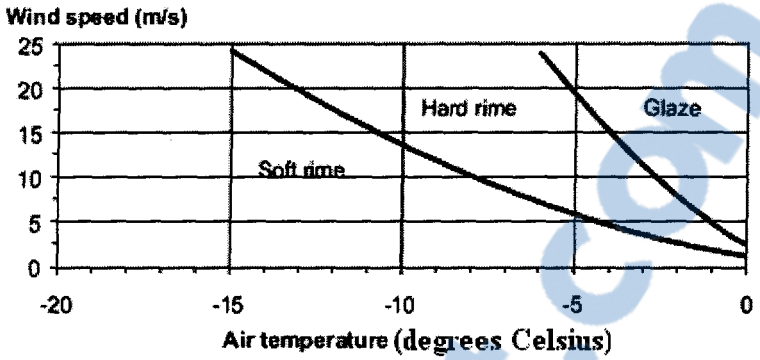

Figure 2.2. Accreted ice type as a function of wind speed/air temperature. The curves shift to the left with increasing liquid water content and with decreasing object size [22].

(A) Glaze: Glaze is the type of precipitation ice having the highest density. This type is caused by freezing rain, freezing drizzle, or wet in-cloud icing and normally causes smooth evenly distributed ice accretion; it may also result in the formation of icicles, in this case, the resulting shape can be somewhat asymmetric. Glaze may be found accreted on objects anywhere, when rain or drizzle occurs at temperatures below the freezing point [36-38]. Freezing rain or drizzle occurs when warm air aloft melts snow crystals and forms rain drops, which afterwards fall through a freezing air layer close to the ground. Such temperature inversions may occur in connection with warm fronts or in valleys, where cold air is trapped below warmer air aloft. The surface temperature of accreting ice is close to the freezing point, and liquid water, under the influence of wind and gravity, may thus flow around the object and freeze on the leeward side as well. This type of ice is dense and applies larger static/dynamic forces to the instruments; it conducts electricity more easily and is more dangerous with regard to the performance of the components of electric networks. The accretion rate for glaze varies mainly with rate of precipitation, wind speed, and air temperature.

(B) Rime: Rime is the most common type of in-cloud icing and often forms vanes on the windward side of linear, non-rotary objects, i.e. objects which will not rotate around the longitudinal axis as a result of having been eccentrically loaded down by ice. Lower temperatures create hard rime and soft rime. Rime ice accumulates when smaller supercooled droplets come

into contact with dry objects below the freezing point [33, 38, 39]. This kind of ice appears mainly in mountains and at low wind speeds. During significant icing on small, linear objects, the cross section of the rime vane is nearly triangular with the top angle pointing windward, but as the width, or diameter, of the object increases, the ice vane changes its form. The liquid water content of the air drops so low at temperatures below about -20°C that practically no in-cloud icing occurs. It results in a more or less cylindrical ice accretion around the string. The most severe rime icing occurs on freely exposed mountains, either coastal or inland, or where mountain valleys force moist air through passes, consequently both lifting the air and increasing wind speed over the pass. The accretion rate for rime varies mainly with the dimensions of the object exposed, wind speed, liquid water content in the air, drop size distribution, and air temperature.

(C) Wet Snow: Because of the occurrence of free water in the partly-melted snow crystals, wet snow is able to adhere to the surface of an object; its accretion therefore occurs when the air temperature is just above the freezing point. The snow will freeze when wet snow accretion is followed by a drop in temperature. The density and adhesive strength of this type of snow vary widely with, among other things, the fraction of melted water and the wind speed.

(D) Other Types of Ice: Hoarfrost is a common occurrence at low temperatures; it is due to a direct phase transition from water vapor into ice thereby forming a thin deposit. This thin layer is of low density and strength with needles oriented away from the surface and normally does not result in any significant load on structures. Frost forms on windless clear nights on surfaces facing the sky [40]. On days when warm, moist air moves over cold-soaked surfaces, frost forms on those surfaces which are coldest having no orientation preference [41]. Frost forms on decks, railings, stairs, handles, and cables, thus presenting a slipping hazard for personnel, even at a thickness of only 0.05 mm [42].

2.4 Surface Ice-Repellency

Creating a surface to which ice would not adhere can be considered as an ideal and economical solution to eliminate applies of de-icing techniques. Such a surface is known as an "icephobic" surface. The creation of an icephobic surface would benefit from knowledge of the physics of ice and ice accretion processes as well as of methods for the prediction of icing events. These ice-repellent surfaces can be created by an appropriate morphological modification of the surface followed by the application of a coating whose chemical components would have a weak chemical interaction with ice. The physical mechanisms involved in the strong adhesion of ice to materials can be divided into three different categories [12, 33, 43, 44], namely, electrostatic forces [12, 43, 45, 46], chemical bonds including hydrogen bonds, dipole-dipole bonds, and dipole induced forces *Lifshitz-van der Waals forces,* and finally diffusion or mechanical penetration. Ice adhesion is generally a property of the ice-solid interface which acts via the strong interaction between ice molecules and a solid surface. In ideal cases, all types of interaction must be eliminated to obtain zero or reduced ice adhesion [47]. Adhesion generally involves secondary attractive forces [48]. These are the *Lifshitz-van der Waals forces,* involving the London dispersion and Debye induction effects, which are believed to be a consequence of the negative electron cloud relative to the positive nucleus of the atom. However, the *Lifshitz-van der Waals forces* are not a main factor in ice adhesion [47]; they involve energies of 2-4 kcal/mol versus 10-98 kcal/mol which are primary bonds. Though most effective at about 0.3-0.50 nm, the *Lifshitz-van der Waals forces* have some effect at considerably greater distances. Even at 10 nm they may be 98 pN increasing exponentially at a closer range; they have been estimated at 5 nm or less to be strong enough (~ 30 pN) to account for satisfactory adhesive bonding [11]. The electrostatic forces between a charge at the ice surface and the charge induced on a solid substrate have been found to dominate, largely, the adhesion of ice to surfaces [44]. The electrostatic interaction energy between ice and metals has been found to be significantly higher than the

hydrogen bonding and *Lifshitz-van der Waals forces* at greater than intermolecular distances [44]. The chemical bonding between ice and metals, which is largely hydrogen bonding seems to be one of the main forces [49]. As explained, ice can bond strongly to nearly all types of surfaces, making it difficult to remove from surfaces. While the majority of techniques actively used at present belong to active de-icing, *i.e.* to the mechanical removal of ice and snow build-up, none of them can be reasonably or even easily applied to various structures considering that they are highly demanding of energy, not environmentally-friendly in the case of anti-icing fluids, and destructive to most surfaces [50].

2.5 Adhesion Forces and the Interface

The force required to detach ice from any given surface is typically termed ice adhesion force. A number of parameters may influence the adhesion of ice to a surface, including, substrate properties, the conditions under which the ice formed, air temperature, freezing rate, water contact area, and droplet momentum. Although knowledge of the fundamental physics of ice adhesion is not yet widespread [44], it has been a well-known fact for over 50 years that, from a thermodynamic viewpoint, an adhesive layer will rupture from within the bulk adhesive rather than at the interface. It is thus difficult to correlate basic adhesion with practical adhesion due to intermolecular forces, the mode of applying stress, the presence or absence of sites of easy failure, *e.g.* weak boundary layers, intrinsic stresses, and the failure mode. Experimental conditions must be carefully defined considering the difficulty inherent in quantifying all these factors [3]. Generally, adhesion failure may occur at five points, these being at the true interface, within either of the bulk phases or at either of the two regions adjacent to the true interfaces. Most failures occur in this inter-phase region adjacent to the true interface [3]. Crucial in icing is the substrate/ice interface, with its chemistry and physics; it is a question as to whether or not these can be modified so as to repel ice. Complete repulsion, displaying zero ice adhesion bond

strength, is unattainable because all matter exhibits some degree of mutual attraction, as between liquid and solid in contact with each other [51, 52]. Reduced adhesion is an attainable objective, however, being well known in adhesion technology. Alteration of the interface, as by dirt, dust, grease, moisture, or poor contact can impair bonding. The chemical nature of the materials is also a factor here [53]. In this section, interface chemistry and forces will be discussed in relation to adhesion with its release or parting. Any system is most stable when its free energy is at a minimum, for example, a mixture of hydrogen and oxygen is only quasi-stable where a spark or a flame can induce a reaction evolving energy, or heat; the resultant water formed is deemed more stable. The reverse reaction requires the application of energy-heat; adhesion is similar. When two surfaces come together, residual surface forces interact, releasing energy. Conversely, it takes energy to create new surfaces, as by pulling apart adhered joints (see Figure 2.3) [54].

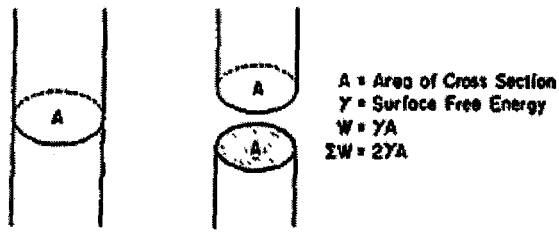

Figure 2.3. Cohesion-adhesion work $W = \gamma A$, $\sum W = 2\gamma A$ [54].

The properties of surfaces are different when compared to the interior or bulk. The extra energy associated with the surfaces or surface free energy arises from an imbalance between the interior and the exterior. This leads molecules to seek the interior, minimizing the surface energy and area. Thus a globule of liquid tends to form a spherical drop, the form which displays a minimum area-to-volume ratio, and hence minimum surface free energy [55]. In the case of liquids, the surface free energy 'γ' results from the residual unsatisfied forces remaining on a surface. This drawing together of molecules, as though enclosed in an elastic sheath, produces an apparent surface tensile force called "*surface tension*". This is also designated 'γ' having a dimension of force per unit length (mN/m) or energy per unit area (mJ/m^2) which is the same

numerically and dimensionally as surface free energy. Many physical and chemical properties are dependent on the micro-structural attributes in the case of crystalline materials. The surface energy of metals has been the subject of numerous theoretical and experimental investigations [56-58]. With regard to Figure 2.3, when a body is separated into two parts, the work to create the two new surfaces is $\sum W = 2\gamma A$, where A is the area of the cross section. When both these cross sections are again brought back together, such a degree of energy is released that the surface forces become mutually satisfied. This is the work of cohesion for a homogeneous material, or of adhesion for dissimilar halves or with an adhesive film between as a separator. Satisfaction of forces is incomplete when contamination is present, when contact is not intimate, or when one surface displays "*low energy*", *i.e.* is so self-satisfied that there is little attraction for neighboring material. It is now a question as to which forces are involved in the process of adhesion. Rarely are they primary chemical bonding, or valence forces, which are ionic-electrostatic or homo-polar (electron-sharing). These are effective only at typical bond lengths of 0.15-0.2 nm which decrease rapidly with distance. Typically, good adhesive joints result from adhesive-adherent interaction at much greater than inter-atomic distance. They have perhaps one-tenth the theoretical strength based on the forces available at the interface [59, 60], due presumably to imperfect matching, contamination, and the non-perfect intimacy of contact. It is also likely that hydrogen bonding is involved in ice adhesion; this is an interaction resulting from the sharing of a proton, or hydrogen atom, between two electronegative atoms [61] which must be small, *e.g.* F, N, or most commonly O. Hydrogen-bonding holds water molecules together in random clusters within the liquid and binds them into the rigid crystal lattice of ice [61]. Hydrogen-bond energies, namely 2-10 kcal/mol [61], are comparable with the weaker primary bonds and generally exceed the *Lifshitz-van der Waals* attraction forces [48]. Their range of action extends beyond that of the latter forces but has the greatest effectiveness at comparable distances, namely 0.1-0.5 nm [12]. Normally, there is a sufficient amount of adsorbed water molecules or oxides on the majority of practical solid surfaces, able to provide the strong interaction required with water molecules during

freezing [62]. The ability of optical flats or gage blocks to adhere when closely pressed or wrung together is evidence of interfacial forces which are effective well beyond atomic distances [61]. Electrostatic forces occur between non-compensated spatial distributions of charge on opposite sides of the interface at greater than intermolecular distances thus contributing significantly to ice adhesion with interaction energy of up to 500 mJ/m^2 [12]. It should be noted that the interaction forces between ice and a metal are greater than those between ice and a dielectric material since charges on ice induce equal and opposite charges on metals. Moreover, several conditions, including purity of materials, uniformity of surfaces, temperature, rate of application of force, and the morphology and composition of the iced surface all play an important role in the adhesion of ice to surfaces, for which any adhesion measurements must be taken with extreme care [3]. In the case of mechanical penetration, such as the presence of microscopic pores in a solid, a water drop can enter and freeze inside the pores. The expansion of water after freezing leads to a strong mechanical interlocking between the ice and substrate.

2.5.1 Ice Adhesion Testing

Various methods are possible for ice adhesion testing, for which a number of devices and methods have been employed at different times and places [63]. Included in these techniques, may be found impact tests [3], the peel test, the blister test [61], the cone or tensile test, scratch methods [64], laser techniques [65], electromagnetic tensile tests [66], the lap shear test, the axial cylinder shear test, the torsion shear test, the cylinder torsion shear test and others, each of which has its own advantages and/or drawbacks. Variability among these tests due to idiosyncratic methods and procedures, or ice formation conditions (*e.g.* the temperature of the air flow and of the supercooled droplets, the air speed, the liquid water content of the air together with droplet size and distribution, as well as the materials used) makes it difficult to compare results or to reproduce them as reported in the literature [18, 67, 68]. The most important factors in ice-

adhesion measurement are reliability and reproducibility of results both of which require uniformity in the force applied to the ice-sample, a sufficiently large iced area and a constant strain rate. Ideally, the results provided should be compared with those obtained on a common standard substrate, *e.g.* stainless steel, Al, or any specified plastic having been tested in the same way. Based on previous studies, the shear strength of refrigerated ice was about 1.72 MPa for Cu and the same variable for artificial ice was found to be between 0.85 MPa for Cu and 1.52 MPa for Al [69]. Ice adhesion tests were carried on several surfaces having different chemical compositions [3]. The adhesive strength for hard rime on Al power cables were shown to vary 0.075 to 0.12 MPa [70-72]. A study of the literature in the field shows that adhesion results from secondary forces yet exceeds normal cohesive strengths; it depends on free surface energy, low contact angle, wetting, cleanliness, and texture. Poor adhesion occurs with low energy surfaces or contaminants, particularly when this is textured or porous. Beams *et al.* [73] and Raraty *et al.* [74] used a rotating centrifugal force method to measure the adhesive shear strength of thin films of ice on the surface of a metal. The adhesive shear strength of ice on the samples was found to be 0.03 to 0.16 MPa at -1 to -15°C [75, 76]. For ice to detach spontaneously, it should be calculated to be 1 cm thick while at the same time the shear stress must be reduced to 98 Pa. [3]. Studies have also shown that Al surfaces treated with the addition of a self-assembled monolayer of silane or fluorocarbon will display reduced ice adhesion in comparison with a bare Al surface [2]. There are volume changes which occur as ice forms and cools; the interface is thus always under stress. Ice on a substrate is a polycrystalline solid with numerous dislocations as a result of always being under stress, especially at temperatures above -6°C. It should be noted that the accumulation of dislocations at ice surfaces subjected to steady stress was also observed to result from the differences in thermal coefficients of expansion and contraction of the ice-solid [3]. Shear forces tend to cause ice to rupture away from the actual interface whereas failures occur as a consequence of crack initiation at the stress points. A common technique for measuring ice adhesion is to carry out a comparative study by creating ice on surface of both a well-known

reference sample and sample in question with the same method and finally stating the results in shear strength change percentage.

2.5.2 Lowering Ice Adhesion

To reduce the adhesion of ice, which is considered to be an adhesive whose liquid form is water, requires reducing substrate wettability, thereby making it more hydrophobic. This property implies reducing both its reactivity and its surface forces, causing it to become more inert and more increasingly incompatible with water. The resulting higher contact angle makes it more likely to occlude air at the interface. Water is prone to hydrogen-bonding, which is the basis of the ice structure; water and ice are thus attracted to a substrate having H-bondable components, *i.e.* oxygen atoms. A low ice adhesion surface should then be free of oxygen atoms, or have them well screened by more inert atoms and groups. While capable of H-bonding in other situations, H as in hydrocarbons [61] and also F as in fluorocarbons [61] have been stated to not H-bond, although Eley [53] does suggest that even F in F-C bonds can exhibit some H-bonding properties. Chemical bonding strength or energy varies with different atom pairs and with what may be attached to them. It thus contributes to the relative activity or inertness of a substrate. A high energy surface, exhibiting high interfacial energy, has a high level of attraction for a contacting fluid and a low energy surface is the opposite. A low energy surface is relatively inert, its residual forces being more self-satisfied. Polymeric fluorocarbons and hydrocarbons have low energy surfaces which is 117 kcal/mole [61]. This reflects both the intensity of bond energies and the size of the atoms involved. Certain of the other single-bond energies are C-H 98, C-Cl 79, C-O 85.5, C-N 73, O-H 111, and C-Br 70 kcal/mol. These energy values show why surfaces of fluorocarbons and hydrocarbons display low energy. They thus show a low attraction for water and low ice adhesion, as in the case of Teflon (polytetrafluoroethylene) and polyethylene, as well

as other organic polymers with similar types of surface. A number of other bonds are of still higher energy, although these are unlikely to appear either alone or in an exposed position, or they otherwise involve O and N. Where not screened, their ability to H-bond enhances their attraction for water and ice, as seen in epoxy and polyester resins. The relatively low adhesion of silicones to ice [61] is explained by structural characteristics which keep their oxygen atoms well screened by methyl groups. Meanwhile, the silicone oxygens may aid the attachment of a silicone coating by H-bonding to an underlying substrate, thereby making it more permanent than wax. On the other hand, in most studies, so-called icephobic products are selected according to their hydrophobic properties, showing water-repulsion qualities [77-79].

The most common hypothesis is that any product having poor chemical affinity with water should also have weak ice adhesion. On hydrophobic films, dislocations occurring during the removal of ice tend to collapse into the surface due to the lower interfacial forces thus producing interfacial defects; this may explain why adhesion failure occurs at or very close to the interface. For hydrophilic surfaces, the interfacial forces are stronger and step formation is inhibited with a subsequent lower concentration of interfacial defects; adhesion failure occurs in the bulk ice, *i.e.* cohesion [3]. A highly glossy surface reduced the shear stress by 41 % and a sanded surface increased the adhesion by 149 % and hydrophobic waxes and PTFE dispersion decreased the adhesion by over 50 % [3].

2.6 Brief Review of Hydrophobic Properties

2.6.1 Wetting, Roughness and Air

Much evidence has accumulated supporting the stance that a liquid-like or transition layer exists on ice, both on free surfaces and at interfaces with solids [61, 80, 81]. Since its thickness depends on temperature and the nature of the surface, the latter must also affect ice adhesion via

this layer. This reinforces the belief that low ice adhesion can indeed be obtained by choosing suitable substrates. The ability of any given material or an applied adhesive layer to "wet" or spread out thoroughly as a fluid on another (substrate) material [52, 82] is critical to good adhesion in aiding the trans-interface transfer of forces. Wetting phenomenon may occur at the point where all three states, whether solid, liquid, or vapor, are in contact; this also includes the behavior displayed by the intersection of the three interfaces, namely, solid-liquid, solid-vapor, and liquid-vapor. For a solid adhesive, this can be brought about by heating or using a solvent where, as the heat or solvent escapes, the adhesive sets. Also, a liquid system may be solidified by polymerization, whether induced chemically or by heat, or by a suitable catalyst. Physical Roughness of texture plays only a secondary role in adhesion. Where wetting is sufficient, roughness can enhance adhesion by increasing the contact area for an exchange of forces, as well as by "*tooth*" or "*anchor*" effects. Conversely, roughness may increase the chance of retention of air [48] or other contamination, such as dust or oil, and can hence further impair wetting and adhesion. The effects of roughness on wettability are discussed below in connection with the contact angle. Interface contamination or imperfections also affect adhesion [48, 52, 60]. Contaminants interrupt the trans-interface exchange of forces. An important contaminant in adhesion is air. When wetting is incomplete, pockets of air are left in hollows or adhering to the surface, reducing bonding. Such pockets also can be loci of stress concentrations, with consequent initiation or propagation of adhesive failure. This is truer for smooth surfaces, where co-planarity of contaminant patches aids propagation of failure cracks. Conversely, a rough surface can minimize contaminant effects by interrupting such co-planarity, as shown in Figure 2.4.

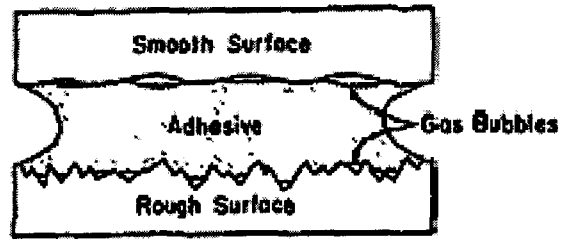

Figure 2.4. Effect of surface texture on adhesion. Co-planarity of occluded bubbles, as on a smooth surface, weakens joint. Interruption of co-planarity, as on a rougher surface, strengthens joint.

Since adequate wetting is a necessity for proper adhesion, poor wetting and occlusion of air may be a way of bringing about poor ice adhesion. Wetting depends on the attraction between applied liquid and solid [52], *i.e.* on secondary and H-bonding forces, which the surface energy 'γ' reflects. For hard solids, 'γ' is 500-5000 mJ/m^2, increasing with hardness and melting point, *e.g.* metals, oxides, nitrides, sulfides, silica and diamond. For soft organic solids, 'γ' is generally less than 0.1 mJ/m^2, *e.g.* waxes and most organic compounds. For liquids (excluding liquid metals), 'γ' is also less than 100 mJ/m^2. Low energy liquids, *i.e.* most organics, typically 'γ' of 20-40 mJ/m^2, creep over and wet solids readily since their internal forces are not strong, as evidenced by the fact that their boiling points are lower than those of higher energy liquids. Water, with γ = 72 mJ/m^2, is one of the latter, owing to the role of H-bonds in holding it together, as is mercury, in which metallic bonding does this function. Added detergents, or wetting agents, improve wetting by water, through a lowering of its surface tension. This also increases the adhesive strength and diminishes the cohesive strength of ice [48, 61]. For the substrate, if its surface energy is high, as for metals, oxides and inorganics, the residual forces are significant [52]. From a practical point of view, any liquid will spread out over high energy surfaces, thereby making them difficult to keep clean. If surface energy is low, as for waxes and numerous polymers, self-satisfied forces provide little inducement for liquids to spread out. It is to this type that researchers must look in order to observe low ice adhesion. Although the surface energy of solids is not as readily measured as it is for liquids, values are obtainable by analogy with the

liquid phase, through specialized measurements [59, 60], contact angles, calorimetric heat of solution, or other relevant thermodynamic considerations.

2.6.2 Hydrophobicity and Contact Angle

Wettability is assessed by the contact angle, CA or θ formed by the liquid and the substrate. Values of θ vary inversely with mutual attraction and ease of wetting ranging from 0° to well over 90° (theoretically to 180°). To date, numerous methods have been developed to characterize the hydrophobicity of the surface, including contact angle, tilt angle, and multiresonance thickness-shear mode sensors [83]; among these, the contact angle measurement is the main method for the characterization of hydrophobic surfaces and for studying the surface energy. Young and Laplace reported that each surface has a specific energy which is called surface energy and is proportional to the number of atoms present on the outermost layer [3, 18]. Figure 2.5 shows the shape of water droplets for wetting and non-wetting liquids in a tube and for typical drops, with the associated force diagram, where γ_{SV}, γ_{SL} , γ_{LV} are the interfacial free energies per unit area of the solid-vapor, solid-liquid, and liquid-vapor interfaces, respectively. The contact angle, θ, is the macroscopic indicator of the surface energy balance. The equilibrium of surface energy can determine the entire shape of a droplet on a solid, provided that the drop is small enough to remain unaffected by the flattening action of gravity. Disorders, impurities, and other defects or energetic effects close to the surface of the material can give rise to increased surface energy. When the surface energy is diminished, the hydrophobicity, or water repellency, is enhanced [18]. Young's equation introduces the water contact angle on rigid homogenous object which does not reshape and for which there is no chance of any liquid penetrating the surface.

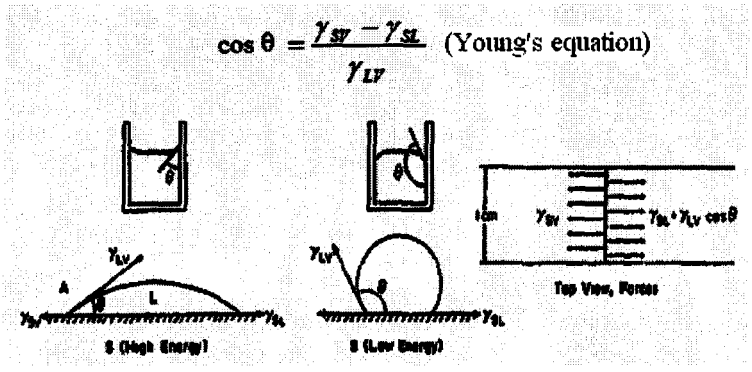

Figure 2.5. Liquid droplet on a surface, its surface energies, CA and force diagrams [54].

The measurement values provide information regarding the bonding energy of the solid surface and the surface tension of the droplet. Because of its simplicity, CA has been broadly accepted for material surface analysis related to wetting, adhesion, and absorption. For a given liquid, a high-surface-energy solid tends to be wetted in contrast to a low-energy surface solid which does not absorb the liquid. On the other hand, when a droplet of high surface tension liquid is placed on a solid of low surface energy, the liquid surface tension will cause the droplet to form a spherical shape, which is the lowest energy shape; a low-surface-tension liquid, however, will simply spread out.

As described previously, wettability of a surface is normally expressed as a CA (θ) of the specific surface, *i.e.* when $\theta > 90°C$ and is called a hydrophobic surface not having any attraction to water; also when $\theta < 90°C$ and is called a hydrophilic surface which indicates that the surface in question has considerable attraction for liquid. Water molecules orient themselves towards a surface due to hydrogen bonding and, depending upon the surface structure of the substrate, super-cooled water layers can occur at low temperatures. For hydrophobic coatings, the orientation of water molecules is much lower in the first layer than in the hydrophilic ones [3]. The greater the contact angle, preferably >150°C, the better the water-repellency and self-cleaning abilities. These surfaces named as superhydrophobic or ultrahydrophobic surfaces [49]. The superhydrophobic states can be further classified by considering the contact angle hysteresis [83] which will be explained in greater detail further on in the text. It is impossible to achieve $\theta =$

180° because hydrophilic sites are invariably present on practical hydrophobic surfaces while the London forces would still act across the interface. It is thus not possible to produce a surface which water would not wet at all [3]. Also, there exists an alternative opinion regarding the border between hydrophobic and hydrophilic surfaces, which maintains that 65° is the turning point [83, 84]. Thus, if $\theta = 0°$, representing extreme hydrophilicity, then water is liable to wet the entire surface entirely, thereby spreading completely to form a thin layer of liquid on the surface. Thermodynamic treatment, in lieu of intermolecular force treatment, led to the reversible system of work of adhesion (W_A) introduced by Dupré in 1869:

$$W_A = \gamma_{SV} + \gamma_{LV} - \gamma_{SL} \qquad (1)$$

This implies that the reversible work of separating the liquid from the solid equals the change in free energy of the system. Substituting for γ_{sv} in the above equation yields the Young-Dupré equation:

$$W_A = \gamma_{LV} (1 + \cos\theta) \qquad (2)$$

Although γ_{SV} and γ_{SL} are difficult to determine in all the above equations, the variables on the right in last equation are easily measured. The higher wettability indicates the higher work of adhesion. Equation 2 shows how work of adhesion, and hence wettability also, relates to θ; when $\theta = 0°$ in that case $W_A = 2\gamma_{LV}$ followed by complete wetting which occurs with excellent adhesion. When $\theta = 180°$, the $\cos\theta = -1$ and thus $W_A = 0$ with no wetting or adhesion. When $\theta = 90°$, then $W_A = \gamma_{LV}$ displaying poor wetting and fair to poor adhesion. In real situations, it is impossible to achieve a surface with $\theta = 180°$ because the *Lifshitz-van der Waals* or *London forces* would always act across the interface between two materials, hydrophilic sites are invariably present on practical hydrophobic surfaces. Thus, it is not possible to produce a surface which water would not wet at all and to which ice would not adhere [51, 52]. Actually, θ may be found to be as large as 110°-115° for water (on waxy or $-CH_3$ surfaces) [51, 61], or as large as 154° for mercury on

steel [85]. Roughness of surface can affect θ [52, 60, 86], decreasing it when θ is less than 90°, and increasing it when θ is greater than 90°. Thus, on rough wax θ is increased to 132° [85].

2.6.3 Methods of Measuring the Contact Angle of Surfaces

Contact angle measurement is an easy-to-adopt method for surface analysis related to surface energy and tension. Contact angles may be used to detect the presence of films, coating, or contaminants with a surface energy which is different from that of the underlying substrate. Static contact angles can be measured by fitting the symmetric sessile droplets where a droplet is placed on a static horizontal solid surface using a goniometer and applying the *Laplace-Young* equation in which a water droplet is deposited on the surface in such a way as to maintain its volume of 3 to 8μL constant during the contact angle measurement. It should be noted that static CA is susceptible to providing the values of equilibrium contact angles. Droplet volume on the surface is time-dependent, thus various parameters such as chemical reaction between the solid and the liquid, liquid evaporation, and dissolving the solid into liquid may have an effect on it; variations of contact angle versus time can thus be obtained during the measurement-taking process. As shown in Figure 2.6, the dynamic contact angle or contact angle hysteresis (CAH) can be measured when a water droplet is allowed to advance in one direction on a surface with the difference calculated between the advancing contact angle, which is the CA at the wetting edge of droplet, θ_A, and the receding contact angle, which is the CA at the de-wetting edge of droplet, θ_R. An additional example is when the volume of the liquid drop increases or diminishes because of injecting or aspirating the liquid into or out of the drop with a hollow needle. The static CA is normally greater than the receding angle, and less than the advancing angle. Numerous methods and techniques have been developed to date to measure the contact angle hysteresis, including the tilt angle (θ_T), the advancing/receding angle, contact angle measurements with surfactant solution, multi-resonance thickness-shear mode sensors [83].

Previous studies show that there is almost no unique relation between the values of CA and CAH. When the static contact angles are (large/wide), however, low hysteresis values may be obtained. The tilt angle refers to the critical angle between the substrate and the horizontal, below which the water droplet begins to move after elevation of one end of the substrate. It should be pointed out, that the tilt angle does not equal, the difference between advancing and receding contact angles but it does, however, reflect it. A schematic illustration of the relationship between the advancing angle, the receding angle, and the tilt angle is shown in Figure 2.6. It is worth noting that the combination of micro- and nano-roughness is helpful in obtaining surfaces with a high CA and low tilt angle [87].

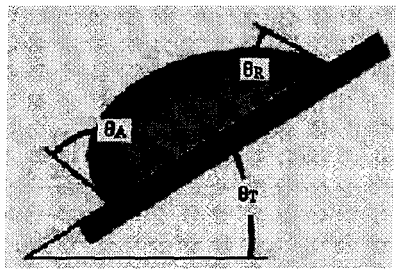

Figure 2.6. Schematic illustration of the relationship between advancing, receding, and tilt angles.

Using a surfactant solution as a probe to measure the contact angle can also reflect the CAH. Gao and McCarthy [88], and Zhang *et al.* [83] have demonstrated that when adding surfactant molecules to water, the CAs on certain superhydrophobic surfaces with high hysteresis appear to become narrower. For superhydrophobic surfaces with low hysteresis, however, the contact angles are similar no matter whether a pure water droplet or a water droplet containing surfactant is used as an indicator. This method can, therefore, be used to distinguish between a self-cleaning surface and a superhydrophobic surface with a high CAH. Kwoun and co-workers [83] introduced a method called *MTSM* sensors, to differentiate superhydrophobic surfaces exhibiting similar macroscopic CAs but a different CAH. This measurement technique operates on the basis of high-frequency shear acoustic waves generated by a piezoelectric quartz resonator thickness-shear mode (*TSM*) sensor. The depth of penetration is of the order of tens of thousands

of nanometers. When a superhydrophobic surface has a low CAH, the water layer can only wet the top of the surface considering that it is almost unable to penetrate the interspaces of the rough structure. The harmonic frequency shift of such a surface is, therefore, much smaller than surfaces with a higher contact angle hysteresis [83]. Contact angles may be judged fairly accurately within 10-15° visually [51]. Measurement of θ is usually made as indicated in Figure 2.7 [60, 85]. In Figure 2.7(a), a slab of solid is partially immersed and its angle is then adjusted until the liquid touching it remains horizontal with no meniscus on one side. When $\theta < 90°$, this condition may be judged from the side, or perhaps more easily by looking down from the top and noting the reflective surface.

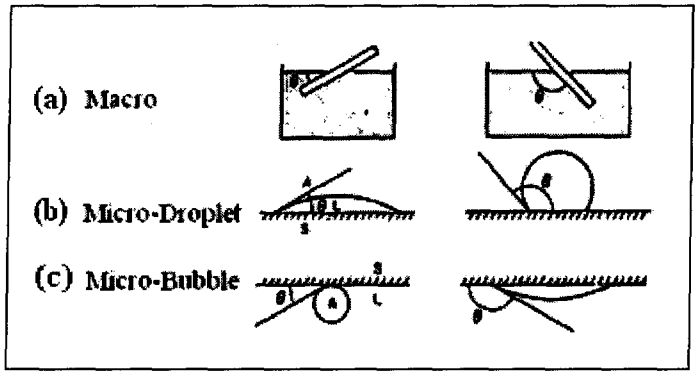

Figures 2.7. Measurement of contact angle on a surface (CA, θ).

For $\theta < 90°$, the slab prevents viewing from above, thus the judgment must be made from the side. Preferably, the test should be made in a completely filled tank, adjusted so that the surface rests above the plane of the water-repellent sides. In Figures 2.7(b) and 2.7(c), θ is measured as a sessile drop or air bubble resting on the test surface, using a microscope with goniometer. In all cases, the angle should be measured as shown, on the liquid side of the intercept. Misleading contact angles can be obtained without care to cleaning the surface, avoiding contamination, and attaining equilibrium. Misleading contact angles are also result of comparing advancing and receding values, which are particularly different if there be contamination.

2.6.4 Other Measurements on Contact Angle Hysteresis

Gao *et. al.* [88] developed a method of distinguishing the CAH by lowering the superhydrophobic surface onto a supported droplet and compressing follow by releasing several times. If the CAH is low enough, this surface will not adsorb the water droplet after release; otherwise, a superhydrophobic surface with high hysteresis has a strong affinity for the water droplet. The bouncing drop method may also be used to characterize the CAH. When a liquid drop lands on a solid surface without wetting it, it bounces with remarkable elasticity [83, 89, 90], thus, the bouncing ability of the water droplet can also reflect the CAH.

2.6.5 Critical Surface Tension (γ_c)

A useful concept in considering the contact angle, wettability, and adhesion is the critical surface tension (γ_c) [52]. The value of γ_c for a given solid is determined by observing the spreading behavior and the angle θ of a series of liquids of decreasing γ_L. A rectilinear relation exists between cosine θ and γ_L on a linear plot in which the intercept of this line with the cos $\theta = 1$ (*i.e.* θ = zero) line gives a value of γ_c for which wetting would be complete. The value of γ_c is independent of the nature of the test liquid and is a parameter characteristic of the solid surface only. To spread on a given substrate, a liquid must have $\gamma \leq \gamma_c$. This approach is most useful for low energy surfaces of $\gamma < 30$ mJ/m^2. Deviations of such plots from linearity are more likely for values of $\gamma > 50$, *i.e.* for liquids of high energy, since they are always of the H-bonding type. Values of γ_c are useful for evaluating the wettabilities of low energy surfaces. Thus, for a monolayer anchored to a substrate by the polar groups acid, alcohol, and ester, wettability is governed by the end groups exposed (-CH_3, -CHF_2, and so forth together with decreases for substituents on an organic carbon chain substance in the order N>O>Cl>H>F [48]. The value of γ_c is useful for comparing the

wettabilities of low energy polymer surfaces, decreasing as shown for the following structures shown in table 2.3 [52]. The lowest value known is $\gamma_c = 6$ mJ/m^2 (see table 2.4), for a condensed monolayer of perfluoric acid, or $F_3C(CF_2)_{10}COOH$, the most non-wettable surface ever reported [52]; every liquid studied was unable to spread on it. The lowest for any solid polymer is $\gamma_c = 10.6$ mJ/m^2, for polymerized methacrylic ester of perfluoro-octanol.

Table 2.3. Values of γ_c for surfaces ended with various groups exposed and structures [52].

structures	γ_c (mJ/m^2)
$-CH_2-CCl_2-$	40
$-CH_2-CHCl-$	39
$-CH_2-CH_2-$	31
$-CH_2-CHF_2-$	28
$-CH_2-CF_2-$	25
$-CHF-CF_2-$	22
$-C_2F_4-$	18

It should be noted that the critical surface tension for spreading (γ_c) defines the wettability of a solid surface by noting the lowest surface tension (γ) a liquid can have and still exhibit a contact angle greater than zero degrees on that same solid.

Table 2.4. Values of γ_c (mJ/m^2), for low energy polymers/surface components [52].

Polymer of hexafluoropropylene $[-CF_2-CF_2-CF_2-]_n$	**16.2**
Polymer of tetrafluoroethylene (PTFE) $[-CF_2-CF_2-]_n$	**18.5**
Polymer of trifluoroethylene $[-CFH-CF_2-]_n$	**22**
Polymer of vinylidene fluoride $[-CH_2-CF_2-]_n$	**25**
Polymer of trifluorochloroethylene $[-CFCl-CF_2-]_n$	**31**
Polymer of ethyl methacrylate $[-CH_2-C(CH_3)COOCH_3-]_n$	**39**
Polymer of vinyl chloride $[-CCl_2-CH_2-]_n$	**40**
Surface constitution of fluorocarbon : $-CF_3$	**6**
Surface constitution of fluorocarbon : $-CH_2CF_2$	**20**
Surface constitution of fluorocarbon : $-CFHCH_2$	**28**
Surface constitution of hydrocarbon : - CH_3 (Crystal)	**22**
Surface constitution of hydrocarbon : $-CH_3$ (Monolayer)	**24**

2.7 Definition of Surface Passivation

Passivation is the process of making a material "passive" in relation to another material prior to using the materials together. As discussed above, impurities, disorders, and other defects or energetic effects near the material surface can give rise to higher surface tension energy [18]. It is possible to alter the surface energy and wettability of surfaces by coating the surface with an appropriate coating, even if it is only as thin as a few layers of molecules; this is called the passivation process. A typical passivation process used in industries is the cleaning out of stainless steel tanks with sodium hydroxide plus citric acid, followed by nitric acid (up to 20% at ~ 48.9°C) then a complete water rinse. These steps help to restore the film by removing metal particles, dirt, and welding-generated compounds or oxides. In the context of corrosion, passivation is the spontaneous formation of a hard non-reactive surface film which will inhibit further corrosion. This layer is usually an oxide or nitride having the thickness of a few molecules. Some corrosion inhibitors help the formation of a passivation layer on the surface of the metals to which they are applied. A common passivation procedure is based on the self-assembly of a number of organic molecules; this is one of the most successful approaches to chemical modification and hydrophobization of numerous hydrophilic surfaces leading to both high static hydrophobicities, defined by the contact angle of water droplet, and low dynamic hydrophobicities, defined by the sliding angle. Such self-assembled coatings are ultimately expected to be potential snow and ice-repellent materials [15], while the molecules usually have a polar unit on one side known as the head and a non-polar long saturated hydrocarbon chain on the other side known as the tail. A typical hydrocarbon molecule used for passivation is stearic acid (SA), as shown in Figure 2.8. The head portion of the stearic acid molecules may be strongly attracted to the high energy surfaces of solids; this may lead to ordered arrangements resulting in considerably lower surface energy.

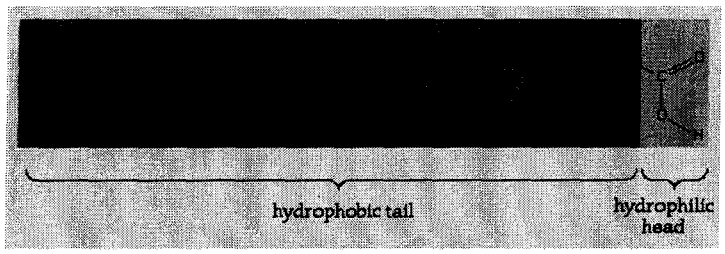

Figure 2.8. Structure of a stearic acid (SA) molecule.

A class of self-assembling monolayers (*SAMs*) widely used for the hydrophobization of various surfaces is based on fluoroalkylsilane or n-alkyltrialkoxysilane precursor molecules, which, through a combined process of adsorption, hydrolysis, and polymerization can form a dense and well-organized layer [15]. In order to form a complete monolayer, silane groups condense with surface hydroxyl groups to form a thin layer of polysiloxane. Figure 2.9 demonstrates self-assembly for a perfluorinated octylsiloxane monolayer, which is similar to that of octadecyltrimethoxysilane *(ODTMS)* based layers used in this study, as described below. The degree of assembly displayed by SAMs depends on reaction conditions and on the substrate.

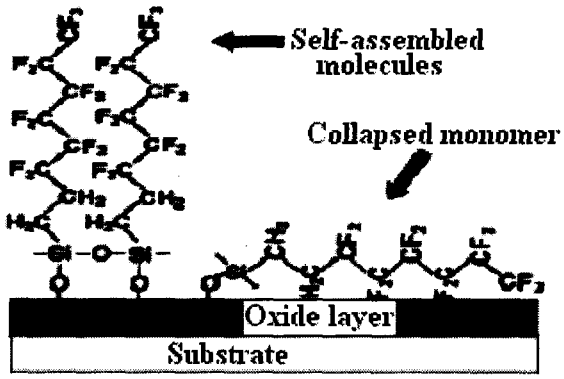

Figure 2.9. Well SAM of FAS-13 molecules (left) and collapsed (right) on an oxide surface.

The fully-grafted surfaces by SAM molecules, which expose their CF_3 (or CH_3) and CF_2 (or CH_2) groups atop may be considered low-surface-energy coatings. The least surface energy relates to the hexagonal arrangements of closely packed -CF_3 factional groups [91]. A variety of fluorinated materials, *e.g.* polytetrafluoroethylene (PTFE or Teflon), have been prepared with excellent resistance to water, oil, and organic solvents. In fact, the reducing of surface energy

which may lead to enhanced hydrophobicity and therefore, to ice or wet-snow repellency also, can be placed in the following order: $-CH_2 > -CH_3 > -CF_2 > -CF_2H > -CF_3$ [18, 92]. It has been demonstrated that both the static and the dynamic water repellency of SAM-coated surfaces may be strongly affected by the degree of self-assembly of fluoroalkylsilane or alkylsilane molecules and by the water coverage of a rough surface, which is susceptible to trapping air [3]. In other words, increasing the assembly degree of SAM molecules, in combination with the desired roughness, can result in the improved hydrophobic properties of the surface, as discussed earlier, thereby probably leading to enhanced icephobic properties [3, 93]. Maccarini *et al.* [2] showed that H-terminated silicon surfaces had lower stability in contact with water with significant changes in the contact angle. Only the surfaces coated with long-chain aliphatic SAMs, such as octadecyltrichlorosilane (*OTS*), however, did not display any appreciable changes even after 24 h of exposure to water. Earlier studies established a typical range of water contact angles of 100° to 120° for the F-containing flat surfaces [94, 95]. Another alternative approach is to use insulating low-surface-energy coatings with higher thicknesses values on the order of tens of nm. A reasonably thick film of diamond-like carbon (*DLC*) is a good choice because of its high hardness and low surface energy. For many years, room-temperature-vulcanizing (*RTV*) silicones have also been used as water repellent coatings and surface treatments. The contact angle of a sessile water droplet, as a measure of static hydrophobicity, is demonstrated to be ~10° higher on flat fluoroalkylsilane-grafted surfaces in comparison with alkylsiloxane monolayers and it is then observed to increase gradually with the assembly order. The difference, however, diminishes when rough substrates with air inclusion are used [93]. Furthermore, a perspective use of various SAM coatings as snow- and ice-repellent materials with low surface energy has been recently reported by several groups [93]. There is still a lack of systematic knowledge, however, on how the microstructure and surface chemistry of SAMs influence the hydrophobic and, in particular, the snow- and ice-repellent properties of the coatings. Alkylsilanes have a direct correlation with the interfacial strength which exists between SAM-grafted surfaces and ice. Such SAMs can be

formed from commercially available organosilanes, namely: 1H,1H,2H,2H-perfluorodecyltrimethoxysilane or octadecyltrichlorosilane (*OTS*), FAS-17 or 1H,1H,2H,2H-perfluorodecyltrichlorosilane, and FAS-13 or 1H,1H,2H,2H-perfluorooctyltrichlorosilane [93]. Increasing the assembly order of SAM_S, in combination with properly designed roughness, leads to the considerably improved hydrophobicity of the surface [3]. Octadecyltrichlorosilane [$CH_3(CH_2)_{17}SiCl_3$] is an organo-metallic chemical, shown in Figure 2.10, which is used in semiconductor industry to form thin films of SAMs on silicon dioxide substrates. This chemical reacts violently with water.

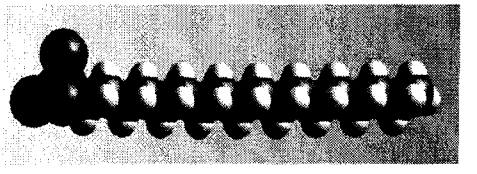

Figure 2.10. Octadecyltrichlorosilane (OTS) molecule configuration.

Dimethyl-n-octadecylcholorsilane (*DMOCS*), belonging to the self-assembled monolayer family, when used on AA6061 surfaces was shown to have the smallest values of ice adhesion compared to other surface treatments, including chemical and mechanical polishing and the use of polymethyl methacrylate (*PMMA*), as a result of using the polar side group -$COOH_3$, and polyimide coatings. In addition, because of their thickness and also the formation of the covalent Si to Al bond, this layer adheres strongly to the Al surfaces and should lead to improved service life under periodic icing/de-icing cycles [2].

2.8 Brief Review of Superhydrophobic Properties

2.8.1 Waterproofing in Nature

Waterproofing is of interest because it, too, involves interactions between air, water, and solids and the apparent preferential "wetting" by air. As Crisp *et al.* [96] described, there are numerous examples of waterproofing in nature. These include (i) insects which require the means

of taking in air without drowning when immersed in rain or dew and yet must also be able to conserve moisture in arid conditions; (ii) plants which need pores for air but must also conserve moisture when humidity is low; (iii) animals whose coats must remain dry to maintain thermal insulation, and (iv) birds whose water-repellent feathers retain air for insulation to conserve body heat as well as for the preservation of buoyancy when floating on water. Closely perforated or hairy structures of hydrophobic character shed water or cause the formation of a "*gaseous plastron*" which protects bird feathers, insects, and leaves. The plastron effect, created by this shield of occluded air, produces the silvery appearance often seen when leaves are immersed. As stated earlier, when θ is greater than 90°, it is larger on rough surfaces than on smooth ones, and the converse holds true when θ is less than 90°. This fact can be rationalized on geometric grounds. A corollary is that a perforated or porous hydrophobic material is one which will not wet readily, *i.e.* rough surfaces which will also neither wet nor allow liquid water to penetrate until a specific entry pressure is exceeded. It derives from the greater θ on a rough surface; it is thus possible to consider the substrate as preferentially inclined towards "wetting" by air, considering that surface tension forces tend to hold the meniscus in the perforations against appreciable pressure. Lowering the surface tension of the water as may be done by adding a surfactant, or wetting agent, will contribute to lowering the θ values and will destroy the water resistance [86]. Scientists have discovered how to make fabrics water-repellent by utilizing similar techniques. Like the fibrils on plants and insects, the hairs on animals, and the interlocking parallel barbs on bird feathers, fibres need to be organized into a compact and regular spacing order, then made hydrophobic, by treatment using wax, silicone, or other hydrophobic agents. Not only fabrics but also porous materials like leather, masonry, soils, and so forth can be thus waterproofed. The non-wettability of the treated matrix, or its preferential "wetting" by air, aided by the relatively high surface tension of surfactant-free water, makes it possible to cause the required repulsion of water.

2.8.2 Superhydrophobic Surfaces

The research carried out on superhydrophobic surfaces and the related phenomena dates back to approximately the beginning of the last century [17, 83, 97-101]. In 1907, Ollivier [83, 102, 103] observed that contact angles of nearly 180° appeared on surfaces coated with soot, arsenic trioxide, and lycopodium powder. Later on, in 1923, Coghill and Anderson [51, 104-106] found that after depositing stearic acid on the rough surface of galena, this same surface showed a high contact angle of about 160°. Previous studies show that the combination of suitable surface roughness and low-surface-energy materials is responsible for superhydrophobicity. Research on superhydrophobic surfaces received continued but relatively limited attention before the mid-1990s [51, 83, 102-112] when all studies focused on the relationship between contact angles and surface geometry [83, 107, 108, 113], on observation of the superhydrophobic phenomena displayed by "*triticum aestivum*" plant leaves, on the surface of ducks' feathers, and on insect cuticles [83, 114, 115]. This line of research became reactivated because of the explanation of the origin and the universal principle of the "lotus effect"' in nature submitted by Nienhuis and Barthlott in 1997 (Figure 2.11) [116, 117]. They revealed that this effect is due to the presence of a rough micro-nanostructure covered with epicuticular wax crystalloids resulting in a water CA greater than 150° [118] which is responsible for their self-cleaning properties. Taking the lotus leaf as an example, self-cleaning means that particles adhere to the surfaces of water droplets on rough surfaces and can be removed easily from the leaves when the droplets roll off (see Figure 2.11). Because most dust has stronger adherence to the water droplet than to the solid surface due to the surface tension, a spherical water droplet on the superhydrophobic surface can roll off the surface with the dust adhered to it under even a tiny disturbance.

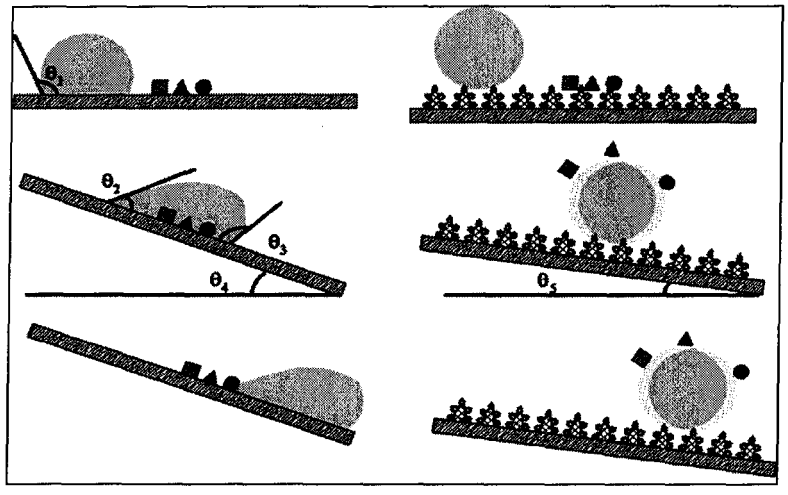

Figure 2.11. Left: normal hydrophobic surfaces do not have self-cleaning properties. Right: superhydrophobic surfaces have self-cleaning properties. The water droplet rests on the surface spherically.

Superhydrophobic surfaces can thus act as self-cleaning surfaces when there is dust accumulated on them. Since then, research on superhydrophobic surfaces has been motivated by mimicking nature on one hand. Much effort has thus been devoted, to understanding the surface structures of different plants and animals [83, 119] then to fabricating similar structures artificially. On the other hand, the impetus of this line of research also derives from the demand for the improved performance of chemical materials through surface modification. Beyond the research on the superhydrophobic fabrication methods, recently, more and more attention has been attracted to the potential functional applications of superhydrophobic coatings in different realms. It is the combination between surface roughness and low-surface-energy coating that leads to superhydrophobicity. Recently, various applications of superhydrophobic surfaces in micro- and nano-materials and devices were reported. The maximum CA which may already be obtained on a flat surface with regularly aligned closest-hexagonal-packed CF_3 groups is equal to ~120° [17]. Several superhydrophobic coatings have been produced using a range of chemical and physical methods on rough surfaces, *e.g.* a CA of 174° using n-alkylketene dimer [120] and a CA of 160° using plasma-enhanced chemical vapor deposition (PECVD) of fluoroalkylsilanes on Al surfaces [121]. Superhydrophobicity means not only a high contact angle, but also a low

hysteresis of the contact angle. The low hysteresis of the contact angle of the superhydrophobic surface is responsible for the self-cleaning properties, which means that a water droplet can easily roll off the surface and remove dust from the surface. Self-cleaning is one of the most important purpose of the application and function of superhydrophobic surfaces. The direct fabrication of superhydrophobic coatings on metal surfaces has provided a solution to the corrosion problem which is a concern to be discussed in detail in the next chapter. It was demonstrated that a water drop can slide off a surface even if the CA is very low, even less than 20°, provided that the CAH is less than 4-5°. On the other hand, a water drop can slide off a surface even if the CAH is higher, provided that the CA is greater than 160°, as a result of the lower contact area between the liquid and the solid [99]. The influence of surface roughness on water-repellency and equilibrium CA values on rough surfaces has been mathematically expressed by the Wenzel and Cassie-Baxter equations, as shown in Figure 2.12 [107, 108]. These regimes are two major models for describing water CAs on rough surfaces. At sufficiently large micro-feature spacing and liquid pressures, the air-water interface can collapse, resulting in a fully wetted Wenzel state.

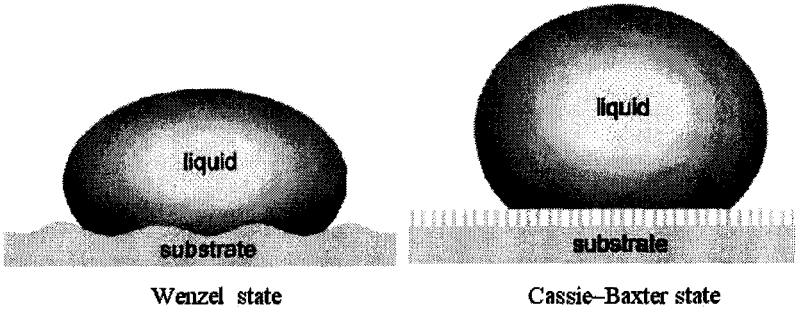

Figure 2.12. Wenzel model and Cassie-Baxter model.

The Wenzel equation is stated as $\cos\theta^* = R\cos\theta$, where θ^* is the apparent CA observed on a rough surface; θ is the equilibrium CA between a smooth surface of the same chemistry and the liquid as defined by Young's law; and R is the roughness factor defined as the ratio of the actual wetted surface area to its geometrically projected counterpart. A roughness factor of R=1 represents a smooth surface; the number is thus expected to increase with increasing roughness.

For a hydrophobic surface, the equilibrium angle will increase in the Wenzel state; however, the CAH is also typically very large. This is due to the contact line being pinned to each wetted feature as it recedes [122]. In the Cassie-Baxter model, an air-water interface is supported between the surface roughnesses [108]. In other words, the Cassie-Baxter model describes the effect of roughness on chemically heterogeneous structures where the apparent contact angle is mathematically derived from the Cassie equation; this phenomenon modifies the CA, θ', such that:

$$\cos\theta' = f_1\cos\theta_1 + f_2\cos\theta_2 \qquad (3)$$

Here, θ' is the contact angle of the composite surface consisting of two components with contact angles θ_1 and θ_2, and their corresponding area fractions of the solid-liquid interface f_1 and f_2. In order to maximize the equilibrium CA, the percent coverage of the air-water interface must similarly be maximized [123]. It is also important to note that the shape and size of the surface protrusions affect the contact angle and the resulting hysteresis [123]. In such a composite system, f_1 is assumed to be the area fraction of the solid surface while f_2 is assumed to be that of air, where θ_2 is 180^0. As $f_1 + f_2 = 1$, the previous equation can be further modified as $\cos\theta' = f_1(\cos\theta_1 + 1) - 1$. This equation explains why, on a rough surface with a large amount of air entrapment in the surface irregularities, (one can/it is possible to obtain a highly superhydrophobic surface with a very small area fraction, f_1, of the surface in contact with the water drop. It should be noted, however, as has been shown, that even with proper spacing of surface features when on a small scale, the roughness cannot sufficiently "*trap*" air, and an increased hysteresis is thus experienced [124]. True superhydrophobic surfaces, therefore, do indeed exist in the Cassie-Baxter mode, but not in the Wenzel state.

2.8.3 Fabricating Rough Surfaces via Chemical-Physical Methods

As mentioned previously, artificial superhydrophobic surfaces are fabricated by combining rough surface morphology and low-surface-energy coatings. In view of the methods for fabricating rough surfaces, two general approaches have been developed, including chemical and physical methods in general. Different methods can be used for fabricating different rough surfaces with their advantages and drawbacks.

A) Lithography

Lithography is a useful method for fabricating rough surfaces with regular structures. For example, Oner *et al.* have used photolithography for transferring the patterns of masks onto silicon wafers [123]. Subsequently, a superhydrophobic surface may be obtained by hydrophobizing the silicon wafer by applying silanization chemistry. Chen and co-workers have used the spin-coating of mono-disperse polystyrene beads for lithography to obtain a patterning of large-area periodic nanosphere arrays [126]. After treatment using oxygen plasma etching, the nanosphere arrays are coated with a 20 nm thick gold film. In this way, a well-ordered, tunable superhydrophobic surface is manufactured with a CA of 132° to 170°. Recently, nano-imprint lithography [127] and femtosecond laser pulses [128] were also developed to form structured surfaces. Besides the above physical methods, chemical etchings are employed for surface roughening on polycrystalline metals, such as aluminium, copper, and zinc [129]. In general, the lithography method is too complicated for the creation of large scale superhydrophobic surfaces.

B) Vapor Deposition and Plasma Techniques

Carbon nano-tube forests are a useful structured matrix for mimicking the lotus effect; the fabrication of a regular carbon nano-tube forest relies on a variety of methods of chemical vapor deposition (*CVD*). Although different methods are available, plasma enhanced CVD is a technique which produces perfectly aligned and untangled carbon nano-tubes with controlled height and diameter. Lau *et al.* created a superhydrophobic surface using the nano-scale roughness inherent in a vertically aligned carbon nano-tube forest together with a hydrophobic PTFE coating [130]. The microwave plasma-enhanced CVD, using organosilicon compounds and Ar gas as starting materials at low temperatures, was developed by Wu *et al.* to prepare ultra-water-repellent films [131]. They also improved upon their method by using CO_2 as an additive gas thereby obtaining an ultra-water-repellent film with enhanced mechanical durability [132]. Simple physical vapor deposition (PVD) is also used to generate films of orderly textured features. For example, superhydrophobic surfaces of n-hexatriacontane can be obtained directly by PVD [133]. Plasma techniques are a relatively simple way of preparing non-wetting surfaces which can provide the as-prepared material with surface roughness and low-surface-energy coatings simultaneously. The plasma polymer vapor polymerization process introduced to fabricate superhydrophobic surfaces of PTFE coatings [134]. At a later date, a series of projects for the fabrication of fluorinated polymer superhydrophobic coatings via plasma treatment of the surfaces was reported [83]. Because the surface roughness of the coatings fabricated by plasma treatment is easily tuned, this method is an appropriate way to prepare superhydrophobic coatings with special optical properties that have strict requirements on surface roughness.

C) Sol-Gel Processing

The surface roughness of the materials fabricated via the sol-gel method can easily be tuned through changing the protocol of the method and the composition of the reaction mixture. Tadanaga *et al.* have fabricated thin films of alumina with a roughness of 20-50 nm by immersing porous alumina gel films in boiling water. After depositing a layer of fluorinated silane, the as-prepared coatings exhibit superhydrophobic properties [83]. Subsequently the sol-gel method was applied to the fabrication of superhydrophobic surfaces by several groups of researchers. By tuning the scale of the surface roughness, the superhydrophobic coating fabricated by means of the sol-gel method can be made transparent. Therefore the sol-gel method is another candidate for the fabrication of transparent superhydrophobic surfaces.

D) Other Techniques Used

Other approaches to the fabrication of superhydrophobic surfaces have been developed and used, these include the template method [83], electro-hydrodynamics/electro-spinning [135], sublimation [136], polymer re-conformation [83], hydrothermal synthesis [137], layer-by-layer methods [138], electrochemical methods [83, 138], bottom-up approach for the fabrication of nano-arrays [83], one-pot reaction [139], and wax solidification [125].

2.8.4 Self-Assembled Monolayer of Organosilanes

SAMs of organosilanes were first introduced by Sagiv [140], who took advantage of the hydrophobicity of the organosilane alkyl chain, and used them to modify surfaces bearing hydroxyl groups, such as silicon wafers, glass slides, silicon nanoparticles, and zeolite to create low-surface-energy coatings [83, 141]. For example, it was shown that after modification of a

rose-like surface using octyltrimethoxysilane, the surface wetting is susceptible to a remarkable change going from super-hydrophilicity to superhydrophobicity with a contact angle as high as 154° and a tilt angle of less than 3° [141]. In addition to alkyl silanes, perfluorinated silanes are also widely used to adjust surface wetting properties.

2.8.5 Self-Assembled Monolayer of Fatty Acids

Fatty acids are among important group of modifiers used to obtain low-surface-energy coatings in the fabrication of superhydrophobic surfaces. Zhou *et al.* used lauric acid to modify the surface of brucite-type cobalt hydroxide, and obtained a superhydrophobic surface [142]. By modifying copper surfaces with fatty acids bearing different lengths of the alkyl chain, surface wetting ability with different contact angles can be obtained [143].

2.8.6 Low-Surface-Energy Modification of Rough Surfaces

In general, two main approaches have been developed to generate superhydrophobic surfaces. One is to increase the surface roughness of low-surface-energy materials directly, as described above. The other is to fabricate a suitable surface roughness using certain materials and then to modify the as-prepared surface with low-surface-energy materials. The latter method is no longer limited to low-surface-energy materials but it can extend the formation of superhydrophobic surfaces to many systems. To date, various low-surface-energy coatings have been developed to modify organic and inorganic rough surfaces to fabricate superhydrophobic surfaces.

There are other approaches and techniques which are used broadly to generate superhydrophobic surfaces, for instance, surface modification with aromatic azides, SAM of alkanethiols, spin-coating perfluorononane, and so forth [17, 83, 137, 138].

CHAPTER 3

ALUMINIUM ALALLOYS AND THEIR CORROSION

3.1 Aluminium and Aluminium Alloys

Reduced ice accumulation on surfaces, especially in the case of metallic surfaces such as Al alloys, is always accompanied by corrosion, which is an unavoidably serious issue when it comes to the outdoor use. Corrosion is defined by the breaking down of fundamental properties in a material due to chemical reactions with its surroundings. Most structural alloys corrode only from exposure to moisture in the air. Since all modern Al alloys use other metal additives to improve the strength of the material, these metal additives precipitate during solidification processes and create second-phase paricles in the Al matrix. This couple, composed of the Al matrix and second-phase particles, inevitably leads to increased unsustainability to the electrochemical corrosion, or galvanic corrosion, of such alloys, especially of those in close contact with water. Galvanic corrosion is an electrochemical process which occurs when two different metals come into electricall contact with each other and are immersed in an electrolyte. As a result, a galvanic couple gets set where the more active metal corrodes at an accelerated rate and the more noble metal corrodes at a reduced rate. Corrosion may be observed to concentrate locally in the form of pits or cracks on the surfaces. Thus, anticorrosive performance becomes a significant issue in-the durability and stability of the coating. Aluminium is noteworthy for its ability to resist corrosion due to the fact that its surface oxide layer (Al_xO_y) forms in air. The corrosion resistance of this metal may be considered excellent due to the presence of a thin surface layer of Al oxide (Al_xO_y) which forms when the metal is exposed to air, thereby

effectively preventing further oxidation. Worldwide, Al is the most frequently used non-ferrous metal, known for its good thermal and electrical conductivity; by weight this element is better than copper which is able to use as a superconductor. Pure aluminium has low tensile strength, but when combined with thermo-mechanical processing to produce Al alloys, it displays a marked improvement in mechanical properties, especially when tempered. Aluminium alloys often contain copper, zinc, manganese, silicon, and magnesium. These alloys are much lighter and more corrosion resistant than plain carbon steel, but not quite so resistant as pure aluminium. Based on the additives used Al alloys may be grouped into different categories (AA2024, AA6061, etc.), each of which has specific properties and a basic grade or 'type'. Some of the most common alloys, together with their chemical composition are listed below in Table.3.1. The strongest Al alloys are less corrosion resistant due to galvanic reactions with alloyed copper or zinc. An Al alloy used extensively to manufacture aircraft is Al 2024-T3; the T3 temper indicates that the stock was solution heat-treated, cold-worked, and naturally aged. The composition of this alloy makes it noticeably prone to corrosion processes. Typically, environmental factors such as moisture and electrolytes are capable of penetrating through the polymer coating layer to form an electrochemical galvanic cell with the Al- and Cu-rich inclusions, resulting in the corrosion of the Al alloy. The propagation of this corrosion makes the metal substrate increasingly vulnerable to the corrosion process [144]. Since second-phase intermetallic particles including copper, zinc, and manganese, having more negative corrosion potential than Al, always precipitate during solidification in Al alloys, the accelerated galvanic corrosion is triggered at this point. Four practical conditions, reported in the relevant literature [159], must be met in order to generate corrosion, especially filiform corrosion; (i) a high relative humidity of 60% to 80% RH, (ii) the presence of halide ions at the coating-substrate interface, (iii) the presence of defects in the coating, and (iv) the permeability of the coating to water and oxygen. The presence of a surface oxide film (Al_xO_y) explains why the surface is resistant to further oxidation and causes the surface to be "passive" or corrosion resistant. It was found that in AA2024, approximately 60%

of second-phase particles greater than about 0.5 to 0.7 μm were Al_2CuMg, namely the S phase. This fraction corresponds to 2.7% of the total alloy surface area which are a reason for localized corrosion [159]. The S phase particles in the AA2024 appeared to be active with respect to the matrix phase; this is consistent with the open-circuit potentials reported in the literature for Al_2CuMg which resulted in severe de-alloying thereby leading to the formation of Cu-rich particle remnants.

Table 3.1. Chemical composition (wt. %) of several typical Al alloys based on different reports. Other elements were also detected at lower levels [145-158].

Alloy	Cu	Mg	Si	Mn	Cr	Zn	Fe	Ti
AA2024-T3	3.8-4.9	1.2-1.8	0.5	0.3-0.9	0.1	0.25	0.5	0.15
	3.8-4.9	1.2-1.8	0.5	0.3-0.9	-	0.3	0.5	0.15
	3.8-4.9	1.2-1.8	0.5	0.3-0.9	0.1	0.25	0.5	0.05
	4.4	1.5	0.5	0.6	-	-	<0.5	-
	4.47	1.42	0.07	0.61	<0.01	0.11	0.16	0.03
AA7075-T6	1.4	1.1	1.0	-	0.2	5.9	-	-
	1.6	2.5	-	-	0.23	5.6	-	-
	1.78	2.91	0.03	0.02	0.21	5.6	0.25	0.04
AA6061-T6	0.2-0.6	0.5-0.9	0.5-0.9	0.2	-	-	-	-
	0.35	0.95	0.5	0.15	0.15	0.25	0.7	0.15
	0.3	1.0	0.6	<0.15	0.2		<0.7	<0.15
	0.2	1.4	0.6	0.1	0.2	0.03	0.09	0.02
AA3003-H14	0.05-0.2	0.05	0.6	1.0-1.5	0.05	0.1	0.7	0.05
	0.5	-	0.6	1.2	-	0.1	0.7	-
	0.12	0.017	0.18	1.05	0.002	0.012	0.52	0.009
AA2014-T6	3.9-5.0	0.2-0.8	0.5-1.2	0.4-1.2	<0.1	-	<0.7	-
AA6082-T6	0.1	0.6-1.2	0.7-1.3	0.4-1.0	0.25	0.2	0.5	0.1

A number of particle remnants remained largely intact and induced pitting on their periphery once ennobled through de-alloying. Other particle remnants decomposed into 10 to 100 nm Cu clusters which became detached from the alloy surface and were dispersed through the mechanical action of increasing corrosion products or solution movement. It should be noted that heterogeneous microstructures are intentionally developed in commercial Al alloys to optimize

mechanical properties. Microstructural heterogeneity also arises as a result of impurities which have been involuntarily introduced during melt processing that such microstructures make Al alloys susceptible to localized corrosion. The inhomogeneous concentration of Cu in second-phase particles and the local depletion of Cu in certain micro-structural regions establish local galvanic cells resulting in a form of localized attack, *e.g.* Al_6Mn type [159]. Results obtained from electron dispersive spectroscopy (EDS) show that the most heavily populated category of second-phase intermetallic particles contain Al, Cu, and Mg exclusively, although the analysis was unable to distinguish conclusively between Al_2CuMg, AlCuMg, $Al_5Mg_2Cu_5$, and Al_6Mg_4Cu chemical types. Electron probe microchemical analysis showed that particles displayed 44 to 46% (by weight) Cu and 14 to 16% Mg as expected for this phase [159]. The θ phase formation takes place during solidification or solution heat treatment. The size of the θ phase category, Al_2C, is greater than 4 μm [159]. The most significant characterization result is that Al_2CuMg was found to be the most predominant type of particle observed in the AA2024-T3. The composition of the Al-Cu-Fe-Mn particles is believed to be Al_6 (Cu,Fe,Mn). These types of particles are typically small in size, as a rule ≤ 4 μm, and regular in shape, whereas the latter are irregularly shaped and coarse usually ≥ 10 μm [160]. Energy Dispersive Spectroscopy indicates that the ratio of Al to the sum of the Cu, the Fe, and the Mn was regularly 6 to 1 on an atomic percentage basis and the average Cu: Fe: Mn ratio was 2:1:1 varying little from particle to particle [159]. Particles of both types impair the resistance of the AA2024 to electrochemical corrosion [160]. The elements of Al-Cu-Fe and Al-Cu-Mn were detected in the third and fourth categories, respectively. These two categories were assigned the Al_7Fe_2Cu and $(Al, Cu)_6$ Mn chemical types which are stable compounds in alloys of this type. Neither phase was detected by EPMA or X-ray diffraction (XRD) techniques [159].

3.2 Corrosion of Al Alloys and Local Dissolution Phenomena

3.2.1 Historical Introduction

The verb "*corrode*" is derived from the Latin word "*rodere*" which means "*to gnaw*". This word entered the French language in 1314 to designate the action of gnawing, progressively wearing away by a chemical effect. The noun "corrosion" was derived at the beginning of the 19th century from the Lower Latin *"corrosio"*, which designated the act of gnawing [161]. The phenomenon of corrosion has been known ever since the discovery of metals. However, the first reported corrosion experiments on Al started around 1890, when the metal was available in sufficient quantities to envision its use in the constructions. The resistance of Al to rainwater and various types of beverage was first assessed at the beginning of the 1890s [161]. As defined earlier, corrosion in metals is caused by an electrochemical reaction between a metal and its surroundings that proceeds according to a complex electrochemical process which is related to the atomic structure of matter. In metals, the electrical environment of atoms is made up of free electrons capable of moving throughout the metal. In the aqueous phase, which is a solution, the following species may be found: positive ions (cations), negative ions (anions) and neutral molecules such as water and various undissociated compounds. At the interface between metal and water, the transfer of electrical charges leads to electrochemical reactions. The fundamental reactions of the corrosion of Al in an aqueous medium have been the subject of a number of studies [162, 163]. In simplified terms, the oxidation of Al in water proceeds according to the equation $Al \rightarrow Al^{+3} + 3e^{-}$. Metallic Al, in oxidation state 0, goes into solution as trivalent cation Al^{+3} upon losing three electrons. In a common aqueous medium having a pH close to neutral, *e.g.* water or moisture, only two reduction reactions can occur; the thermodynamic considerations involved are the reduction of H^{+} protons and the reduction of the oxygen dissolved in water. Aluminium corrosion results in the formation of Al hydroxide, $Al(OH)_3$, which is insoluble in water and precipitates as a white gel observed in corrosion pits as white gelatinous flakes. The

corrosion of Al, however, is the sum of two electrochemical reactions, namely, oxidation and reduction:

$$Al \rightarrow Al^{+3} + 3e^{-} \quad \text{(oxidation)} \quad \textbf{(1)}$$
$$3H^{+} + + 3e^{-} \rightarrow 3/2\ H_2 \quad \text{(reduction)} \quad \textbf{(2)}$$
$$Al + 3H^{+} \rightarrow Al^{+3} + 3/2\ H_2 \quad \textbf{(3)}$$

or

$$Al + 3H_2O \rightarrow Al(OH)_3 + 3/2\ H_2 \quad \textbf{(4)}$$

As it was explained before, that approximately 60% of second-phase particles were Al_2CuMg, or the S phase, which corresponds to 2.7% of the total alloy surface area liable to cause localized corrosion [159]. The polarity of the local S phase-Al galvanic couples determines whether particles were selectively dissolved or whether the matrix pitting found on the particle periphery was induced. Buchheit *et al* [159] explained that the S phase is active and that S phase particles show either significant peripheral pitting or apparently selective dissolution. X-ray investigations showed a strong Cu signal at S phase particle sites, but a Mg signal that is weaker than the Mg signal from the matrix phase. Since the S phase particles originally contained 17% Mg and the matrix phase originally contained 1.5% Mg, strong selective Mg dissolution from particles on the corroded surface is indicated. Aluminium, together with Mg, is selectively dissolved from S phase particles leaving behind Cu-rich remnants [159]. The result reveals a porous sponge-like structure in the particle remnant as might be expected from a de-alloying process based upon which it may be deduced that this porous structure is comprised predominantly of metallic Cu. Although de-alloying S phase particles produces two types of pit morphology, there appear to be no obvious metallurgical or microstructural factors influencing whether it is peripheral matrix pitting or selective particle dissolution which occurs. A maximum in the total pit density and in the density of pitting due to selectively dissolved particles was observed at pH 4.2. This pH is close to the solubility minimum for Al which occurs at

approximately pH 5. The density of the pits formed on the S phase particle periphery was observed to be independent of the solution pH, although the ratio of peripheral pitting to selective dissolution pitting clearly varies with the pH level. De-alloying S phase inclusions can produce Cu particles which are no longer attached to the metal surface. These Cu particles may remain mobile under the influence of local mechanical action due to moving solution or corrosion products [159].

3.2.2 Types of Corrosion on Aluminium Alloys

Different types of corrosion, more or less visible to the naked eye, can occur on Al. The predominant type of corrosion will depend on a certain number of factors which are intrinsic to the metal, the medium, and the conditions of use. There is, however, no form of corrosion which may be considered specific to Al and its alloys. Certain types of corrosion occurring on Al alloy surfaces can be classified among others as galvanic corrosion, uniform corrosion, pitting corrosion, trans-granular and inter-granular corrosion, exfoliation corrosion, stress corrosion, filiform corrosion and so forth each having its own characteristics and conditions. For instance, galvanic corrosion has appeared ever since two different metals were first placed together in a liquid medium, that is to say, since the Iron Age. From its ranking on the scale of potentials shown on the electro potentials table, Al is more electronegative than most common metal elements including Fe (steel, stainless steel), and Cu (cuprous alloys). When two dissimilar metals are in direct contact with each other in a conducting liquid, experience shows that one of the two may corrode through a process of galvanic corrosion. The second metal will not corrode; it may even be protected under these conditions. Unlike other types of structural corrosion, galvanic corrosion does not depend on the texture of the metal, or on its temper. Galvanic corrosion may occur with any metal, as soon as two of them are in contact in a conductive liquid. It works like a battery built out of two electrodes, namely the cathode, where reduction takes

place, and the anode, where oxidation takes place. These two electrodes are plunged into a conductive liquid called an electrolyte, which is normally a diluted acid solution, or a salt solution or even moisture extracted from the environment. The appearance of galvanic corrosion is characteristic; it is not dispersed like pitting corrosion, but highly localized in the contact zone with the other metal. This affected zone often has a shinier aspect than the rest of the surface. All types of Al alloys undergo identical forms of galvanic corrosion which is based on the same principle, in which the following three conditions must be met simultaneously, the presence of at least two different types of metal, the presence of an electrolyte, and electrical continuity between the two metals.

3.3 Anticorrosive Action *via* Long Aliphatic Chain Silanes

Besides the utilization of cerium salts and Zirconates, a persistent protective action against Al corrosion can be obtained by applying treatments having silane molecules containing a long aliphatic chain, as for example, n-octadecyl-trimethoxy-silane, or ODTMS, which can increase the barrier properties of the silanic coating significantly [164]. The use of hexavalent chromium for the surface treatment of metals has a long history. Both for environmental reasons and for worker safety concerns, however, the replacement of this hexavalent chromium treatment became a major priority and research activities increased to develop alternative non-toxic treatment processes. At variance with other silanic compounds, the layers of ODTMS, as well as that of OTMS, although not uniform, tend to cover the entire Al surface. Such coatings are characterized by minute defects, as found in the case of self-assembled-monolayers (*SAMs*) on various metal substrates [164]. The flexible long hydrocarbon chains, however, can contribute to the healing of small sized defects. There are examples of SAM application to the surface of a hydroxylated polymer or to hydrophilic metal oxide surfaces [12]. The complex surface chemistry of metal alloys is certain to have a certain number of significant effects on the self-assembling process and

the properties of the resulting thin films [144]. Self-assembled monolayers, often made from amphiphilic hydrocarbon molecules, are expected to function as a barrier against the permeation of corrosion accelerants such as moisture and electrolytes into the metal substrate, thereby improving the corrosion resistance of the substrate materials [144]. The presence of a sufficiently long aliphatic chain in the base silane molecule affords satisfactory and continuous protective properties to the coating. The *Lifshitz-van der Waals* interactions between long alkyl chains of ODTMS favor the formation of dense and ordered protective layers which may even include a poly-molecular layer. The formation of oxane bonds, Al-O-Si, through the interaction of the silanol groups of silane compounds with the hydroxylated metal oxide surface, namely surface condensation, improves the protective performance of the native Al oxide film [164]. An ODTMS film tends to hinder both the cathodic oxygen reduction and the anodic oxidation of Al to a limited extent [164]. In the absence of the alkaline treatment of the Al surface, the anodic reaction is not at all affected since the formation of the hydrogen-bonded silane layer or the surface condensation process was not able to proceed through lack of a suitable hydroxylated surface. With the aging process, however, the inhibiting action exerted by the silane film is enhanced and the most interesting results are produced [164]. In ref. [164] the authors clearly showed that the longer the aliphatic chain of the alkyl–silyl derivatives, namely the OTMS and the ODTMS, the most hindered the cathodic reaction. The protective effects for the propyl derivative C_3 were poor, for OTMS they were fair, and marked for ODTMS. While all silanic layers inhibit the cathodic reaction, only ODTMS succeeds in inhibiting the anodic reaction, even in the presence of chlorides [164]. The thickness of an ODTMS coating, which is a multilayered structure of around 160 Å, was much greater than that of OTMS which is possibly a monolayer of around 5 Å, accounting for the impaired protectiveness and higher permeability of the latter. The aqueous salt solutions may permeate through this layer, but with greater difficulty than in the other cases mentioned. On the other hand, the contact angles of the panels modified by ODTMS [$H_{37}C_{18}Si(OMe)_3$] and OTMS [$H_{17}C_8Si(OMe)_3$] are ~108° which corresponds well with the results

of previously reported work by Maege *et al.* on octadecyltrimethoxysilane [144]. In contrast to the above silane-modified samples, the contact angle of a $C_{18}SiMe_2Cl$-modified Al surface is extremely small (~40°). This small CA value suggests the presence of a much more hydrophilic surface than even the unmodified Al panels in view of the fact that the $H_{37}C_{18}SiMe_2Cl$ molecules formed a monolayer film with alkyl chains anchored onto the Al substrate, with the functional moieties oriented towards the solution phase which displays an opposite molecular orientation. The hydrolysis of the –Si–Cl bond leads to the formation of the –Si– OH bond, a fairly hydrophilic functional group. Because these polar groups are oriented away from the surface, the Al panel becomes more hydrophilic compared to the unmodified panels thereby causing greater penetration of water molecules into the surfaces leading to accelerated corrosion. Three categories of molecules are commonly used for self-assembled monolayers; these include fatty acids with carboxylic end groups forming electrostatic interactions with metal substrates, alkylthiols that link to the steel substrate through iron-sulfur bonding, and alkylsilanes that react with the metal oxide from the metal and metal alloy substrates [144]. The fatty acids and the phosphonic acid tend to bond with Al_2O_3 from the Al substrates through electrostatic interactions, while the long alkyl chains interact together by means of van der Waals interactions to form the stable monolayer films. For alkylsilanes, a two-dimensional hydrolysis-condensation reaction occurs between the silane and Al_2O_3 from the Al substrate, leading to a polymerized monolayer film, as illustrated in Figure 3.1. The metal alloy surface becomes much more hydrophobic due to film formation, while the corrosion resistance of the substrate was found to increase significantly. The surface properties of metal alloys are often affected by surface cleaning and the treatment protocols applied, as is the molecular self-assembling process on the metal alloy surface [144]. When they are dissolved in water, certain silane compounds may form superficial protective layers on Al and other metals by a simple dipping treatment, followed by a proper thermal curing cycle. Siloxane-anchored SAMs began attracting interest as surface modifiers as a result of the work of Sagiv in the early 1980s [165].

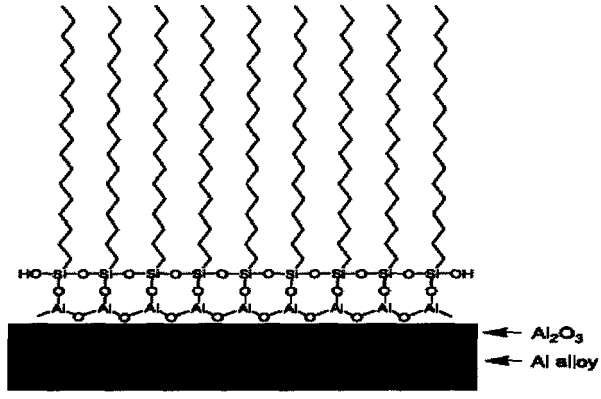

Figure 3.1. Self-assembled monolayer film of alkylsilane molecules on Al alloy substrate.

Bis-silanes are particularly reticulation stages which are susceptible to augmenting the hydrophobic properties of these coatings [166]. It was found that 1,2-bis-trioxymethyl-silyl-ethane *(BTSE)* can be used as an efficient corrosion inhibitor because of the presence of a long alkyl chain in their molecular structure, *e.g.* by using methoxysilanes in the prevention of the atmospheric corrosion of iron [166]. The thickness of the *BTSE* thin film deposited on Al surfaces was investigated using spectroscopic ellipsometry which is 250 to1700 nm [167]. This improvement is related to an increase in layer thickness, creating a noticeable obstacle to the penetration of the aggressive aqueous solutions; this type of layer covers the Al surfaces completely, although not uniformly. Organofunctional silanes are hybrid organic-inorganic compounds which can be used as coupling agents across the organic-inorganic interface [164]. The most commonly-used silane coupling agents have the structure $X_3Si(CH_2)_nY$, where X represents a hydrolysable group such as methoxy or ethoxy species, and Y an organofunctional group such as chlorine, amine, epoxy or mercapto. Non-functional silanes or di-silyl derivatives bear a close resemblance to functional silanes in structure, except for the fact that they have hydrolysable Si-O-C bonds on both ends of the carbon chain in the form of cross-linking agents. A further cross-linking step may lead to the formation of Si-O-Si siloxane bonds which increase the protective action of these coatings [164]. As proposed by Plueddemann [167], organofunctional silanes can bond with the metallic surface via the formation of oxane bonds

induced by the interaction of silanol groups with the metal oxide surface. This reaction may be expressed by the general equation:

$$\text{Me-O-Si-R} + H_2O \rightarrow \text{Me-OH} + \text{HO-Si-R} \qquad \textbf{(5)}$$

It should be noted that the immersion of Al alone in a hydro-alcoholic silane solution is not sufficient for the production of particularly effective systems, since an aging and curing process is required besides a hydroxylated surface. Tetraethyl orthosilicate, shown in Figure 3.2, is another organosilane molecule which can be used to modify the Al surface as an underlayer. Such an "*anchoring layer*" can be then covered with a SAM-forming silane, forming a thicker and denser coating comprising two layers. Tetraethyl orthosilicate is a tetrahedral compound having the formula ($C_8H_{20}O_4Si$) often abbreviated to TEOS.

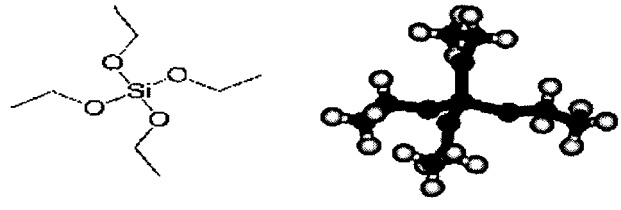

Figure 3.2. TEOS molecule and its spatial configuration.

This molecule consists of four ethyl groups attached to a SiO_4^{4-} ion. Tetraethyl orthosilicate (TEOS) is used mainly as a cross-linking agent in silicone polymers. This application exploits the reactivity of the Si-OR bonds. It may be hypothesized that a multilayered system can be obtained through repeated sequences of *Lifshitz-van der Waals* interactions between the long octadecyl chains of molecules displaying the opposite orientation; or else obtained through the condensation between facing silanol groups. This multilayered film formation on Al alloys has been reported by Wang *et al.* [168], it is possible to form a poorly-bonded, easily penetrable, thick outermost silane layer forming at variance with the strongly-bonded innermost protective layer.

3.4 Alkanoic Acid Layers on Al_2O_3 Surfaces

A molecule known to be structurally related to octadecylsilane is stearic acid. The carbon backbone of stearic acid [CH_3 $(CH_2)_{16}COOH$, SA] has the same number of carbon atoms as ODTMS and octadecyltrichlorosilane [CH_3 $(CH_2)_{17}SiCl_3$] (*OTS*), which is an amphiphilic molecule consisting of a long-chain alkyl group ($C_{18}H_{37}$-) and a polar head group ($SiCl_3$-), which forms SAMs on various oxidic substrates. Previous studies show that the films formed by self-assembly of stearic acid (SA) tend to be well-ordered, while the alkyl chains extend away from the Al_2O_3 surface. The Al oxide layer is highly adsorbed to contaminants from the ambient environment, thereby affecting the adsorption kinetics of the alkanoic acids significantly [169]. These results suggest that surface defects and/or monolayer defects may play an important role in the adsorption process and completion of film formation, the poor quality of which can be verified by Raman spectroscopy. Observations indicate that alkanoic acids adsorb to Al_2O_3 surfaces at Lewis acid sites through a single oxygen atom tilted 10° off true perpendicular. Alkanoic acids, however, adsorb to Ag surfaces through both oxygen atoms as a carboxylate *via* a delocalized double bond which may reduce the *Lifshitz-van der Waals* interactions of the alkyl chains and create a slightly less-ordered film with the alkyl chain extending away from the surface along the surface normal. These orientations are shown schematically in Figure 3.3.

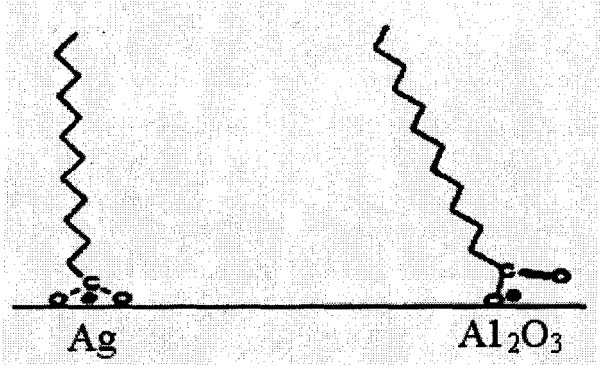

Figure 3.3. Schematic diagram of the stearic acid adsorption to a smooth Ag and Al_2O_3 surfaces.

3.5 Chromate and Permanganate Conversion Coatings

The term "*conversion coating*" *(CC),* as used in the metal finishing industry, refers to the conversion of a metal surface into a surface which will more easily accept applied coatings, thereby offering corrosion resistance in the event that the secondary coating is breached. These coatings are relatively thin, not over 600 nm, easily and rapidly formed on Al. To date, the most successful CC systems used on Al are based on hexavalent chromium, generally known as chromate and used as a "yardstick" system [170]. A cold applied version of CC, which reacts in a few seconds, has been available for the processing of large scale items, such as aircraft for several decades. It is now well-documented that such behavior is provided by chromate conversion coatings *(CCCs),* which contain a certain amount of chromate anions capable of migrating to local sites of mechanical damage and oxidizing them, thereby restoring the corrosion protection factor involving active corrosion protection [160]. The CCC provides ideal alloy protection against pitting and filiform corrosion on AA [172]. Such processes were also observed in vanadate and cerium-oxide based conversion coatings [160]. Since Cr (VI) compounds are carcinogenic, many attempts have been concentrated over the years on producing chromate-free systems in order to replace chromates and related coatings gradually in large-scale applications [170, 171]. Few researches have been made to duplicate the coating formed by chromate-based CC systems using a trivalent chromium system which is non-toxic, unlike those based on Cr (VI) [170]. In the presence of Al, the hexavalent chromium is reduced to various trivalent chromium compounds which are not carcinogeneous forming a soft gel-like mixture which, when dry, initially has an open porous structure easily accepting applied organic coatings. After eight hours, these coatings lose their open porous structure due to the formation of inorganic coating; it is this polymer which is primarily responsible for the excellent corrosion resistance shown by these CC systems [170].

One alternative approach is to produce coatings by oxidizing Al with the permanganate anion, followed by Mn (IV) deposition. Permanganates, which have long been used to purify drinking water, are attractive for large-scale applications, in contrast to Cr (VI) compounds which may be used as a safe alternative to CCCs; they can be successfully used to protect Al alloys [160]. There is a certain amount of similarity between the physical and chemical characteristics of Cr (VI) compounds and MnO_4^- compounds based on the rule in the periodic table of elements. Moreover, permanganate conversion coatings *(PCCs)* provide the advantage of higher thermal stability [160]. Thus, as in the case of chromates, the permanganate-generated conversion coating system contains a mixture of manganese in place of the chromium and Al_xO_y. The corrosion characteristics of the permanganate-based system are identical with those of the chromate-based system with the exception of alloys (containing high levels of) copper or zinc) as in the aircraft alloys 2024 and 7075. These systems are deemed environmentally-friendly since they will not generate water soluble manganese compounds under normal conditions in the absence of any strong reduction agents [170]. The primary function of a CC is to provide for a corrosion resistant surface as insurance against failures in the secondary coating while at the same time providing for excellent organic adhesion characteristics [170]. There are several reports that, at high pH values, Mn is capable of inhibiting the corrosion of Al-based alloys which is probably due to the fact that the reduction of Mn (VII) in an alkaline medium typically leads to the formation of MnO_2, confirmed by IR spectroscopy, as a less soluble species [160]. The recommended range of process temperatures is 38–82°C, while the solution pH must lie between 9 and 10 [160]. At lower temperatures, the process requires a longer time, up to 60 min at room temperature, whereas at 68°C a coating can form itself in 1 min [160]. To apply high-quality corrosion-resistant coatings to Cu- or Zn-rich alloys, treatment in a silicate solution is necessary to block the process inducing defects and cracks in the coating [170]. The trivalent chromium pre-treatment followed by a $KMnO_4$ post-oxidation on aluminium alloy contributes good pitting corrosion resistance which is probably due to the presence of Cr (VI) in the post-treated film. Drying these

pre and post-treated Al samples provides good filiform corrosion protection, as shown in Figure 3.4. [172].

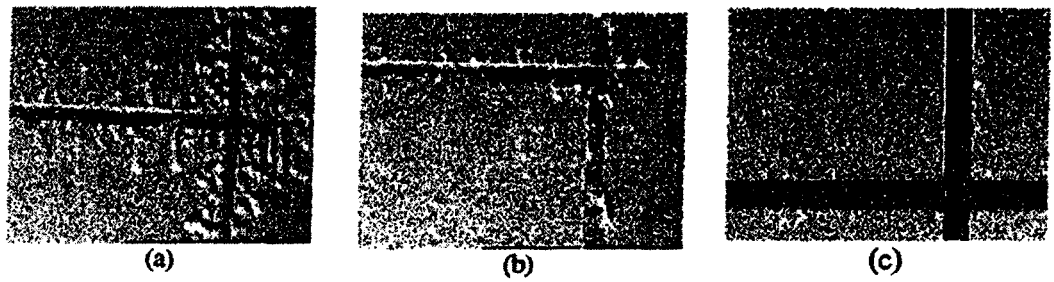

Figure 3.4. Results of filiform corrosion tests performed on trivalent chromium (pre-treated) and $KMnO_4$ post-oxidized Al samples without drying (a), with drying (b), and chromated samples (c).

The thickness of the PCC and the Al_2O_3 layer remain on the AA substrate exceeds ~ 5–10 nm at permanganate treatment times longer than 5 min. The coatings on most of the Al-Cu-Fe-Mn particles display cracks, which developed during drying due to large thickness of the PCC. It appears that the development of cracks in the coatings on larger particles containing Fe and Mn is associated with their large size and irregular shape. Another type of defect was also observed, namely cracks along the perimeter of certain particles which is probably due either to the difference in thickness between the coatings on the particle and the surrounding alloy matrix or to the fact that, during electrochemical deposition of PCCs, the matrix adjacent to a particle dissolves more rapidly. The Mn content of the coatings on the intermetallic particles far exceeds that to be found on the matrix. As may be seen in Figures 3.5(c) and 3.5(d), most defects in the PCC are concentrated in the vicinity of large intermetallic particles. These defects are cracks in the thick coatings on the irregularly shaped Al-Cu-Fe-Mn particles, as shown in Figure 3.5(c); they may also be seen as peripheral cracks at the particle-matrix interfaces, occurring more commonly in the vicinity of large Al-Cu-Mg particles, as shown in Figure 3.5(d). Both types of crack seem to develop during the period of time covered by the drying of the coatings. The PCC on the surface of the major phase of the alloy, as shown in Figure 3.5(b), is fairly uniform in morphology and displays no well-defined traces of defects or cracks; this fact concords well with

the lesser thickness of the PCC in this region. It is, therefore, reasonable to assume that it is the high cathodic activity of second-phase particles in AA2024, containing, a more noble element compared to Al, namely Cu, which is responsible for the formation of the defects in question [160].

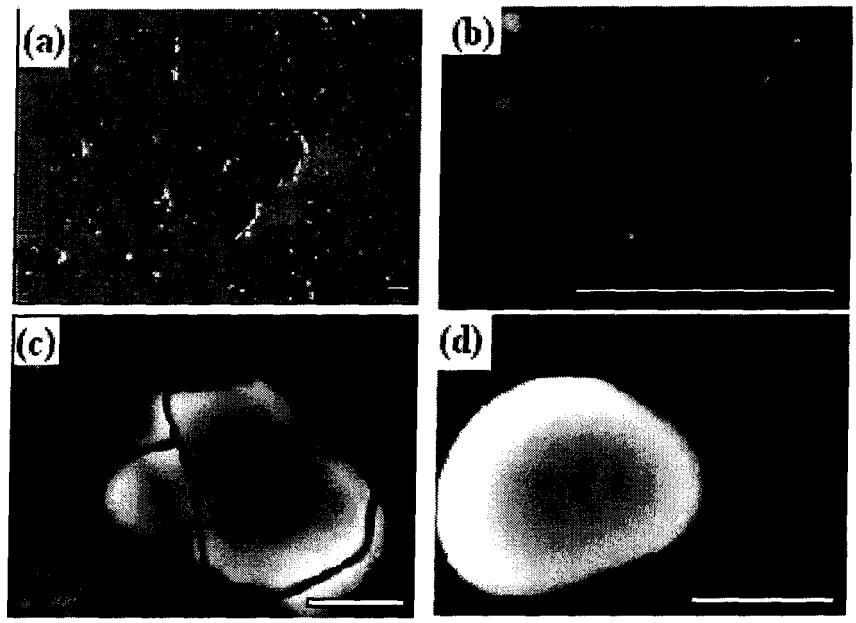

Figure 3.5. SEM images of permanganate treated AA2024 surfaces; (a) after 20 min when particles are covered and PCC have just appeared on matrix; (b) Al matrix after 210 min; (c) Al-Cu-Fe-Mn particle after 210 min; (d) Al-Cu-Mg particle after 210 min. (Scale bars are 5 μm.)

Therefore, in this project, organic and inorganic anticorrosive coatings on Al alloy surfaces with due attention to review literature of this chapter have been prepared. Moreover, the combination of corrosion protection with ice repellent properties *via* the one layer or the multilayer approach, has involved considering under layers and upper layers. All these have been detailed in the relevant research objectives subchapter. Such coated Al surfaces were characterized and tested with the pertinent procedures as will be discussed in detail in the subsequent methodology section.

CHAPTER 4

EXPERIMENTAL FACILITIES AND TEST PROCEDURES

4.1 Introduction

On the basis of the specialized literature pertaining to ice adhesion, testing, and experience with countermeasures as well as in order to achieve the objectives listed, a set of experiments was systematically carried out on the icephobic and hydrophobic properties of prepared coated Al surfaces, evaluated together with their stability in contact with water. The objective of this chapter is to introduce and discuss in detail the methods used and the instruments involved in the study for preparing and characterizing the assembled low-surface energy and anticorrosive thin films on AA surfaces using the available facilities. The preparation of the coating, the morphology, and their performance were also analyzed by applying a set of surface analysis and characterization techniques which are explained in this current chapter. This chapter consists of two separate sub-chapters; sample preparation procedures and sample characterization including facilities description and their principles along with corresponding explanations.

4.2 Experimental Procedures

4.2.1 Sample Pre-Treatment (Polishing and Cleaning Protocol)

The as-received AA6061-T6 (Al 97.9 wt.%, Mg 1.0 wt.%, Si 0.60 wt.%, Cu 0.28 wt.%, Cr 0.20 wt.%) and AA2024-T3 (Al 93.50 wt.%, Mg 1.40 wt.%, Si 0.50 wt.%, Cu 4.10 wt.%, Cr 0.10 wt.%, Mn 0.40 wt.%) AA panels from industrial rolled sheets were cut into smaller plates

with dimensions of 1×1 and 5.1 × 3.2 cm^2 which were used as substrates. The thickness of the plates used here was ~2.5 mm. Prior to coating, they were mechanically polished first using 600-grit sand paper, then successively finer SiC abrasive papers lubricated with water, and finally aqueous 1.0 μm alumina slurry to obtain mirror-polished surfaces. All of the larger Al substrates had two holes on one side to connect to an icing test beam. The polished Al plates were then cleaned and degreased ultrasonically in organic solvents; that is to say, in acetone (99.5%, EMD), methanol (99.8%, MAT) and iso-propanol (99.8%) consequently, each for 5-10 min followed by cleaning in a Turco Redoline 53D alkaline solution. The freshly cleaned Al_xO_y layer was created on the surfaces by easy reaction between the Al_xO_y layer on the Al surface and the Turco Redoline 53D alkaline solution OH-anions, obtained by soft etching, for the removal of an old Al_xO_y layer and to produce a fresh and reproducible one. The cleaned and polished Al plates were blow-dried in a N_2 gas flow and then placed in baths with different chemicals. Polished surfaces inspected by optical microscopy showed no evidence of particle-matrix pits or local corrosion. While the smaller samples were used to test the stability of the coatings in water, the larger ones were used to evaluate their ice-repellent performance.

A number of well-cleaned and unpolished Al panels were also etched in HCl (~14.8 wt%) to produce a roughened Al surface; this was followed by rinsing and washing ultrasonically in deionized water to remove any unstable or loose particles on the surface resulting from the etching process. The etched samples were dried in a N_2 flow and were dried in an oven at 70°C atmospheric air temperature and then subsequently placed in corresponding chemical baths. The deposition baths used in this study will be described in greater detail below.

4.2.2 Deposition Baths

A) Potassium Permanganate ($KMnO_4$) Solution

The deposition bath used in this study was 5 g/L (0.1 M) of $KMnO_4$ from Sigma-Aldrich + 0.05 M $Na_2B_4O_7.10\ H_2O$ in deionized water as a solvent. De-ionized water with a conductivity of

~0.32 μS/cm was prepared using a four-step filtration system from Millipore Corporation. A permanganate-based system produces a yellow-gold color coating which is almost equivalent to the color produced by the chromate-based system indicating that the CC has properly formed. A simple one-stage treatment in a proprietary preparation of permanganate solution at 70°C for 3-5 min will be sufficient for surface coating. It would be possible to extend the time involved while at the same time decreasing the temperature to diminish the potentially destructive results of high temperatures on a prepared (layer/coating). The above process produces a uniformly yellow-gold CC thereby preparing it for a further coating of a top layer of ODTMS. The corrosion protection is caused by the presence of a thin layer of MnO_2 and in the majority of cases, adhesion and corrosion protection proved to be excellent. It was demonstrated previously that AA6061 and AA2024 pre-treated with permanganate CC have no surface corrosion effects after 336 h exposure in 5% neutral salt spray [159]. A two-component solution including 0.1 M $KMnO_4$ and 0.05 M $Na_2B_4O_7.10\ H_2O$ with borax as a buffer reagent, was used to keep the solution pH constant at pH ~9 during coating deposition on AA surfaces. The composition of the solution was close to one of the formulations proposed by Bibber *et al.* [170]. The same $KMnO_4$ concentration was used earlier by Danilidis *et al.* on AA 6061 samples [154].

B) Octadecyltrimethoxysilane (ODTMS) Solutions

A 1% (v/v %) solution of as-received ODTMS, $C_{18}H_{37}Si(OCH_3)_3$, from Sigma-Aldrich, in methanol-water, namely 90% CH_3OH + 9% distilled water, was also prepared and used. The immersion time in deposition baths was 15 min for the ODTMS treatment. Another deposition bath of ODTMS 1% (v/v %) was also prepared in isopropanol-water to trace any effects of the solvent. Prior to use, the baths were vigorously stirred for 3 h to allow for dissolution and/or hydrolysis according to the following reaction (1):

$$\mathbf{R\text{-}Si(OMe)_3 + 3\ H_2O \rightarrow R\text{-}Si(OH)_3 + 3\ MeOH} \qquad \mathbf{(1)}$$

Several coatings based on stearic acid and alkylsilane were prepared on flat rough Al alloys. After sample coating and prior to tests, all the samples treated were removed from the solutions then rinsed with copious amounts of the relevant solvents and washed ultrasonically for 10-15 s in methanol and blow-dried with N_2. They were finally cured at 80°C in air for ~10 h to improve layer cross-linking with good barrier properties. Alkylsilanes covalently react with surface hydroxyl groups of the Al_xO_y surface forming Al-O-Si bonds while releasing H_2O as a by-product. The initial contact angles of the pre-prepared samples were measured immediately after organosilane-based deposition. These samples were used to investigate coating stability in water by means of CA measurements on samples immersed in deionized water for different periods of time, from 0 to 1200 h, subsequently evaluating their ice-repellent performance as well. Different ODTMS coating parameters and procedures are presented in Table 4.1.

Table.4.1 Experimental details of an Al alloy sample coated with octadecyltrimethoxysilane.

Sample	SO1	SO2	SO3	SO4	SO5	SO6	SO7	SO8	SO9	S10
Immersion time in ODTMS (min)	1	5	10	30	5	5	5	5	5	5
Alkaline treatment	+	+	+	+	+	-	-	-	+	+
Annealing (at ~ 100°C for 2 h)	+	+	+	+	+	+	+	-	+	-

C) Stearic Acid Chemical Bath Solution

A 5 mM stearic acid solution, $CH_3(CH_2)_{16}COOH$ obtained from Alfa Aesar, in 300 ml of methanol used as a solvent, was prepared. The as-prepared flat rough aluminium samples, with an oxide layer, Al_xO_y, coated at an oven temperature of 80°C with stearic acid (SA). The immersion time in deposition baths was 24 h for the stearic acid bath. Prior to use, the bath was magnetically stirred for 2 h to complete the dissolution and hydrolysis processes as much as possible. After coating the Al samples and prior to experiments, each sample was removed from the solution and rinsed with plentiful amounts of methanol, then rinsed ultrasonically for 10-15 s in methanol and blow-dried with N_2. They were finally cured at 80°C in air for ~10 h.

4.2.3 Other Passivation Baths Used

1) 1H,1H,2H,2H-Perfluorodecyltriethoxysilane Chemical Bath Solution (FAS-17)

As-prepared etched Al samples were immersed in diluted 10% (v/v) methanol of 1H,1H,2H,2H-perfluorodecyltriethoxysilane, $C_{16}H_{19}F_{17}O_3Si$, FAS-17 (see Figure.4.1) for 50 min to complete the self-assembly of a monolayer of FAS-17 molecules on the surface of samples. The coated samples were then blow-dried in N_2 and annealed in an oven for 2 h at 50°C prior to surface characterization. These coatings, constituted of a fluorine-containing organosilane compound, possess low surface energy providing enhanced hydrophobic properties. The contact angle as well as contact angle hysteresis of the prepared samples before and after each icing/de-icing cycle were measured. The stability of the coatings in water and their ice-repellent performance were also carefully investigated.

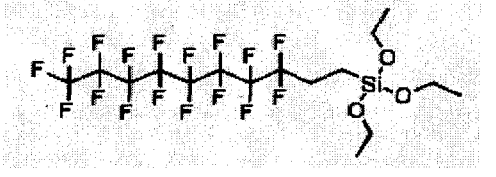

Figure 4.1. Molecular structure of FAS-17.

2) 1H,1H,2H,2H-Perfluorooctyltrichlorosilane Chemical Bath Deposition (FAS-13)

A number of etched Al samples were immersed in a diluted solution composed of 5 ml of 1H,1H,2H,2H-perfluoro-octyltrichlorosilane, namely $C_8H_4F_{13}Cl_3Si$ (FAS-13, see Figure.4.2) in 20 ml methanol for 50 min followed by drying in N_2 and annealing in an oven for 2 h at 50°C. The same investigations and experiments which were conducted for FAS-17 coatings were also carried out on FAS-13 coatings.

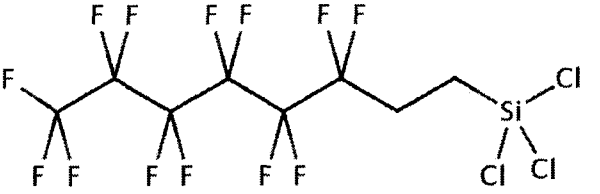

Figure 4.2. Molecular structure of FAS-13.

3) 1,2-Bis(Triethoxysilyl)ethane (BTSE) Chemical Bath Deposition

An additional chemical bath was prepared by mixing 4.7 ml of BTSE ($C_{14}H_{34}O_6Si_2$) in deionized water and methanol (MeOH) for 5 h at room temperature prior to use for silane deposition as an under layer. These conditions offer the best compromise between silane hydrolysis and condensation, leading to improved stability of the solution [19]. Polished and cleaned flat Al panels were dipped into the BTSE solution for different immersion times [166, 167] followed by blow-drying in an N_2 gas flow. The BTSE treated samples (series B) were then immersed into 1% (v/v %) ODTMS solution for different immersion times of 1, 5, 20, 60 min, and 5 hours. One sample was also immersed in a similar ODTMS solution for 20 min followed by washing ultrasonically in methanol for 15 s to monitor any effect of ultrasonication.

4) Tetraethyl Orthosilicate (TEOS) Chemical Bath Deposition

An additional chemical bath was set by using pure as-received tetraethyl orthosilicate (TEOS, $(CH_3CH_2–O)_4Si$, 98%). This chemical has the remarkable property of easily converting itself into silicon dioxide; the reaction occurs upon the addition of water according to the following equation (2):

$$\mathbf{Si(OC_2H_5)_4 + 2\ H_2O \rightarrow SiO_2 + 4\ C_2H_5OH} \qquad \mathbf{(2)}$$

This hydrolytic reaction is an example of a sol-gel process. The reaction proceeds through a series of condensation reactions that convert the TEOS molecule into a mineral-like solid *via* the

formation of Si-O-Si linkages. Flat cleaned Al samples were layered with a thin layer of SiO_x by soaking the samples in a undiluted TEOS bath for 20s followed by immersion in deionized water for hydrolysis to occur, so as to obtain a hydrated silicon under layer followed by drying with N_2. These Al samples were successively immersed in the TEOS bath to create further layers, namely from 2 to 5 layers, with the aim of investigating the effects of multi-layers on coating performance. This type of treatment involving organic silicate, the immersion in water, and drying in N_2 flow constitutes a cycle. After a number of cycles, all pre-treated samples were immersed in 1% (v/v %) ODTMS solution for different immersion times, similar to series B, and then annealed in an oven at 100°C for 6 hours. All samples were also annealed for a further 2 h at 80°C to assure all possible poly-condensation in the coatings.

4.3 Surface Analysis Tools

4.3.1 Morphological Analyses

A) Atomic Force Microscope

An atomic force microscope, (Veeco AFM E-scope) was used to study and characterize the surface morphologies, with the surface roughness of coated samples. The AFM images were gathered in tapping mode, with a silicon probe, Si, from Nanosensors™ administered at room temperature under normal air pressure. The three dimensional (3-D) topography of the surface was mapped *via* lightly tapping the surface with an oscillating silicon nitride probe and monitoring the changes in the cantilever oscillation amplitude while scanning the surface. This type of AFM probe has a typical tip radius of less than 10 nm and a length of 10 μm set on a cantilever of 220 μm length and 35 μm width, with a high mechanical Q-factor for high sensitivity and fast scanning ability.

B) Scanning Electron Microscope

A scanning electron microscope together with energy-dispersive X-ray spectroscopy (SEM/EDS) were used to investigate the morphologies of coated surfaces in the current study with their surface chemical composition; the data-sheet records accelerating voltages from 500 V to 25 kV for a Hitachi S 4700 Field Emission SEM. This SEM/EDS microscope provides high beam brightness and high resolution images in high magnifications. Flat samples were coated with a very thin film of platinum prior to imaging to prevent or diminish surface charging effects during the scanning. Scanning electron microscopy measurements provide a two dimensional image of the morphological features of the surface as well as the chemical composition of the material *via* energy dispersive X-ray analyses; SEM can image surfaces with a maximum degree of roughness. Normally, a 20 kV beam was used during scanning with magnifications of up to ×1000 k.

4.3.2 Wettability Tests

A) Contact Angle Measurement at Room Temperature

The contact angle measurements were performed on a fully automated contact angle goniometer, DSA 100 from Krüss GmbH Co. having a controllable volume of water drops which applies the sessile drop method of 4 μL and feed rate of 195 μl/min on the sample surfaces, as shown in Figure 4.3 (a). It is also possible to control injection volume and rate using the related software. A light source exists to illuminate the sample surface and a camera connected to a computer where the droplet shape can be analyzed.

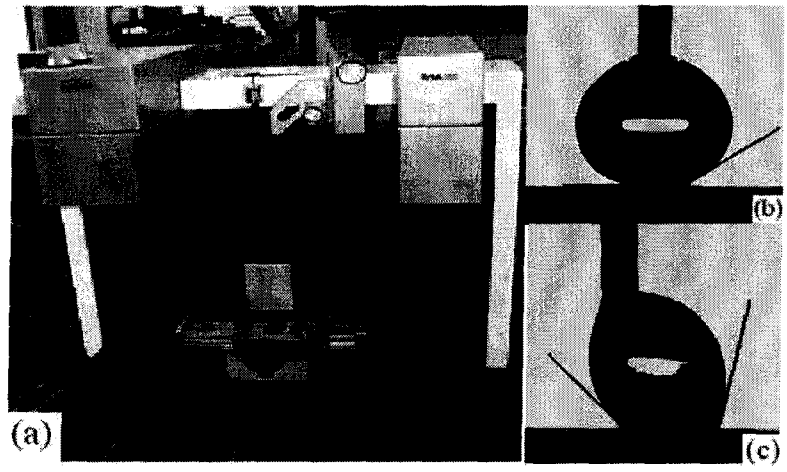

Figure 4.3. (a) contact angle goniometer (DSA100, Krüss) for contact angle measurements. The CAs measured: (b) static and (c) advancing (θ_A) and receding (θ_R) CAs.

The droplet shape was fitted according to the Young-Laplace method which is theoretically considered as the most accurate since the distorted droplet shape due to the liquid weight was first taken into account [5]. It is also possible to calculate the contact angles by curve fitting methods. As pointed out in a previous chapter, hydrophobic properties of a surface can be considered as a prior property leading to icephobicity. For each sample, CA measurements were made on at least seven different randomly selected spots on a horizontal surface and measured. The static contact angles in this study, as shown in Figure 4.3 (b), were measured by putting the symmetric water droplet containing a pre-measured preferred amount of water (4 μL) on a completely horizontal sample in a dark room in order to obtain the most accurate results. In the case of superhydrophobic surfaces, settling the water droplet on the surface should be carried out scrupulously to prevent the drop from rolling off. The contact angle hysteresis, the difference between the advancing (θ_A) and receding (θ_R) contact angles as shown in CAH, Figure 4.3 (c) were measured by applying a standard experimental approach to the asymmetric water drops using the tangent-2 method [173, 174]. A water droplet (4 μL) was injected from the syringe needle and brought into contact with the sample surface while still suspended from the needle. The droplet was maintained in contact with the sample surface with the stationary needle in it.

After that the advancing and receding contact angles were measured while moving the sample in one direction. This method allows measuring the advancing and receding contact angles and thus evaluating the value of CAH.

B) Ice Accretion Tests in a Wind Tunnel

Since the subzero tests need to be performed in a subzero environment, the samples to be investigated were placed in a wind tunnel to accumulate glaze ice at subzero temperatures in order to study how ice growth proceeds on prepared coated sample surfaces as discussed in the preceding chapters. The wind tunnel used was adjusted and maintained meticulously under conditions similar to those in nature which lead to glaze ice accretion during freezing rain, as shown in Figure 4.4. The effects of wind tunnel parameters which are controllable and adjustable, such as air speed, temperature, and liquid water content were also considered; the experimental conditions for these will later be explained. Briefly, the atmospheric icing wind tunnel used for these tests was based on room temperature water injection through three warm nozzles into a cold air stream provided by three nozzles on the spray line. The distance between the nozzles and the samples was chosen so as to be long enough to reach thermodynamic equilibrium for all the droplets sprayed into the wind tunnel [176-180].

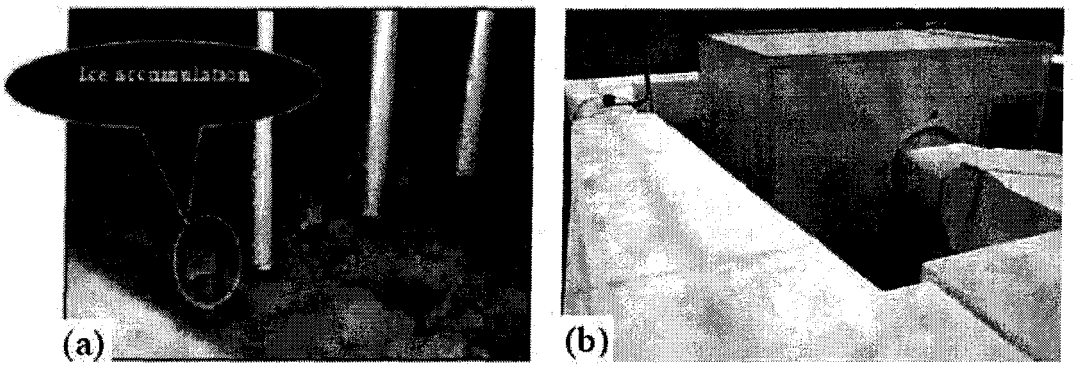

Figure 4.4. (a) Ice accumulation process on samples in a wind tunnel; and (b) top view of refrigerated wind tunnel used.

To prepare glaze ice on the sample surface, the wind tunnel was set at a wind speed of 11 m/s, air temperature -10°C, with a water feed rate of 2.5 g/m^3 and an average droplet size of ~80 μm [181] during the experiment. The requisite time in the tunnel for preparing glaze ice of up to ~1 cm thick was varied for different flat and/or rough samples. Prior to icing, all samples were placed in the tunnel for approximately 8 to 15 min to cool down.

C) Ice Adhesion Evaluation Method

As a final point, the adhesion of ice to the coatings was tested on the relevant surfaces in order to find out what parameters govern these properties. This series of ice-adhesion evaluation tests was conducted on Al beams with artificially iced samples spun in a home-made centrifuge apparatus and placed in a climatic chamber at -10 ± 0.1°C; this procedure was established as a standard method for determining the rotational speed at which ice detachment from the sample surface occurred, having been introduced by the Anti-icing Materials International Laboratory (AMIL), University of Québec at Chicoutimi [182]. The exact rotational speed at the time of ice detachment was determined and recorded by the related software. The centrifuge test machine can accelerate an iced sample beam from 0 to 10000 rpm with an acceleration rate of ~300 rpm/s [183]. The samples attached to the beams were iced by freezing drizzle in a wind tunnel at a fixed wind speed of 11 m/s, an air temperature of -10°C, a water feed rate of 2.5 g/m^3 during the experiment, and an average droplet size of ~80 μm [181] in order to prepare glaze ice of up to ~1 cm in thickness, or 3 to 5 g weight, over the sample area of ~3.2 × 3.0 cm^2 on an Al beam having the approximate dimensions of 320 × 31 mm in width and in length, respectively. This ice geometry was sufficient to avoid cohesion failure and provide easily reproducible results during de-icing. The average density of the ice was ~0.87 g/cm^3. The samples were placed vertically in the wind tunnel, perpendicular to the direction of the freezing drizzle flow. The beams were covered with a U-shaped Al air-foil so that only the tested area of each sample was exposed to the

droplets; this was also done in such a way as to avoid any possible turbulence. The accumulated ice mass and the surface area covered with ice were carefully evaluated both after icing and de-icing for each iced sample. To balance the beam in the centrifuge, a counter-weight was used on the other side, as shown in Figure 4.5. The iced samples were maintained at -10°C for ~15 min prior to the centrifuge adhesion test to ensure that, as far as possible, the state of thermal equilibrium at the ice-solid interface be attained. As mentioned, the artificially iced samples were spun in the centrifuge placed in a climatic chamber at -10°C to determine the rotational speed at which ice detachment from the sample surface occurred.

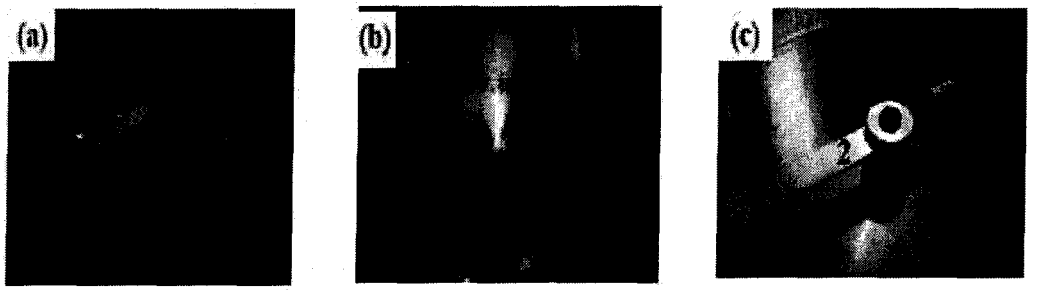

Figure 4.5. (a) Sample covered with artificial glaze ice, (b) centrifuge adhesion test machine, and (c) sample with coating in centrifuge set-up measuring ice adhesion where (1) sample, (2) aluminium beam, (3) counter-weight.

At the moment of detachment, as detected by sensors embedded in the centrifuge walls, the adhesion strength of ice is assumed to be equal to the centrifugal force, $F = mr\omega^2$, where m is the ice mass, r is the beam radius, and ω is the rotational speed in rad/s. The shear stress, correspondingly, was calculated as $\tau = F/A$, where A is the apparent de-iced area of the sample surface. Consequently, to reduce the influence of any experimental errors, the adhesion reduction factor (*ARF*) was finally used rather than absolute values of shear stress. This factor was calculated as the ratio of the shear stress of ice detachment on bare Al to that observed on samples with icephobic coatings, $ARF = \tau_{(Al)} / \tau_{(coating)}$, provided that all the tests, for both uncoated and coated samples, were run under identical conditions. For each flat alkyl-terminated coating

studied, three samples were subjected to at least 12 successive icing/de-icing events and 24 icing/de-icing cycles in the case of the rough coated samples. Each measurement was made on three duplicate samples (prepared under identical conditions), and the values shown are the average of the three. From these results, the ice adhesion strength of each coating was analyzed as a function of the number of icing/de-icing cycles. On the as-received, uncoated or bare Al, used as a reference sample, the shear stress of the ice detachment value, $\tau_{(Al)}$, was measured as 445 ± 20 kPa, which is in full agreement with the data provided in the relevant literature [182, 184]. The *ARF* parameter was calculated for different icephobic coatings in comparison with the bare aluminium. The higher the *ARF* values are, the greater the reduction of ice adhesion to the surfaces will be; it should be noted that the *ARF* of bare Al is 1. Further experimental details relating to this technique and procedure description will be found elsewhere [5, 184].

CHAPTER 5

EXPERIMENTAL RESULTS AND DISCUSSION: INVESTIGATION OF HYDROPHOBICITY AND STABILITY CARRIED OUT ON FLAT AL ALLOY SURFACES

5.1 Introduction

As mentioned earlier in Chapter 4, pre-treated Al substrates were coated with different materials in order to obtain a hydrophobic surface, thus several coatings were used based on permanganate conversion coating, stearic acid, octadecyltrimethoxysilane, FAS-13, FAS-17, and BTSE. All these chemicals were applied to Al substrates by means of various experimental parameters, including a variety of solvents, annealing steps, and sonication effects. This range of experimental parameters was used in order to observe and investigate any possible correlation between the wetting behavior of coated samples, their stability in water, anti-corrosion performance, and ice-repellency together with these parameters. Considering that hydrophobic surfaces are referred to as icephobic surfaces in this research work [77-79, 186], preparing hydrophobic surfaces was accorded priority; for greater detail Chapter 2 may be consulted. It is thus evident that the coatings must be packed in such a way that water molecules cannot penetrate through the surface beneath. Among the various techniques available, chemical bath deposition was used in this work to produce hydrophobic surfaces because of the simplicity of the technique and the minimal costs incurred [185]. The chemical bath deposition method has recently seen widespread use for the purpose of preparing uniform thin films on flat substrates at room temperature. Even though a number of these organic coatings, including stearic acid, or FAS-13,

[183, 186] was previously examined in this laboratory, nevertheless, the systematic study of hydrophobic properties, the stability of these coatings under water for long periods of time, the icephobic behavior during several icing/de-icing events and hydrophobicity following several icing/de-icing cycles has not yet been undertaken formally. These parts are scarce; this research work was thus carried out to investigate the previously mentioned properties on coated Al surfaces.

Chapter 5 describes how hydrophobic properties on Al surfaces were obtained by means of a chemical bath deposition of different substances, followed by a discussion of the results obtained for the hydrophobicity identified on such surfaces and their stability in contact with water.

5.2 One Layer Approach

5.2.1 Stearic Acid (SA) Based Coating on Flat Al Surfaces

Briefly, a series of experiments was carried out by coating the as-prepared flat Al surfaces with stearic acid. The immersion time in the stearic acid deposition bath was 24 h. Prior to use, the bath was magnetically stirred for a period of 2 h. After coating the samples and prior to tests, each sample was removed from the solution, rinsed with copious amounts of methanol solution, a solvent, then rinsed ultrasonically in methanol and blow-dried with N_2 , finally, they were annealed at 80°C for ~10 h. In this series of experiments, 3 Al samples coated with SA were prepared and studied so as to obtain more accurate and reliable results. The results shown here are based on the average of the results obtained for these three samples. For each sample, CA measurements were also made on at least seven different randomly selected locations on a horizontal surface. All three samples displayed similar behavior.

5.2.1.1 Study of Sample Hydrophobic Properties

The initial CA values of the coated samples studied were measured by means of a water contact angle goniometer; these indicated that CA >106° implied well coated flat hydrophobic surfaces. The average contact angle of ~108 ± 5° with a minimal error deviation of 4.5% was found for all three samples (Figure.5.1). It was also observed that without any sample treatment with SA, the polished and mirror polished bare samples display an average CA of 55° and 65°, respectively, indicating a relatively high surface energy. Now the question is that are the SA coatings dense enough to prevent water molecules from penetrating through the coating or not? And also what kind of behavior will be observed for those coatings in terms of their stability under water for a long period of time (time-dependent water-CA)? With this intention, a set of experiments including time-dependent water CA measurements under deionized water and surface characterization were carried out.

5.2.1.2 Influence of Sample Immersion in Water on CA Values (Stability Test)

Figure 5.1 presents CA values as a function of immersion time in deionized water for the SA treated sample. A decrease in hydrophobic properties of the coating may be observed from this figure; this decrease may be ascribed to the loss of the SA layer either partially or completely leading to a decline in the CA beyond ~1200 h. Figure 5.2 shows water droplet images on SA coated surfaces before (left) and after 1200 h immersion in water (right). These layers of SA were believed not to be dense enough to prevent water molecules from penetrating through the coating.

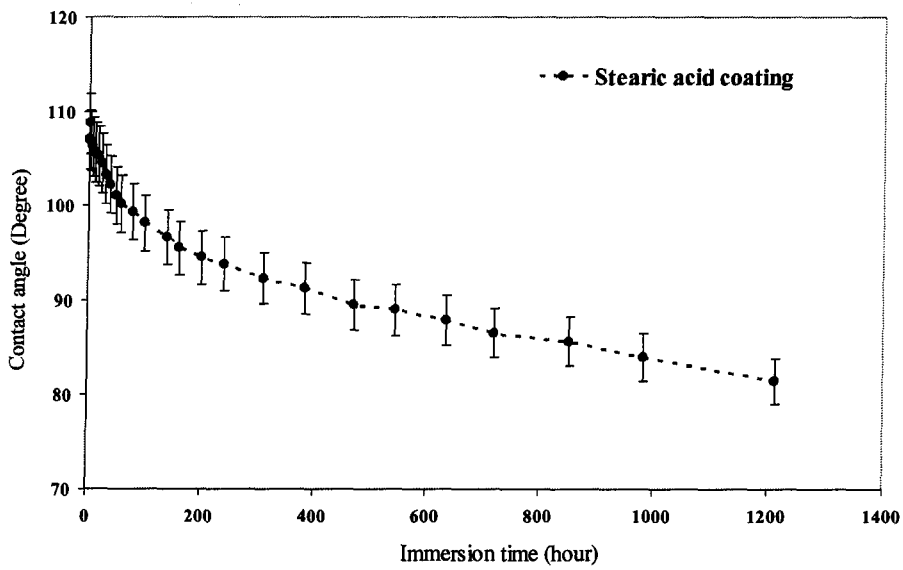

Figure 5.1. Contact angle *vs.* immersion time in deionized water for SA treated Al surface.

A significant decrease in surface hydrophobicity may clearly be observed in Figure.5.2 (right), implying some decay of the coating layer. As was mentioned, Al samples coated with SA were seen to demonstrate initial values of CA >106° (Figure.5.1, left), indicating well coated flat hydrophobic surfaces [93].

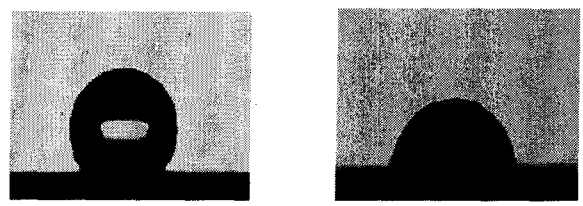

Figure 5.2. Water droplet images on SA coated Al surface before (left) and after 1000 h immersion in water (right).

It will be observed, however, that the CA values decrease with immersion time. In fact, all the coatings studied were found to lose their hydrophobic properties gradually after ~1200 h of immersion in water; this is associated with a considerable decrease of their water contact angle values (e.g. Figure.5.1, right). Meanwhile, the samples treated with SA showed very similar behavior as coated samples with ODTMS in terms of hydrophobic properties and their time-dependent degradation that it will be presented in the next part.

5.2.1.3 Scanning Electron Microscopy and Optical Microscopy Images (Corrosion Observation)

Scanning electron microscope (SEM) images of the coated Al samples with SA before and after immersion in deionized water were taken using a Hitachi S-4700 Field-Emission SEM instrument with accelerating voltages from 500 V to 25 kV and in high-vacuum mode, typically at 15 keV. Since both SA Since both SA and ODTMS molecules have comparable lengths, it is reasonable to assume that their monolayers also demonstrate very similar thickness, i.e. of ~2 nm [19, 166, 167, 169]). These images are presented in Figure.5.3. While extensive corrosion appeared on the unmodified samples after only 20-30 h of deionized water exposure, the first trace of any considerable corrosion products or pitting in either matrix region and/or around second-phase particles after 520 h immersion in water was observed on SA coated samples. Corrosion products, as well as the pits around second-phase inter-metallic particles appearing after ~520 h of exposure to water, can be observed easily from this morphological analysis.

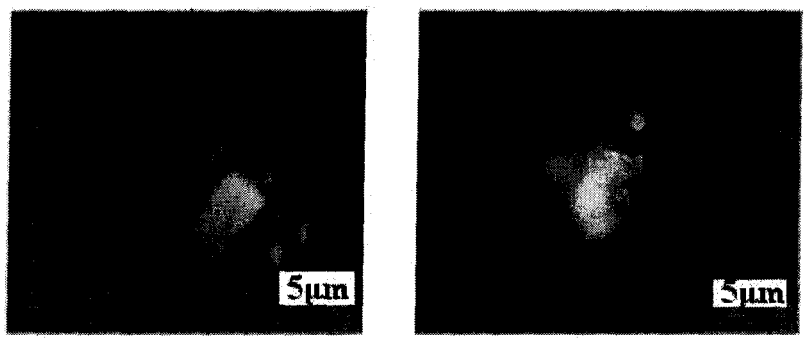

Figure 5.3. SEM images of stearic acid treated sample after 520 h exposure to water.

The images produced by optical microscopy taken of both the mirror-polished Al surface and the one treated with SA, however, show traces of some small black dots or pits prior to water exposure (Figure.5.4). A closer look at these black dots reveal the presence of very small locally corroded areas, visible on the micrometer scale, having also been observed and reported on by other researchers [144].

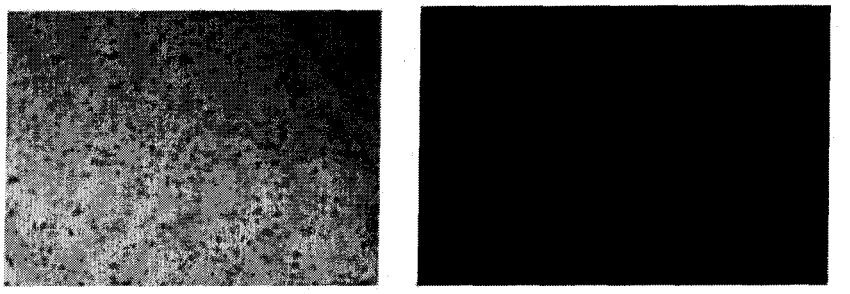

Figure 5.4. Images obtained through optical microscopy of mirror-polished Al surface (left), and Al sample coated with stearic acid (right), at a magnification of ×100.

These small locally corroded spots probably occurred either during sample pre-treatment such as mechanical polishing of the sample surfaces (caused by the finer used), or during the ultrasonic sample washing which could cause the removal of some inter-metallic particles, or even during the sample coating process due to the effects of the solvent used in the SA chemical bath for Al surfaces. As was pointed out earlier, the SA coatings studied were found to lose their hydrophobic properties gradually after ~1200 h of immersion in water upon which the water CA values decreased noticeably (Figure.5.1, right). Indeed, the corrosion products (Figure.5.3) are also believed to have contributed to the decrease in hydrophobic properties over time (Figures.5.1 and 5.2 (right)).

5.2.2 Octadecyltrimethoxysilane (ODTMS) Based Layers on Flat Al Surfaces

Another set of experiments was conducted by coating the flat polished Al surfaces with ODTMS. The immersion time in ODTMS deposition baths was 15 min. Two different types of ODTMS bath, one in isopropanol-water and one in methanol-water with a different pre/post treatment (Table 5.1) were used to trace any possible effects of these various parameters.

Table 5.1 Experimental details of Al surfaces coated with octadecyltrimethoxysilane.

Sample	SO1	SO2	SO3	SO4	SO5	SO6	SO7	SO8	SO9	S10
Immersion time in ODTMS bath (min)	1	5	10	30	5	5	5	5	5	5
Alkaline treatment	+	+	+	+	+	-	-	-	+	+
Annealing (at ~ 100^{0}C for 2 h)	+	+	+	+	+	+	+	-	+	-

Prior to use, the baths were magnetically stirred for 3 h to allow for the hydrolysis process to be set in motion. The initial contact angles of all samples receiving different pre/post treatment are summarized in Table 5.2.

Table 5.2 The initial values of CAs on ODTMS-treated flat Al_2O_3 substrates.

Sample	SO1	SO2	SO3	SO4	SO5	SO6	SO7	SO8	SO9	S10
Initial values of C.A.	107.5	108.2	108.4	108.7	108.1	107.2	107.3	106.7	108.2	107.2

5.2.2.1 Stability of Samples Immersed in Water

Figures 5.5 and 5.6 present CA values for the abovementioned prepared samples as a function of immersion in deionized water producing no significant effect of a variety of applied pre- and post-treatment protocols on coating durability, *i.e.* alkaline treatment, different immersion times in the ODTMS bath, and/or the annealing process, as was described in Chapter 4. All the coatings under investigation demonstrated the initial values of CA > 105° (Figures 5.5 and 5.6, left) indicating well coated flat hydrophobic Al surfaces. It is clear, however, in Figures 5.5 and 5.6 that the samples lose their hydrophobic properties gradually after about 550 h of immersion in water. This decrease in surface hydrophobicity may be ascribed to a considerable drop in water CA values (Figures 5.5 and 5.6, right).

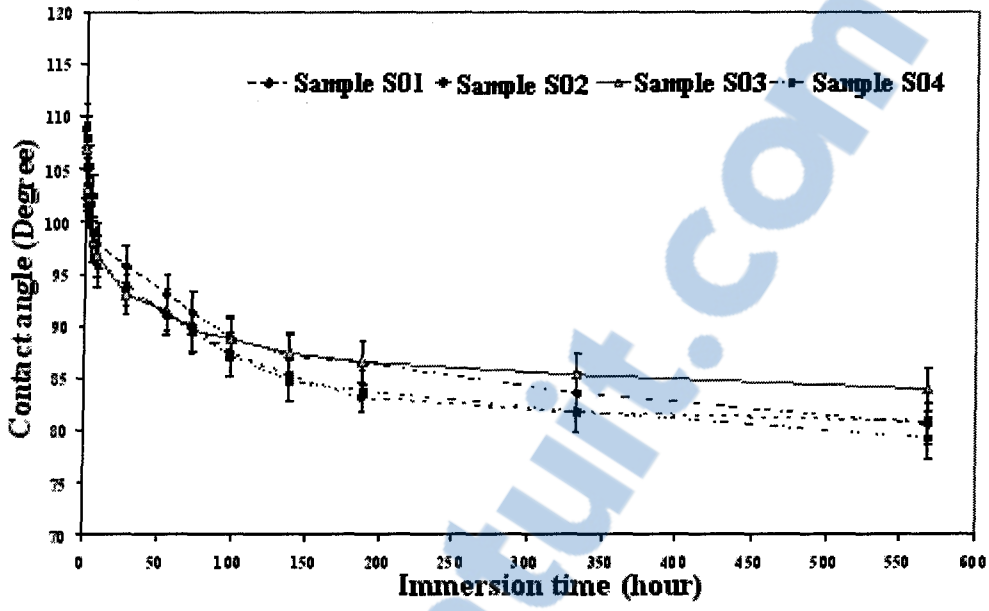

Figure 5.5. Contact angle *vs.* immersion time in deionized water for ODTMS (SO1 to SO4) treated samples.

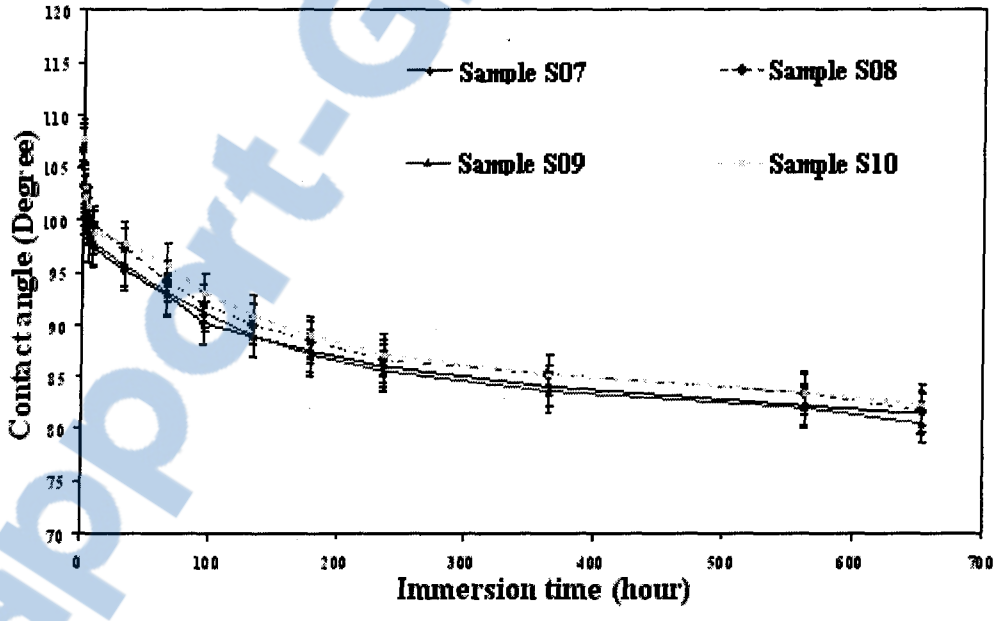

Figure 5.6. Contact angle *vs.* immersion time in deionized water for ODTMS treated samples (S07 to S10).

In fact, the hydrolysis/condensation reaction between trimethoxysilane (R-Si-OH) molecules and hydroxilated surface (Al-OH) is slow and reversible; water molecules can thus

penetrate and hydrolyze the Al-O-SiR bond and therefore, the Al-OH and RSi-OH components were generated and for which a decrease of surface hydrophobicity was ultimately observed [144].

5.2.2.2 Effect of Sonication on Sample Hydrophobicity

Two samples, SO5 and SO6, were sonicated in deionized water for 30 min immediately after coating with ODTMS to investigate any effect of sonication on coating stability. Both samples of coating showed a rapid slump in the CA values, displaying a negative slope from a CA > 105° to 92.2° and 89.9°, respectively, which implies insufficient stability in relation to the ODTMS coatings on Al surfaces. It is likely that the significant amount of decay observed in the coatings may have been caused by a breakdown of the coating bonds during the process of sonication.

5.2.2.3 Effects of Solvent, Alkaline Cleaning and Curing on Sample Hydrophobicity

As is evident from Figures 5.5 and 5.6, no observable effect of the various pre- and post-treatment protocols such as alkaline treatment, varied immersion time in the ODTMS bath or the annealing process were observed in terms of coating stability under water. All the coatings gradually lost their hydrophobic properties after ~550 h of immersion in water, upon which the water CA values dropped. Neither coating stability nor durability was greatly affected by the pre/post treatment conditions applied.

5.3 Two Layer Approach

5.3.1 Potassium Permanganate Conversion Coating (Pre-Treatment) Grafted with ODTMS (Post-Treatment)

5.3.1.1 Introduction

The conversion coating process is self-limiting and will not continue beyond the formation of a thin uniform yellow-gold film [170]. According to an earlier study [160], the surface layer is no more than (~10nm). The XPS analysis showed that the major component of the PCCs was MnO_2, on condition that the films were composed predominantly of Mn and O. The corrosion protection provided by permanganate CC is a result of the presence of this thin layer of MnO_2. The native oxide on Al is unstable in the alkaline medium, namely pH ~9, as used for this study, tending to dissolve in the aqueous solution in accordance with the following equation:

$$Al_2O_3 + 2OH^- + 3H_2O = 2Al(OH)_4^- \qquad (1)$$

The oxidation of the metal and the reduction of Mn (VII) to Mn (IV) can be represented by:

$$Al + MnO_4^- + 2H_2O = Al(OH)_4^- + MnO_2 \qquad (2)$$

The surface morphology and thickness of the Al samples treated for 3-5 min at 70°C approached that of the samples treated at room temperature for 210 min in accordance with earlier reports [160]. After producing a uniform yellow-gold potassium permanganate CC as an under layer, the surface was then ready for further coating with a top layer of ODTMS.

5.3.1.2 Surface Hydrophobicity of Al Substrates Coated with $KMnO_4$/ODTMS

An evaluation by means of contact angle measurements was carried out on the hydrophobic properties of samples pre-treated with $KMnO_4$ and post-coated with ODTMS, in isopropanol as a solvent, S1, or ODTMS, in methanol as a solvent, S5. When the first contact

angles of both the coated samples in question were measured, it was indicated that they possessed values of CA > 105°. These values of CA imply well coated flat hydrophobic surfaces. A slight difference between the contact angle values obtained from thin films of S1 and S5 may be found (the average contact angle of ~105 ± 5° and 107 ± 2°, respectively) with the minimal error deviation of 5% in both cases (Figure.5.7).

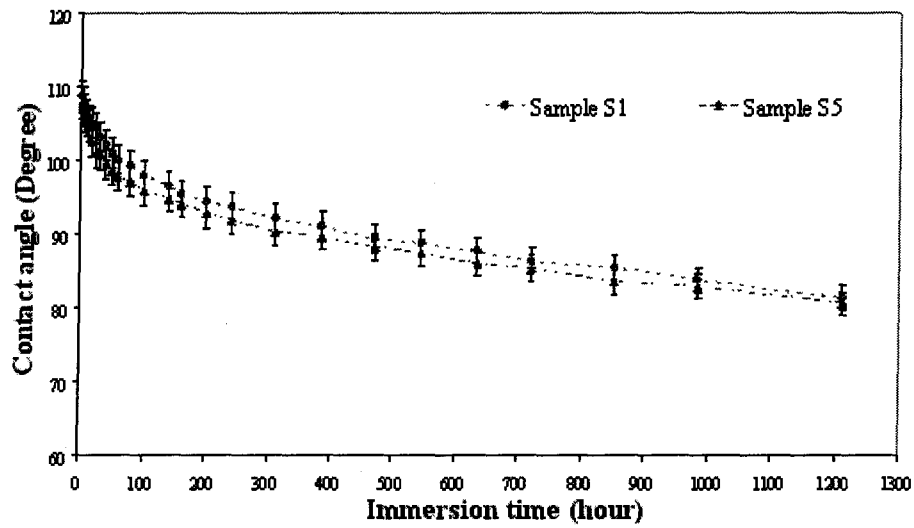

Figure 5.7. Contact angle *vs.* immersion time in water for $KMnO_4$/ODTMS in IP (S1) and MeOH (S5) treated samples.

5.3.1.3 Stability of Al Samples Coated with $KMnO_4$/ODTMS under Deionized Water through CA Measurements

As it was shown earlier, both samples demonstrate the gradual loss of their hydrophobic properties over time through sample immersion in deionized water. A decrease in CA values of the coatings can be observed in Fig.5.7 which may be ascribed to the loss of the ODTMS layer, both partially and entirely, leading to a degradation of the hydrophobic properties of the sample beyond ~1200 h. Both samples treated with SA and $KMnO_4$/ODTMS, however, showed similar behavior in terms of their hydrophobic properties and their time-dependent degradation, as shown in Figure 5.8. These ODTMS layers were not supposed to be sufficiently dense to avoid water

molecule penetration through the coating. Figure 5.8 compares CA values as a function of immersion time in water for SA and $KMnO_4$/ODTMS/IP treated samples. Both samples demonstrate the initial values of CA > 105°, as shown in Figure 5.8, left, which is representative of well-coated flat hydrophobic surfaces [93], although all the prepared coatings gradually lose their hydrophobic properties beyond ~1200 h of immersion in water; this is observed to be associated with a considerable decrease in water contact angle values, as may be seen in Figure 5.8, right.

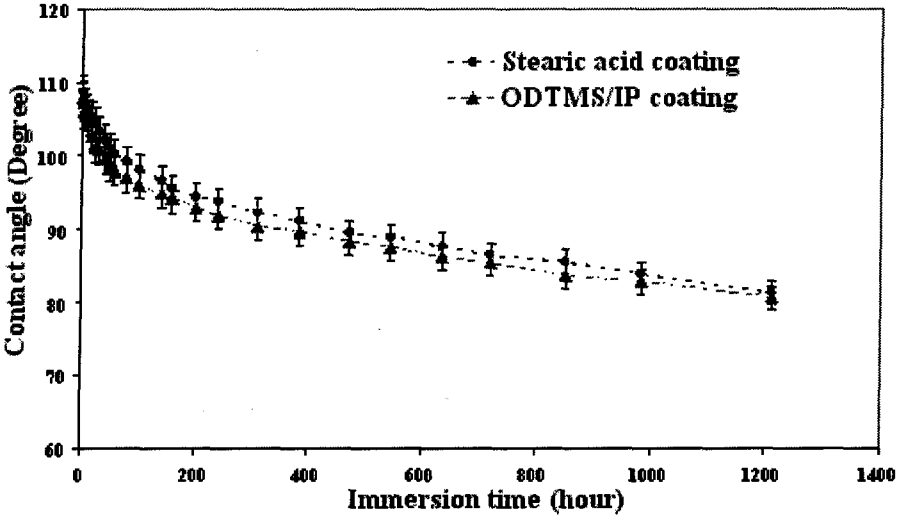

Figure 5.8. Contact angle *vs.* immersion time in deionized water for stearic acid and ODTMS treated samples.

5.3.1.4 Effects of Solvent on Surface Hydrophobicity and Durability

This series of hydrophobic samples was obtained by coating Al samples with $KMnO_4$ as an under layer, followed by a covering layer of ODTMS prepared with isopropanol and methanol used as a solvent, to ascertain the existence of any of the possible effects that a solvent used in the ODTMS chemical bath might have on sample hydrophobicity and durability. As shown in Fig. 5.7 for both cases, the first contact angle values were CA > 105° with a slight difference observed

between the sample values, S1 and S5; the averages obtained were CAs of ~105 ± 5° and 107 ± 2°, respectively. Both coatings, however, showed similar behavior in terms of sample stability under water, losing their hydrophobicity after the same period of time immersed in water.

5.3.1.5 Surface Analysis : Corrosion Observation *via* Images from Scanning Electron Microscopy

Images of the coated Al surfaces, before and after immersion in deionized water, were obtained using a scanning electron microscope. As expected, little or no corrosion products or pitting were observed either in the matrix or around the second-phase particles after 520 h immersion in water for the samples coated with $KMnO_4$/ODTMS/MeOH or $KMnO_4$/ODTMS/IP; whereas extensive corrosion was clearly observed in the case of unmodified samples (as-received Al surfaces) after only 20–30 h of immersion in deionized water. The SEM images of samples coated with $KMnO_4$/ODTMS/MeOH are presented in Fig.5.9. There was no significant difference between both the S1 and S5 treated samples, implying the existence of a minor solvent effect occurring during the deposition of ODTMS. This type of film on Al surfaces may be considered in the same way as a closely packed barrier film against the penetration of water molecules and can therefore act as an anti-corrosion coating as well. Permanganated surfaces are known to be well protected and inert in water. Recently, SEM images have proved that the harder insulating layer of MnO_2 is certainly thicker on second phase particles than it is in the Al matrix. The presence of reversible Red/Ox interactions between the solution and the substrate leads to a more rapid deposition of the MnO_2 layer on particles compared to Al matrix. In other words, fast dissolving process of deposited layer on Al matrix in comparison to particles can create the thicker layer of MnO_2 layer on second phase particles than Al matrix [160, 170].

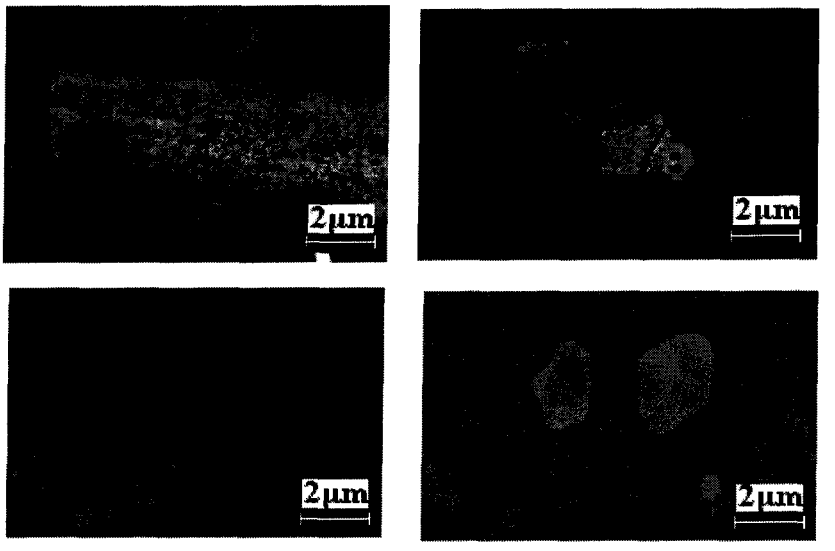

Figure 5.9. (Top Row) SEM images of $KMnO_4$/ODTMS in MeOH treated samples; and (Bottom Row) in IP treated samples after 520 h exposure to water.

However, some cracks can be observed in the layer covering the particles. These cracks occurred when coated sample was removed from the bath and then cured in the oven. It is obvious that these cracks belong to MnO_2 layer only and not to ODTMS based layer.

5.3.2 Coating of Al Alloy Surfaces Applying TEOS and BTSE (Pre- Treatment) Grafted with ODTMS (Post-Treatment)

5.3.2.1 Introduction

The baths of BTSE/MeOH and as-received TEOS were prepared at room temperature for the under layer and further silane deposition for the top layer on clean polished flat Al samples. Immersion in the BTSE/MeOH solution was completed for different immersion times. The BTSE treated samples, series B, were then immersed in the ODTMS solution for varying immersion times of 1, 5, 20, 60 min, and 5 hours. In addition, one sample was also immersed in the ODTMS solution for 20 min followed by ultrasonic washing in methanol for 15 s to search for any effect

of sonication. These under layers were used to produce silicon dioxide and ultimately to form Si-O-Si linkages *via* the following sol-gel process by reacting with water:

$$Si(OC_2H_5)_4 + 2\ H_2O \rightarrow SiO_2 + 4\ C_2H_5OH \qquad (3)$$

Flat Al samples were soaked in a bath of pure TEOS for 20s followed by immersion in deionized water for hydrolysis. These samples were successively immersed in a TEOS bath in order to obtain more layers as a cycle, specifically 2 to 5 layers, to investigate the effects of multi-layers on coating performance. After a number of cycles, all the pre-treated samples from series T were immersed in the ODTMS solution for different immersion times similar to those of series B and then annealed in an oven at 100°C. More details can be consulted in chapter 4. XPS analysis of the surfaces confirmed the presence of silicon on the surface of both TEOS pre-treated and ODTMS grafted samples. The relative amount of oxygen in the surface goes up after applying the silica layer and goes down after applying the SAM. The relative amount of cupper goes down with SiO_2 attachment and up with SAM attachment. The very high O/Si ratio after SiO_2 attachment is consistent with a surface that is not uniformly covered with SiO_2, but rather a surface with patches of SiO_2 intermixed with other metal oxides. Reduction of this ratio after SAM attachment is to be expected.

5.3.2.2 Hydrophobicity of Aluminium Samples Coated with TEOS/ODTMS and BTSE/ODTMS Layers

The initial contact angle values of this series of samples, B and T, were ~107 to 109°. This range of CA values revealed hydrophobic properties of these coated surfaces which covered uniformly. In other words, self assembly of ODTMS molecules on these surfaces have completed with a sufficient amount of assembly degree during formation which can result in improved

hydrophobic properties, and thus enhanced icephobic properties. The influence of solution concentration, sonication and film curing step were also investigated.

5.3.2.3 Stability of Prepared Coated Samples in Deionized and Tap Water over Time

A) Deionized Water

All the coatings studied were found to lose their hydrophobic properties gradually as a result of ~550 h of immersion in deionized water and ~350 to 380 h of immersion in tap water, for series B and T, respectively; this is presumed to be associated with the considerable drop in water CAs observed in Figure 5.10. The effects of all earlier conditions on coating durability were investigated showing that the coatings degrade within several days of immersion in water, while the contact angle decreases with immersion time. By subjecting Al surfaces to a wet environment, the ODTMS layer of ~2 nm will undergo some degree of degradation initially compared to the BTSE or TEOS layers which are thicker by ~100 nm and 10 nm, respectively [164].

B) Tap Water

This series of experiments, as shown in Figures 5.10 and 5.11, was carried out by immersing certain samples in deionized water with a water conductivity of ~0.32 μS/cm and other samples in tap water with a water conductivity of 87.6 μS/cm at 19 ^{0}C. This tendency to lose surface hydrophobic properties is, in all likelihood, due to the rupture of the R'Si-O-SiR bond between the ODTMS molecules and the BTSE layer caused by the hydrolysis of these bonds. In other words, a hydrophilic surface including -OH groups is formed. More hydrophilic properties of the surface, or a decrease in water CA values, were thus observed. It is also evident from Figures 5.10 and 5.11 that losing hydrophobic properties is a slightly faster process for coated

samples immersed in tap water than it is for samples immersed in deionized water. The cause of this difference may be attributed to the influence of salts dissolved in tap water leading to accelerated coating deterioration. These layers are, thus, not dense enough to prevent water molecules from penetrating through the coating.

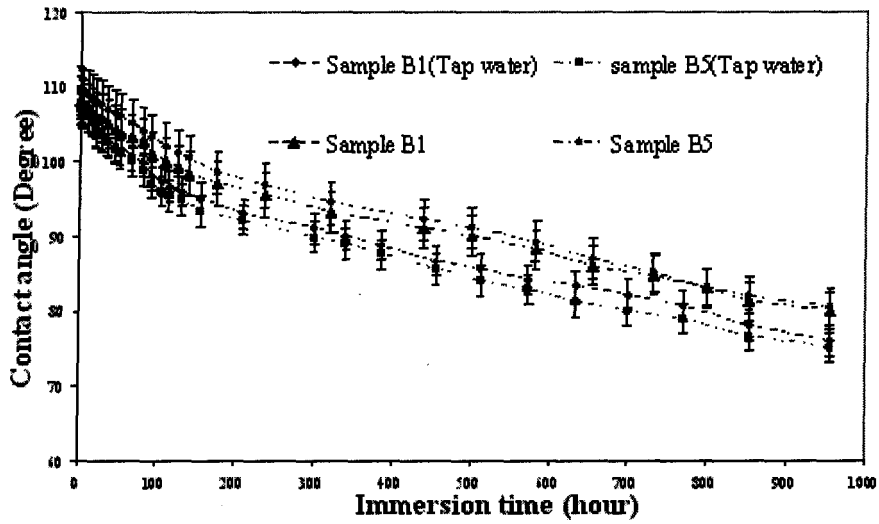

Figure 5.10. Contact angle *vs.* immersion time in water for BTSE/ODTMS treated samples in deionized and tap water.

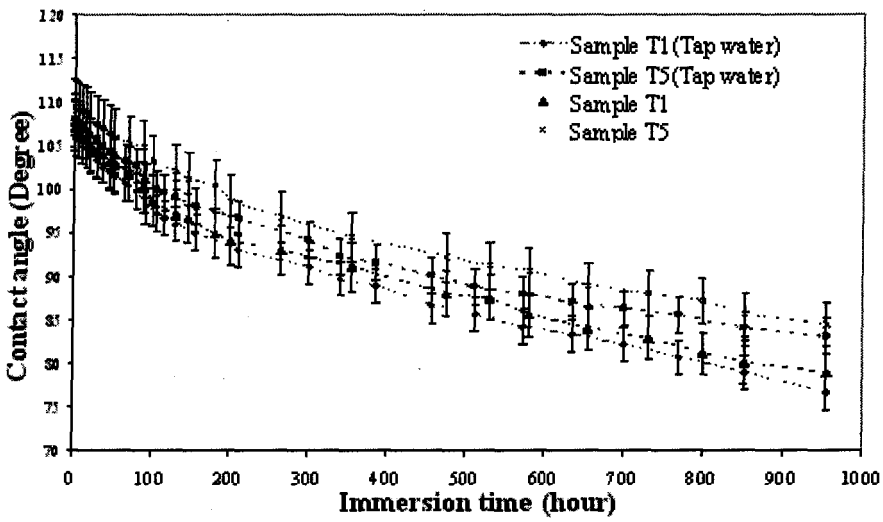

Figure 5.11. Contact angle *vs.* immersion time in water for TEOS/ODTMS treated samples in either deionized water or tap water.

5.3.2.4 Effects on Hydrophobicity of Sample Sonication and Annealing

The ultrasonication of coated samples with BTSE/ODTMS or TEOS/ODTMS for short periods of time, mainly 10-15s, resulted in greater surface uniformity of appearance in comparison with non-sonicated samples. Dense and more compact BTSE layers were obtained by applying the sample curing step, since BTSE films are dependent on such deposition conditions as bath concentration, immersion time, and curing. The optimum conditions reported by other researchers [167] were used in this series of experiments. The curing step augmented the barrier properties of the BTSE film and also thereby improved corrosion resistance of the silane layer in an aggressive environment.

5.3.2.4 Effects of pH and Solution Concentration on Prepared BTSE/ODTMS and TEOS/ODTMS Coatings

As mentioned above, the most important parameters and optimum conditions reported by other researchers [167] were considered in connection with this series of trials. In particular, attention was paid to maintaining the pH levels of the solution in the range of 4.5 to 5.0. In this range of pH solution, a maximum amount of reactive silanol groups are able to interact with Al_xO_y surface. It should be noted that a major challenge with regard to Al surface modification is avoiding the use of chloride ion releasing materials either as SAM precursors or in subsequent manipulations of the SAM-coated substrates. These ions are liable to cause chloride-induced pitting corrosion [165]. Thus, it is essential to choose appropriate materials for coating Al surfaces aiming at their hydrophobicity while at the same time considering their response to corrosion phenomena. Increasing the concentration of the BTSE solution increases the barrier properties of the BTSE/ODTMS film covering of Al surfaces and as a result improves the anti-corrosion properties of the silane layer in aggressive environments.

5.3.2.5 Effects of Various Immersion Times in an ODTMS Solution on Prepared BTSE/ODTMS and TEOS/ODTMS Coatings

All the BTSE and TEOS pre-treated samples from series B and T were further immersed in an ODTMS solution for a variety of different immersion times ranging from 1, 5, 20, and 60 min to 5 hours in order to reveal the influence of various immersion times in ODTMS for the top-layer on coating stability and hydrophobicity. Based on the results obtained for this series of samples, no significant difference was observed in the initial CA values, nor was their durability or stability under deionized water affected in any way as might be evidenced by an improving or worsening effect on their hydrophobic properties.

5.3.2.6 Surface Characterization (Corrosion Observation)

As explained earlier, based on previous observation by other research groups on the corrosion phenomena of Al surfaces, the first corrosion products appeared on the unmodified samples after exposure to only 20–30 h of deionized water. However, morphological analysis of Al samples coated with BTSE/ODTMS and TEOS/ODTMS according to an SEM survey, both before and after immersion in water, revealed the earlier traces of corrosion products or pitting around second-phase particles beyond ~750 h exposure to water, as shown in Figure 5.12. In addition, a number of inter-metallic second phase particles were dissolved and removed from the matrix.

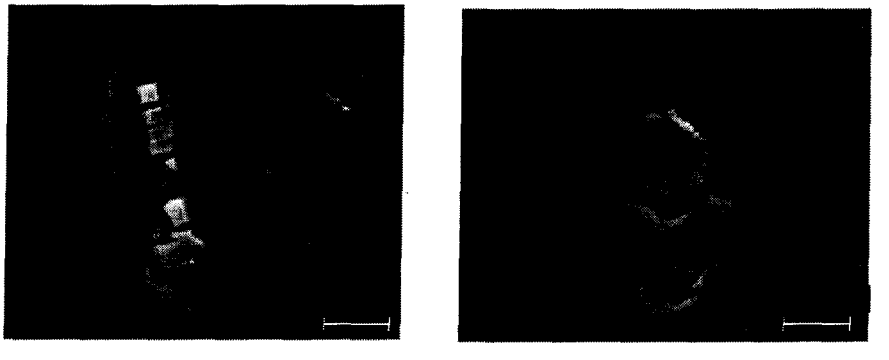

Figure 5.12. SEM images of BTSE/ODTMS (left) and TEOS/ODTMS (right) treated samples after 750 h exposure to water. (Note: Bars stand for 2 μm.)

Investigation by means of EDS revealed that the surface morphology and chemistry of Al samples coated with BTSE/ODTMS and TEOS/ODTMS was altered. Figures 5.13 (a) and 5.13 (b) show the SEM images in the insets and the corresponding EDS spectra for BTSE coated surfaces prior to and following stability tests. It is evident from the SEM images that significant morphological changes are apparent following the immersion test. While a Si peak is detected by EDS before sample immersion in water, as shown in Fig.5.13 (a), indicating a mixed BTSE/ODTMS layer, there is no significant amount of Si to be observed in the same sample after 750 h immersion in water, as shown in Figure 5.13 (b). This finding supports the above described assumption that water molecules hydrolyze the -O-Si-R bond and gradually destroy silane layers. The peaks of C and O also refer to the contaminations on the surfaces. Similar results were observed for the TEOS/ODTMS coating analyzed. Hence, similar processes are expected upon immersion of both samples in water.

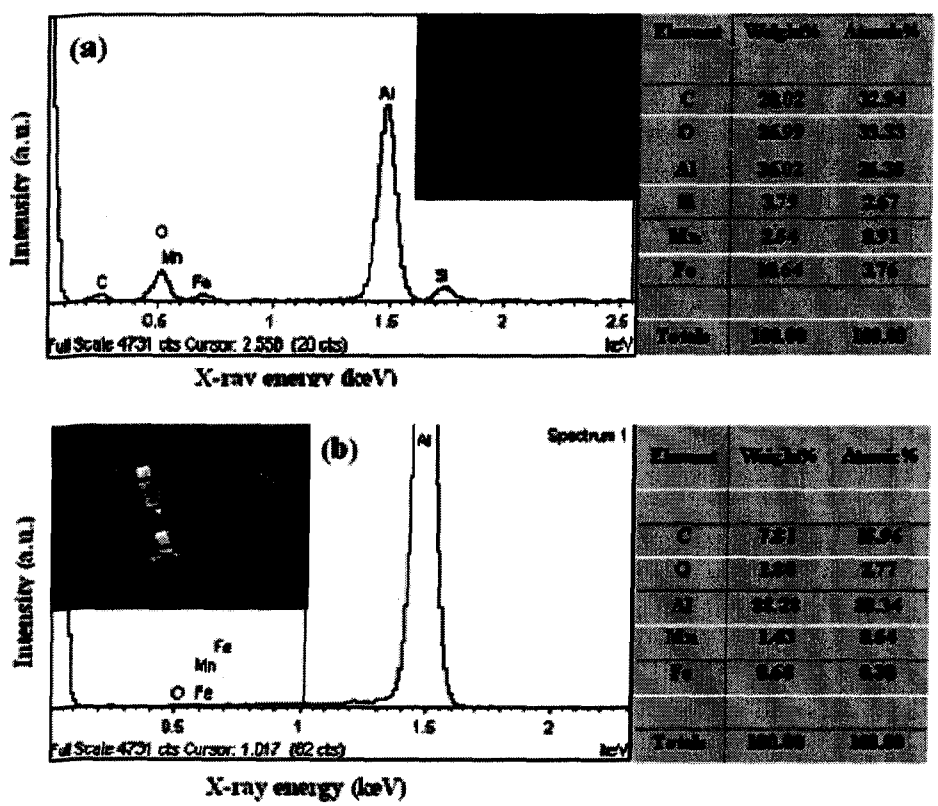

Figure 5.13. EDS spectra and SEM images of BTSE/ODTMS coated Al surface (a) before, and (b) after stability test.

The AFM and optical microscope images of mirror-polished bare Al and of BTSE/ODTMS or TEOS/ODTMS coated Al surfaces demonstrated well-uniform flat coated Al surfaces. All these prepared coated Al samples including the mirror-polished Al sample have a root-mean-square (rms) roughness as low as ~2 nm. However, after immersion in deionized water for the stability tested hydrophobic coatings beyond ~750 h, as shown in the previous section for the SEM results, a certain amount of agglomerated black pits and/or corrosion-products are clearly observable through an optical microscope, as shown in Figure 5.5. These black dots are small locally corroded areas [144]. Figure 5.14 presents images from optical microscopy of flat Al surfaces coated with BTSE/ODTMS before and after immersion in deionized water at a magnification of ×100.

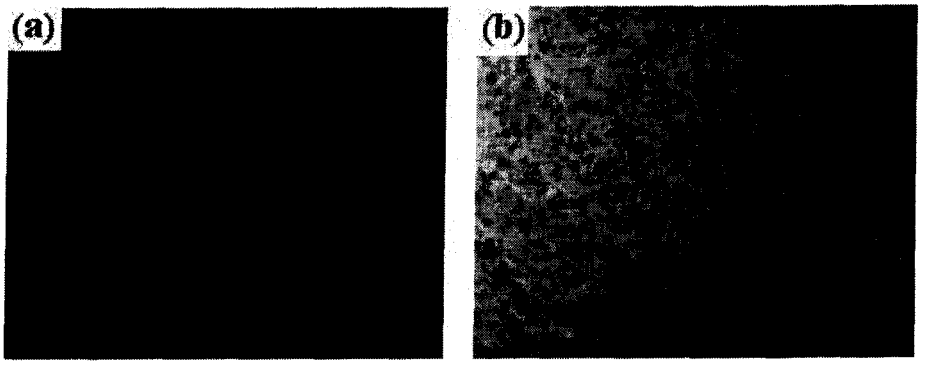

Figure 5.14. Optical microscopy images of flat Al surfaces coated with BTSE/ODTMS, (a) before and (b) after immersion in deionized water (magnification of ×100). Note: Bars stand for 2μm.

CHAPTER 6

EXPERIMENTAL RESULTS AND DISCUSSION: INVESTIGATION OF HYDROPHOBICITY AND STABILITY ON ROUGH ALUMINIUM ALLOY SURFACES

6.1 Introduction

As mentioned in Chapter 2, the essential conditions for creating a superhydrophobic surface are generating an especially-designed type of asperity on the surfaces and applying low free surface energy materials, known here as hydrophobic material, for the outermost layer. With this aim in mind, a range of well-cleaned unpolished Al samples was etched with HCl, ~14.8 wt %, to produce a rough Al surface. They were then rinsed ultrasonically in deionized water to remove any loose particles on the surface resulting from the etching process. After that, these etched samples were dried at 70°C in a furnace and then placed in the corresponding chemicals baths. The deposition baths used in this series of experiments, as explained in detail in Chapter 4, were: 1H,1H,2H,2H-perfluorodecyltriethoxysilane (FAS-17), 1H,1H,2H,2H-perfluoro-octyltrichlorosilane (FAS-13) and stearic acid. An investigation was also carried out on the enhanced wetting behavior, stability/durability under water, and ice-repellent properties of this group of coated samples. The chemical bath deposition method was used for coating rough surfaces to produce superhydrophobic surfaces. These superhydrophobic coatings were formerly studied in this laboratory; however, the stability and durability of those coatings under deionized water, icephobic behavior through several icing/de-icing events, and the hydrophobic properties following each icing/de-icing cycle have not yet been systematically studied. This set of experiments was conducted to and acquire a better understanding of the earlier listed properties relating to coated rough Al surfaces.

6.2 Coating of Etched Al Surfaces Using Stearic Acid (SA)

6.2.1 Introduction

The previously etched Al surfaces were coated with stearic acid/MeOH with an immersion time in the stearic acid deposition bath of 24 h. After coating the samples with a layer of SA prior to tests, each sample was removed from the SA/MeOH solution and rinsed with the appropriate solvent, methanol. After that, they were rinsed ultrasonically in methanol, dried and annealed at 80°C for ~10 h to improve the cross-linking of layers. These coated samples were immersed in deionized water to test their stability under water over time by means of CA measurements.

6.2.2 Hydrophobic Properties

Contact angle values as a function of immersion time in water for samples coated with SA on rough Al surfaces are presented in Figure 6.1. The Al samples coated with SA are seen to demonstrate the initial values of contact angles greater than 150°, as shown in Figure 6.1, left. This contact angle value implies the presence of a well-coated superhydrophobic surface.

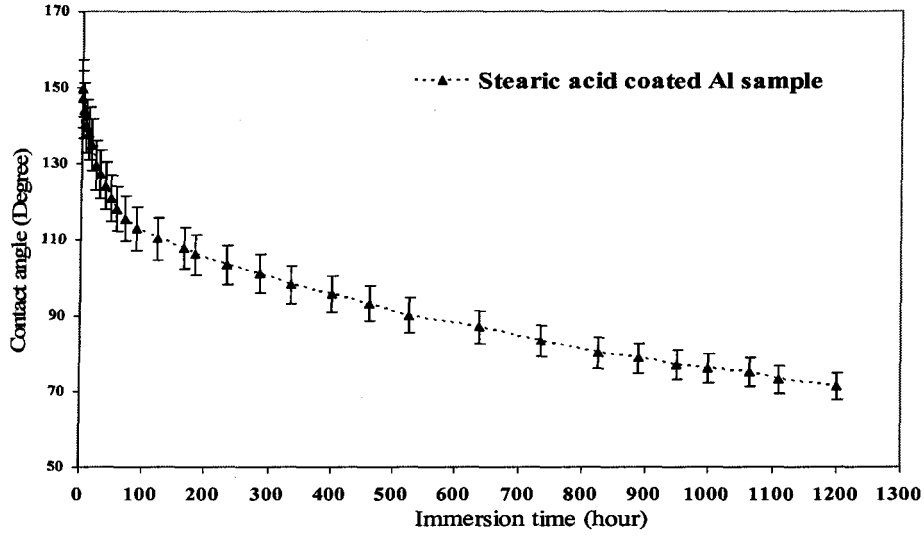

Figure 6.1. Contact angle *vs.* immersion time in deionized water for rough Al sample coated with SA.

By immersing the samples in deionized water, however, the CA values were observed to decrease over time. In fact, SA coatings were found to lose their hydrophobic properties gradually after ~800 h of immersion in water, which is associated with a considerable decrease in the water CA values, as shown in Figure 6.1, right. A considerable decrease in surface hydrophobic properties will easily be observed in Figure 6.1. This tendency to lose surface hydrophobicity is due in all likelihood to the decay of the low surface energy layer coated on Al surfaces, whether partially or completely. Thus, a decrease in surface hydrophobicity was observed for this coated sample over time by turning to lower values of CA (Fig.6.1) after ~800 h immersion in water. It can be referred to an insufficiently dense SA layer prepared on Al surface to stop water molecules penetrating through the coating.

6.2.3 Surface Characterization

Figure 6.2 presents images acquired by Atomic Force Microscopy of scan size of 20x20 μm for SA on rough Al (a) and flat Al surface (b) obtained following the surface coating. This technique is capable of providing 3-dimensional topography images of the surface as well as information concerning features of the surface including the z-height surface roughness. These analyses show that flat Al surfaces possess a root-mean-square (rms) roughness value of as low as ~2 nm and ~400 nm in the case of etched coated Al surfaces. In all of the etched samples, rough structures were observed, implying air entrapment in the structures when a water droplet is placed on top of it. As surface asperities were well separated in all cases, a high CA and "*slippery*" surface state can be expected for water drops on all samples, which is consistent with the CA values in Figure 6.1. The presence of a layer of coating on the rough surface is found to retain the morphological features of the substrate.

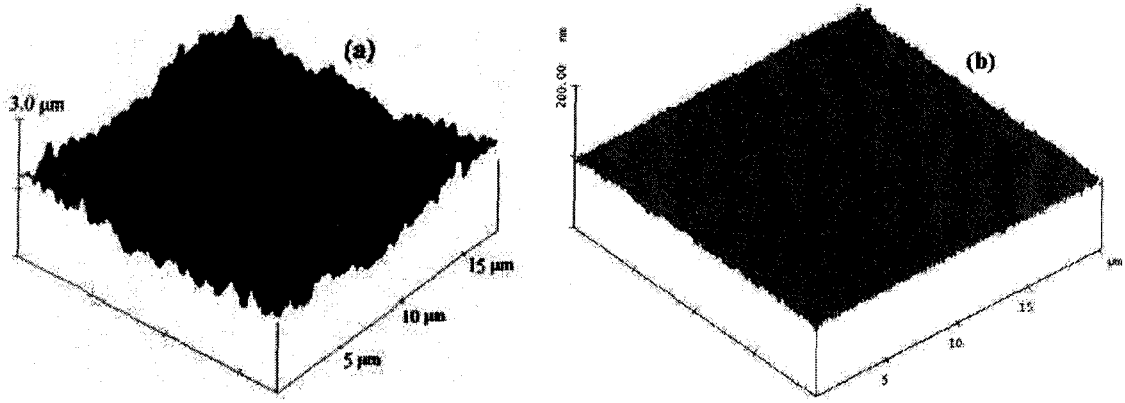

Figure 6.2. 3-D AFM images of (a) rough Al sample coated with SA and (b) flat Al sample coated with SA.

This observation is evident from SEM images of the SA film on the etched Al substrate (top) and non-etched (mirror-polished) Al substrate (bottom), as shown in Figure 6.3. This was also observed in the optical microscopy images of rough Al samples coated with SA Figure 6.4. Corrosion products are also believed to play an important role in decreasing hydrophobic properties (Figure 6.1). That is, the top-layer partially destroyed by water may expose patches of un-protected bare Al surfaces which may become corroded upon coming into contact with water molecules. The corrosion products, which are normally hydrated oxides of metals, have intrinsic CA values which are much lower than those of SA coating, thus contributing to the decreased CA observed in Figure 6.1 over time.

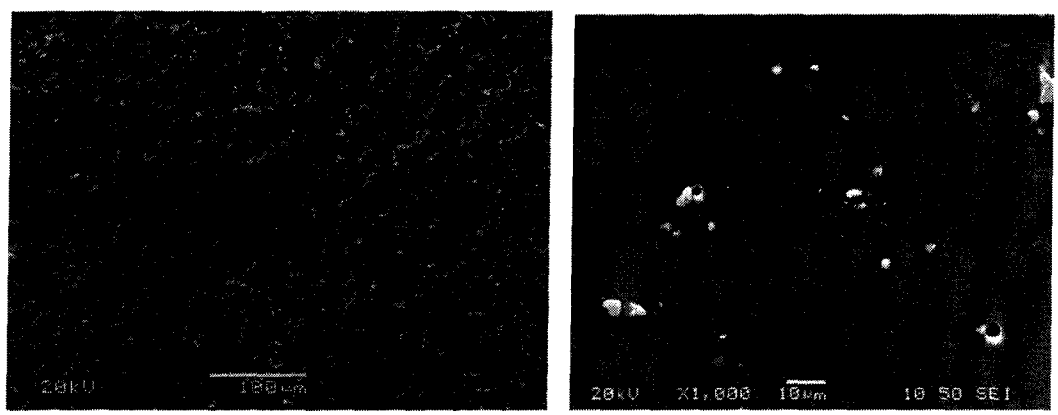

Figure 6.3. SEM images of rough Al surface coated with SA (top) and non-etched (mirror-polished) Al surface coated with SA. Magnification is ×1000.

Figure 6.4. Optical microscopy image of rough Al surface coated with SA. Magnification is ×40. The inset image is mirror-polished Al surface to compare with rougher one.

More research on rough superhydrophobic surfaces is needed to acquire a better understanding of how they deteriorate upon contact with water.

6.3 Coating of Etched Al Surfaces *via* FAS-13 and FAS-17

6.3.1 Introduction

The as-prepared Al surfaces etched in HCl were coated with 1H,1H,2H,2H-perfluoro-octyltrichlorosilane (FAS-13) and 1H,1H,2H,2H-perfluorodecyltriethoxysilane (FAS-17)/MeOH. The immersion time in FAS-13 and FAS-17 deposition baths was 50 min. These coatings were believed to cover Al surfaces *via* self-assembling of FAS-13 and FAS-17 molecules. After coating, each sample was rinsed ultrasonically in methanol (MeOH) and annealed in an oven for 2 h at 50°C prior to any experiments or surface characterization. As explained in Chapter 2, fluorine-containing organosilane compounds have low surface energy and they can thus provide enhanced hydrophobic properties on surfaces. Both CA and CAH measurements were made on the prepared samples before and after each icing/de-icing cycle. Coated samples were immersed in water to examine the stability of the coatings in water over time. The ice-repellent performance of these samples was also carefully investigated, the result of which will be presented in the upcoming chapter.

6.3.2 Hydrophobic Properties

The first contact angles studied of rough Al samples coated with FAS-13 and FAS-17 were measured by means of a water contact angle goniometer, they registered a CA >150° indicating superhydrophobic surfaces. Figure 6.5 presents contact angle values as a function of immersion time in deionized water for these samples. The average initial contact angle of ~155 ± 5° with the minimal error deviation of 4.5% was found for both samples.

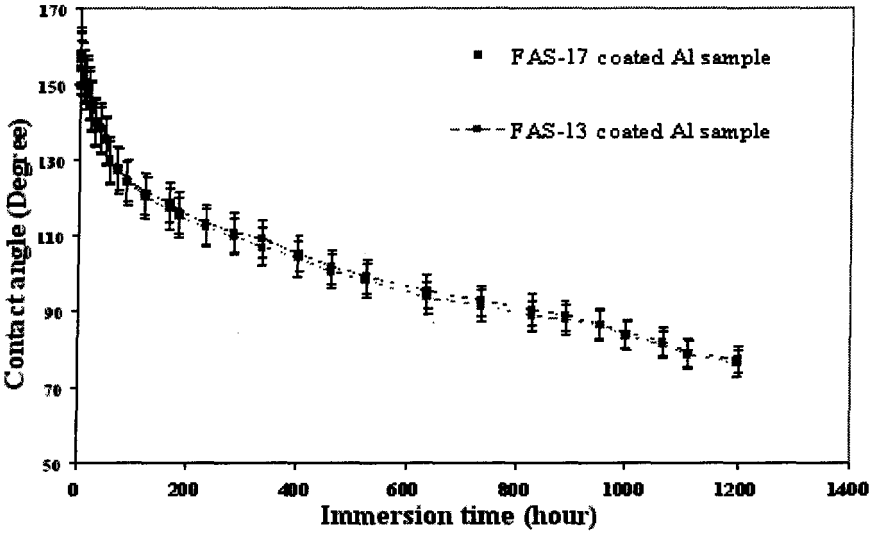

Figure 6.5. Contact angle *vs.* immersion time in deionized water for rough Al samples coated with FAS-13 and FAS-17.

The same tendency of CA values deteriorating over time, as was observed in the case of rough Al samples coated with SA, was also established for these fluorinated samples. Indeed, by immersing samples in deionized water, the CA values were observed to decrease gradually over time. It was established that both coatings slowly lost their hydrophobic properties after ~800 h of immersion in water. This may be observed as a considerable decrease of water CA values (Fig.6.5, right). It is clear that the surface hydrophobic properties of these rough coated Al samples decrease significantly over time. This tendency to lose hydrophobicity is in all likelihood due to the partial or complete decay of the low surface energy layer coated on Al substrates. The hydrophobic properties were thus decreased after ~800 h immersion in water, as shown in Figure

6.5. The observed deteriorating in sample hydrophobicity can be referred to not dense enough SA layers prepared on Al surfaces to stop water molecules penetrating through the coating. Figure 6.6 shows water droplet images on FAS-17 coated aluminium surfaces before (left) and after 1100 h immersion in water (right). These layers of FAS were once again believed to be insufficiently packed to prevent water molecules from penetrating through the coating. A significant decrease in surface superhydrophobicity may clearly be observed in Figure 6.6 (right), which implies some decay of the coating layer.

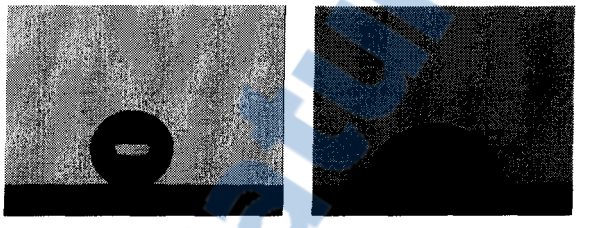

Figure 6.6. Water droplet images on FAS-17 coated Al surface before (left) and after 1100 h immersion in water (right).

Figure 6.7 presents contact angle values as a function of immersion time in deionized water for the rough Al samples coated with SA, FAS-13 and FAS-17 to facilitate comparing the results obtained. As is evident, Al samples coated with FAS compounds, as well as with SA, were seen to demonstrate superhydrophobic surfaces with an initial CA >150°, as shown in Figure 6.6, left.

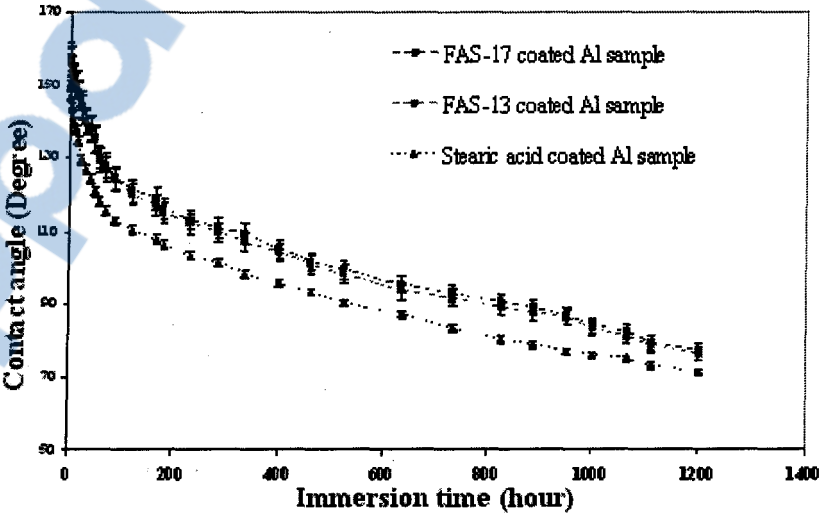

Figure 6.7. Contact angle *vs.* immersion time in deionized water for rough aluminium samples coated with SA, FAS-13 and FAS-17.

All the coatings, however, were found to display the same tendency whereby they lose their superhydrophobic properties after several days of immersion in water, as shown in Figure 6.6, right. Indeed, the corrosion is also believed to have contributed to the decrease in hydrophobic properties for samples immersed in water over a significant period of time.

6.3.3 Surface Characterization

SEM/EDS images of the etched Al samples coated with FAS-13 and FAS-17 were taken with accelerating voltages of 20 kV and presented in Figure 6.8.

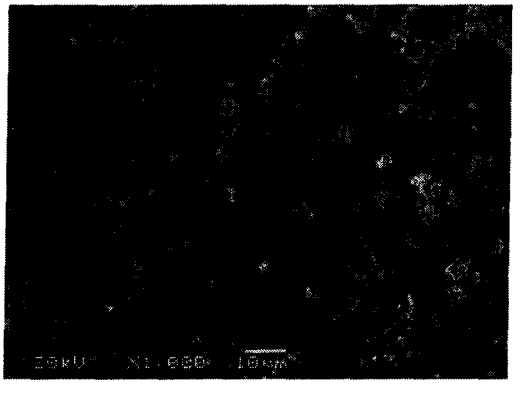

Figure 6.8 SEM image of rough aluminium surface coated with FAS-13.

Layers of FAS-13 and FAS-17 on the rough etched surfaces are observed to maintain the morphological features of the etched substrate, as shown in Figure 6.8. Analysis by electron dispersive spectrography was used to investigate the chemical composition of the surfaces under discussion. Figure 6.9 illustrates the EDS spectra of FAS-17 (before and after immersion under water) and of non-coated etched Al substrates; these results show significant chemical changes following the sample immersion in deionized water. While a Si peak is detected before sample immersion in water, as shown in Figure 6.9 (b) implying the presence of a layer of FAS-17 on Al surfaces, there is no significant amount of Si remaining on the same sample after 800 h immersion in water, Figure 6.9 (c).

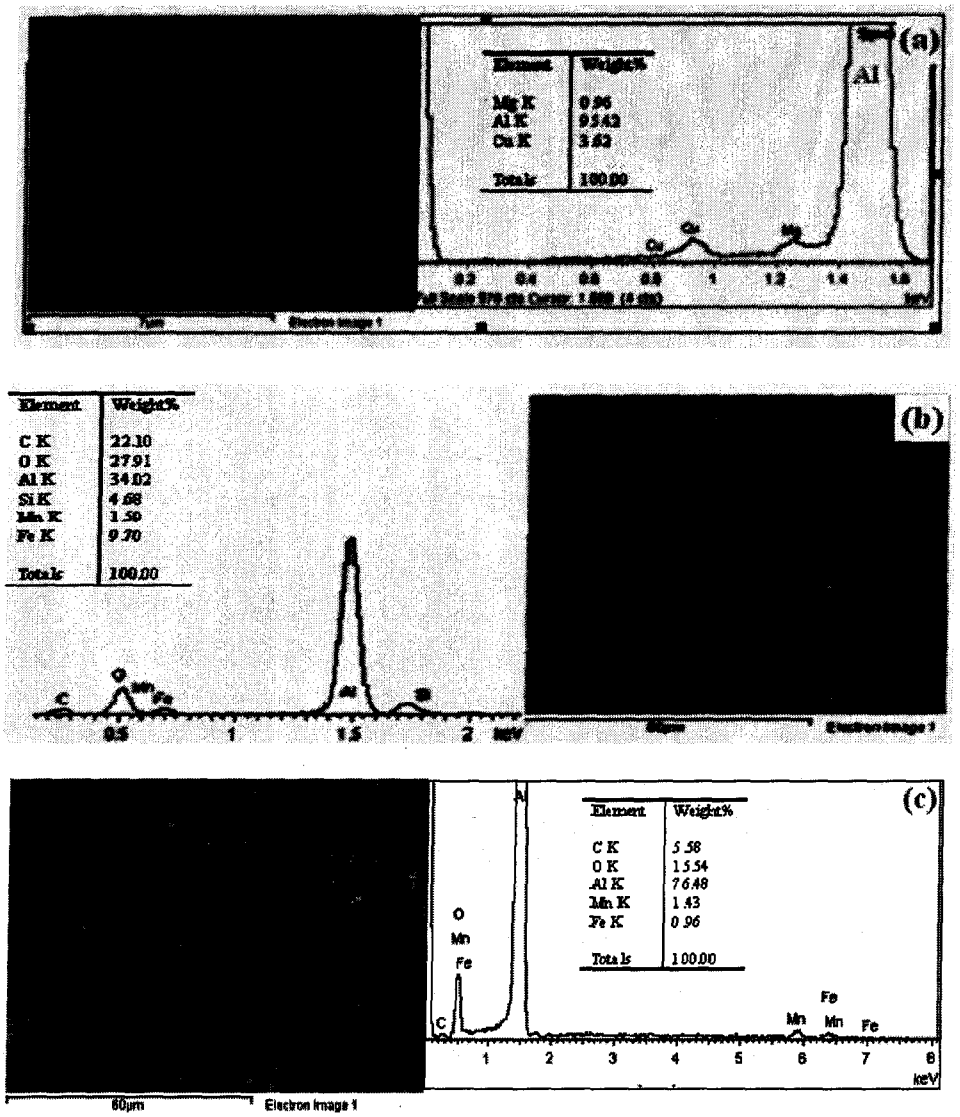

Figure 6.9. SEM images and corresponding EDS spectra of (a) the non-coated and the etched Al substrates coated with FAS-17; (b) before and (a) after the stability test.

It may be ascribed to the hydrolysis of the -O-Si-R bond through the penetration of water molecules and the gradual decay of the FAS-17 layer. The peaks of C and O correspond to contamination on the surface. Similar results were also observed for the FAS-13 coated rough Al samples. Optical microscopy images illustrated the rough features on Al samples coated with FAS-13 and FAS-17. The images of the FAS-17 coated Al sample may be observed in Figure 6.10. Figure 6.11 presents a 3-dimensional topography AFM image of a rough Al surface coated

with FAS-17 in a scan size of 20x20 μm taken following surface coating. Analyses obtained by means of AFM techniques demonstrated the rough features of etched coated surfaces with root-mean-square (rms) roughness values of ~400 nm.

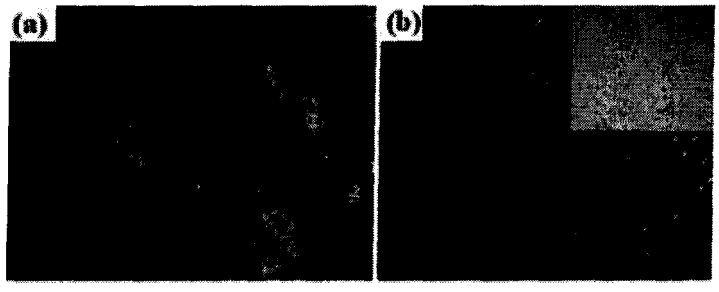

Figure 6.10. Optical microscopy images of a rough Al surface coated with FAS-17. Magnification is (a) ×40 and (b) ×100. The inset image is mirror-polished Al surface (magnification is ×40).

In both samples coated with FAS-13 and FAS-17 (only the AFM image of the sample coated with FAS-17 is provided below), rough structures were obtained and thus based on the Cassie-Baxter model, air entrapment into the structures occurred when the water droplet was placed on top. As mentioned in the earlier part of this section, high CA values, as well as low CAH (see chapter 7), were obtained on such surfaces. Thus, in the same way was observed in the case of the SA coated rough surfaces, a "*slippery*" surface state was observed for water droplets on the FAS-13 and FAS-17 samples.

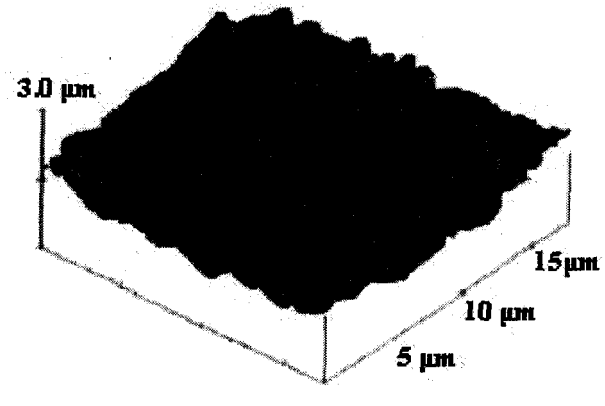

Figure 6.11. 3-D AFM image of rough Al sample coated with FAS-17. The root-mean-square (rms) roughness value was about 400 nm.

CHAPTER 7

EXPERIMENTAL RESULTS AND DISCUSSION: ICE-RELEASING PERFORMANCE OF COATED AL ALLOY SURFACES

7.1 Introduction

The investigation of anti-ice performance, as well as the study of hydrophobic and superhydrophobic properties following ice adhesion tests, were all subsequently conducted on the pre-prepared hydrophobic and the superhydrophobic Al samples under atmospheric icing conditions. As a result of applying low-free surface energy coatings on flat Al samples with hydrophobic surfaces as well as the reduced contact area of water droplets in the case of rough surfaces for the superhydrophobic samples, therefore, it is expected that ice will adhere less to those surfaces. As explained earlier, either hydrophobicity or superhydrophobicity can be considered prerequisites for icephobicity, and can thus lead to preventing ice from adhering to a substrate surface or at least to minimizing the strength of ice adhesion to the surfaces. The results of the above investigation will be presented and discussed in the current chapter.

Briefly, ice can adhere to all types of surfaces. The strength of ice adhesion to aluminium or stainless steel varies from ~0.03 to 2 MPa depending on the test conditions applied and the surface features [186]. In this study, the ice adhesion strength of flat and rough hydrophobic coatings, based on different materials and with different surface topography, was evaluated in order to assess the icephobic nature of the coating applied. This made it possible to compare ice adhesion strength on non-coated as-received and mirror polished Al, flat passivated Al sample having a CA of ~105° and hydrophobic micro-structured Al surfaces displaying high water

CA $\geq 150^{\circ}$ or more. Several techniques and methods do exist to evaluate ice adhesion strength values; most of them, however, are expensive and complicated to use. In this study, the ice adhesion strength was evaluated by spinning the samples in a centrifuge adhesion test machine at a constantly increasing speed to determine the rotational speed at which detachment of the ice from the sample surface occurred; this technique is simple and was used several times by other groups and researchers [73, 74, 182]. Artificially created glaze ice, similar to the naturally accreted form, was deposited on these surfaces by spraying super-cooled micro-droplets of water in a wind tunnel at subzero temperature (-10°C). The ice adhesion strength was evaluated by spinning the samples in a centrifuge at a constantly increasing speed. Ice adhesion strength, the ice adhesion reduction factor *(ARF)* and surface hydrophobicity/superhydrophobicity after several icing/de-icing cycles were evaluated by means of a centrifuge adhesion test machine in conjunction with CA and CAH measurements. For further details regarding this series of experiments and the tools used, kindly refer to Chapter 4.

7.2 Flat Hydrophobic Surfaces

7.2.1 Shear Stress of Ice Detachment *vs.* Icing/De-Icing Cycles for Flat Al Surfaces Coated with SA and ODTMS

To determine the percentage of ice adhesion reduction on coated surfaces, ice adhesion to as-received and mirror-polished Al samples was also measured under the same conditions as those prevailing before the experiments. Figure 7.1 shows the shear stress of ice detachment on different flat coated samples tested as a function of icing/de-icing cycles. Adherence measurements were made in a cold room maintained at -10°C, with glaze-type ice having a measured density of 0.87 g/cm^3 ± 0.02. For each coating studied, one sample was subjected to at least 12 successive icing/de-icing operations. Polished bare Al was used as a standard showing

an ice detachment shear stress of 445 ± 20 kPa, which is comparable to the values recorded in the relevant literature [159, 167]. The corresponding value for the mirror-polished Al surface (350 ± 19 kPa) is also shown in Figure 7.1. Ice adhesion values measured on the coated hydrophobic surfaces varied between 191 to 205 kPa with an average standard deviation of 12-15%. The numerical differences fall within the boundaries of experimental error. The hydrophobic properties of the surfaces were examined after ice removal. All samples treated with a coating showed noticeably close shear stress values, implying the presence of similar ice adhesion strength values on all alkyl-grafted flat samples. The uncoated polished flat sample showed an average ice detachment shear stress of ~445 ± 20 kPa, while its counterparts coated with alkylsilane or stearic acid coatings showed reduced values of ~195 kPa. This reduction may be attributed to the presence of low surface energy coatings on the samples. It will be observed that all samples allow for values of ice adhesion strength at least ~1.5 times lower than those obtained on the mirror-polished sample, and ~2 times lower than those on the as-received Al alloy sample having a rougher finish. It will also be seen that the ice-releasing performance of the samples did not change greatly after 12 icing/de-icing cycles, as only a small increase in ice adhesion strength may be observed after these events. The ice adhesion strength values of nano-particle-based coated surface were presented in Figure 7.1 to compare with values obtained for flat surfaces coated with stearic acid or alkylsilane. This sample was spin-coated by using a methanol/ethyleneglycol (20:1 v/v) suspension of Ag nano-particles (100-600 nm in size), after which the coating was annealed (2h at 200°C in air), dip-coated in a water- Zonyl 8740 (10:1 v/v) solution for 1h, and finally dried in air at 100°C for 3 h to remove any volatile components. This sample was expected not to be mechanically strong as its rough structures were based on relatively loose Ag nanoparticles sintered during annealing to better bond to each other followed by passivating the final rough structure with a thin fluoropolymer later [183, 187].

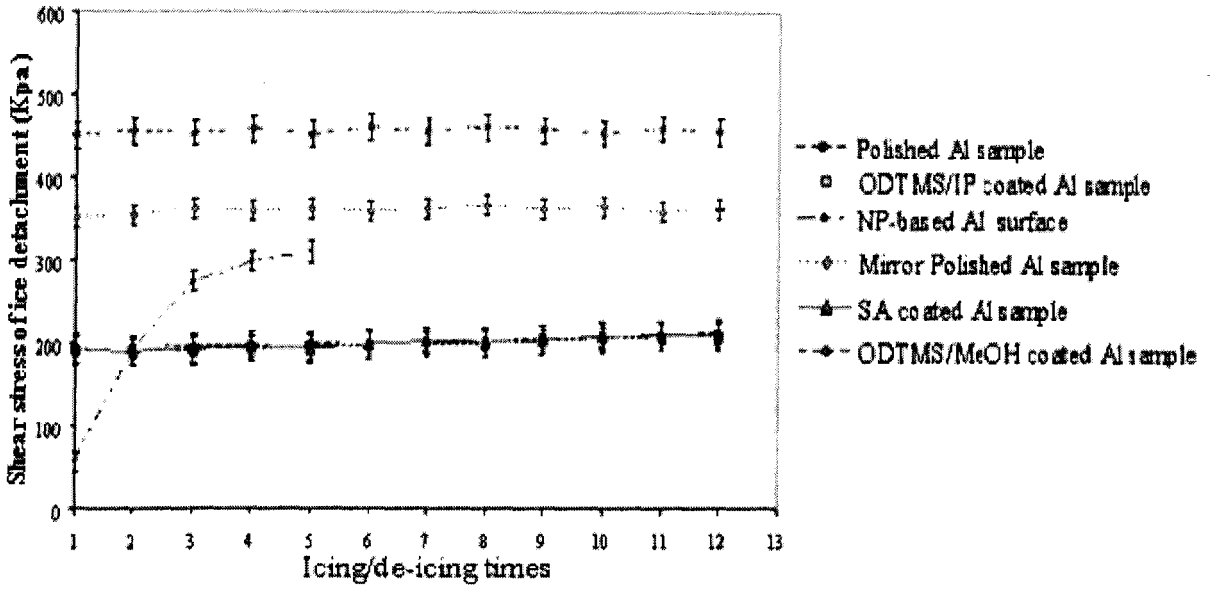

Figure 7.1. Shear stress of ice detachment *vs.* icing/de-icing cycle number for polished, stearic acid, nano-particle based and ODTMS coated Al samples.

Alkylsilane coated flat surfaces show higher adhesion strengths of ~195 kPa compared to the nano-particle-based coated surfaces displaying strengths of ~55 to 60 kPa. However, the latter value remained lower only during the first icing/de-icing cycle as will be seen clearly in Figure 7.2 then increasing rapidly as opposed to the number of icing/de-icing cycles. This observation implies unstable ice-releasing properties of the superhydrophobic, or rough, sample based on a mechanically soft material composed of loose nano-particles passivated with a fluoropolymer [137]. Further investigations were carried out by determining the adhesion reduction factor *(ARF).* The highest *ARF* value of at least 1.8 was obtained on the ODTMS/IP coated Al surface compared to 1.5 on the SA coated Al sample, see Figure 7.3. These results show that ice adhesion is at least two times lower on the coatings in comparison with the mirror-polished Al sample, which would lead to easier removal of the adhered ice from those surfaces, as shown in Figure 7.3. Only a slight decrease in *ARF* values may be observed after as many as 12 icing/de-icing events in most cases. This reduction is believed to be associated with a partial decay of the coatings caused by their contact with super-cooled water droplets, similar to those consequences observed for experiments with sample immersion in deionized water.

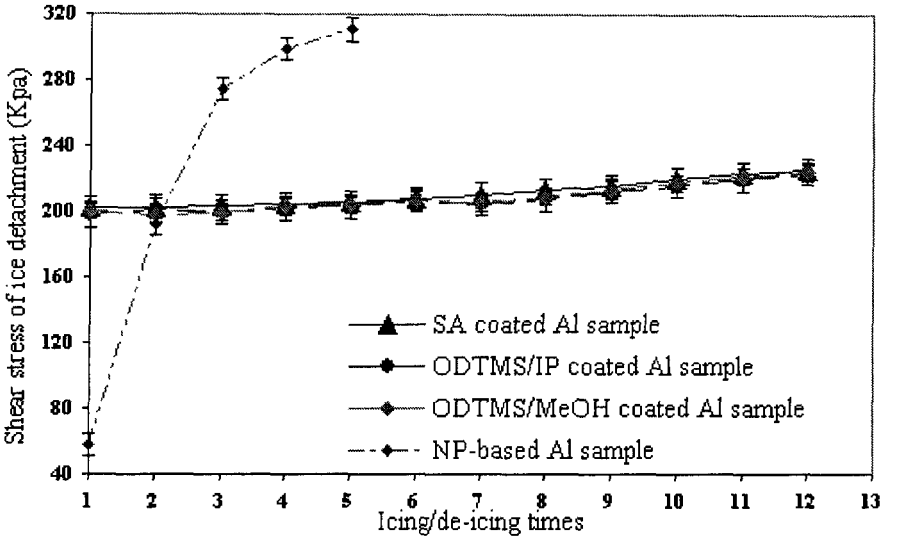

Figure 7.2. Shear stress of ice detachment *vs.* icing/de-icing cycle number for flat Al samples coated with stearic acid, ODTMS/IP, ODTMS/MeOH and rough nano-particle based Al samples.

A similar dependency of ice adhesion strength was also obtained for Al samples coated with ODTMS/MeOH. Since the SA film deposition conditions applied in this study differed from those used in work [183], the properties of the resultant film (including surface coverage, stability, hydrophobicity and ice repellency) were found to be different from those previously reported in [183].

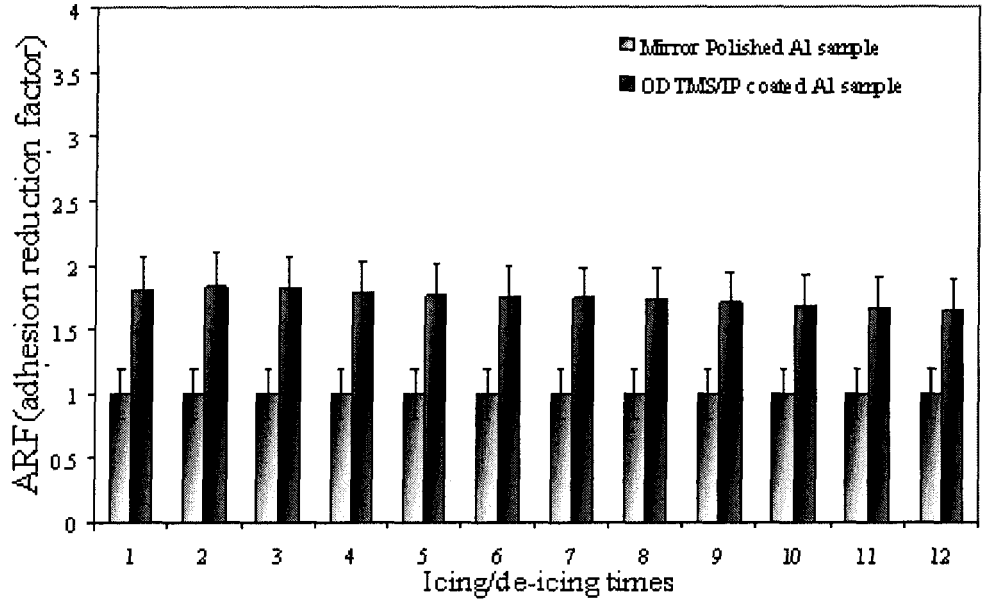

Figure 7.3. Ice adhesion reduction factor (*ARF*) as a function of icing/de-icing cycles on mirror-polished and ODTMS/IP treated Al surfaces.

The question is whether these hydrophobic properties persist following ice detachment from the coated surfaces or not? This was studied by means of a set of experiments, performing contact angle measurements on the samples in question after each icing/de-icing event.

7.2.2 Contact Angle as a Function of Icing/De-Icing Cycles for Flat Al Samples Coated with ODTMS and Stearic Acid

An "icephobic" coating can reduce the adhesion of ice; the ice can thus be more easily removed, or de-iced with less force, ideally just by means of wind and natural vibrations [184]. A slight decrease in their CA values was observed after almost each icing/de-icing cycle, as shown in Figure 7.4. In other words, the hydrophobic properties of each coated sample were gradually reduced after icing/de-icing events. All samples, however, allowed for ice adhesion shear stress values (IAS) of at least ~1.5 times lower than those obtained on the mirror-polished sample, and ~2 times lower than those on the as-received AA sample, as shown in Figure 7.1 and Figure 7.3. The ice-releasing performance of the samples did not change to any great extent after 12 icing/de-icing cycles.

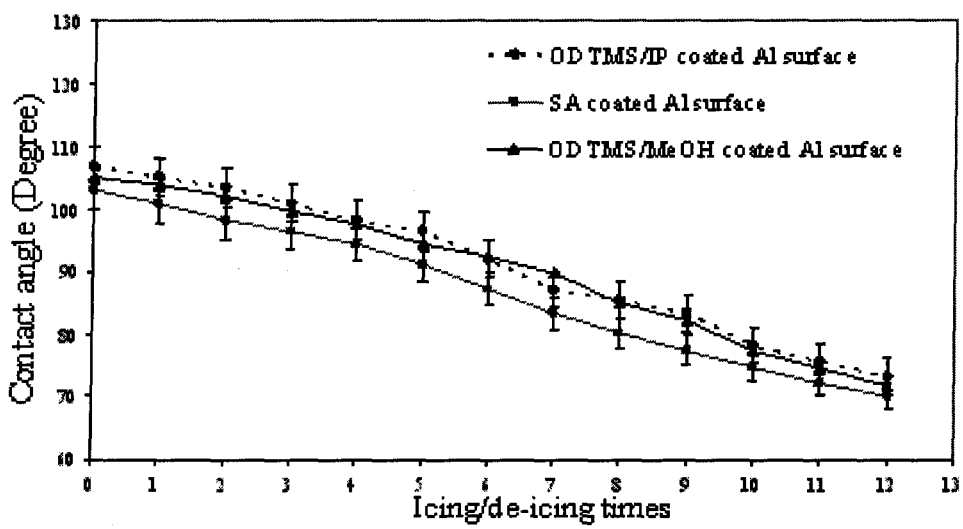

Figure 7.4. Contact angle as a function of icing/de-icing cycles for ODTMS/MeOH, ODTMS/IP and stearic acid coated samples.

7.2.3 Shear Stress of Ice Detachment *vs.* Icing/De-Icing Cycles for Flat Al Surface Coated with BTSE/ODTMS and TEOS/ODTMS

Figure 7.5 shows the shear stress of ice detachment values on both coated Al samples with BTSE/ODTMS and TEOS/ODTMS as a function of icing/de-icing cycles. All experimental conditions were discussed in detail in Chapter 4. For comparison, ice adhesion on as-received and mirror-polished Al was measured under the same conditions as on standard samples showing ice detachment shear stresses of 445 ± 20 kPa and 350 ± 19 kPa, respectively. As is evident from Figure 7.5, both coated samples show greatly similar ice adhesion behavior.

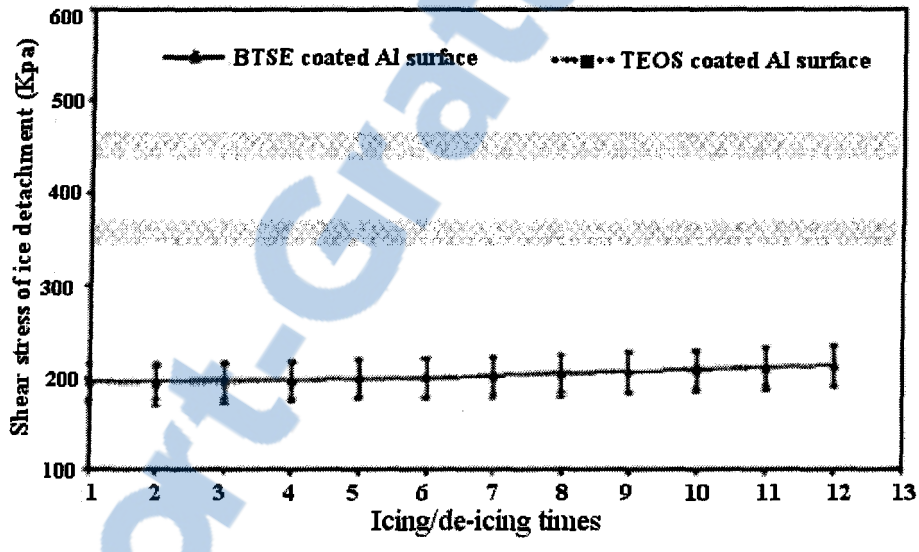

Figure 7.5. Shear stress of ice detachment *vs.* icing/de-icing cycle number for as-received, mirror-polished, BTSE/ODTMS and TEOS/ODTMS treated samples. Grey horizontal bands indicate corresponding results on non-coated as-received and mirror-polished Al surfaces.

While the uncoated as-received sample showed average ice detachment shear stresses of ~445 ± 20 kPa, its counterparts coated with BTSE/ODTMS or TEOS/ODTMS showed reduced values of ~193 to 198 kPa. This reduction can be ascribed to the presence of the low surface energy coatings on the samples. Both samples allow for values of ice adhesion strength (IAS) at least ~1.5 times lower than those obtained on the mirror-polished sample, and ~2 times lower than those on the as-received AA sample. Only a small increase in IAS may be observed after

12 icing/de-icing events, thus the ice-releasing performance of the samples did not appear to change greatly.

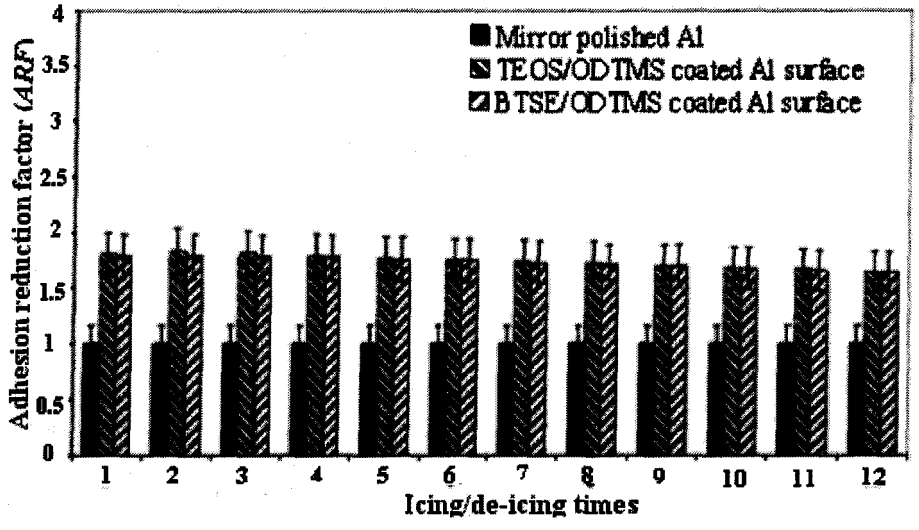

Figure 7.6. Ice adhesion reduction factor (*ARF*) as a function of icing/de-icing cycles on mirror-polished, BTSE/ODTMS, and TEOS/ODTMS treated Al surfaces.

The *ARF* results show at least 1.5 times lower ice adhesion on the coatings in comparison with bare Al, as may be observed in Figure 7.6. Only a slight decrease in these values may also be observed after as many as 12 icing/de-icing events in most cases. It is a result of incomplete degradation of the coatings on Al substrates caused by their contact with ice.

7.2.4 Contact Angle as a Function of Icing/De-Icing Cycles for Flat Al Samples Coated with BTSE/ODTMS, TEOS/ODTMS

For Al samples coated with BTSE/ODTMS and TEOS/ODTMS, measurement of the contact angle as a function of icing/de-icing cycles was also conducted to investigate sample hydrophobicity following ice detachment. For this series of samples, a slight decrease in CA values was also observed after each icing/de-icing event possibly attributable to the partial loss of the hydrophobic coating on Al surfaces after 12 icing/de-icing cycles, as may be seen in Figure 7.7.

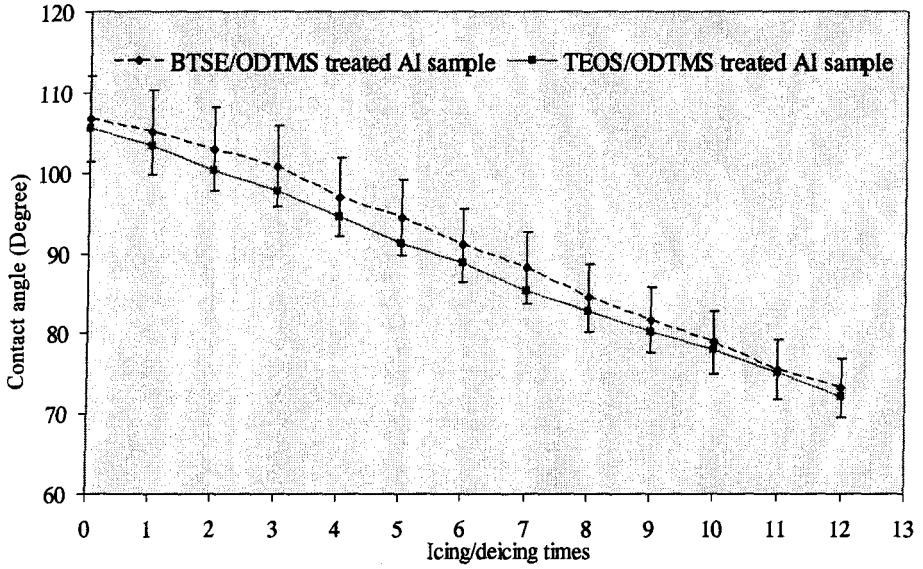

Figure 7.7. CA as a function of icing/de-icing cycles for BTSE/ODTMS, TEOS/ODTMS coated samples.

We thus assume that the ODTMS silane layers degraded on BTSE and TEOS under layers in a manner similar to that on polished Al surfaces. This implies that water could attack the R-Si-O- bond, hydrolyzing it and thus resulting in loose silanol species and hydrophilic –OH group on the surface.

7.3 Rough Superhydrophobic Al Surfaces

7.3.1 Shear Stress of Ice Detachment *vs.* Icing/De-Icing Cycles for Rough Superhydrophobic Al Samples Coated with FAS-13, FAS-17 and SA

Figure 7.8 shows the shear stress of ice detachment on the etched coated samples as a function of the number of icing/de-icing cycles. Initial values on the rough surfaces varied between ~55 and ~90 kPa. The Al sample coated with FAS-17 generally showed lower values of shear stress due to a larger amount of surface F-atoms that leads to lower free surface energy and therefore greater icephobicity.

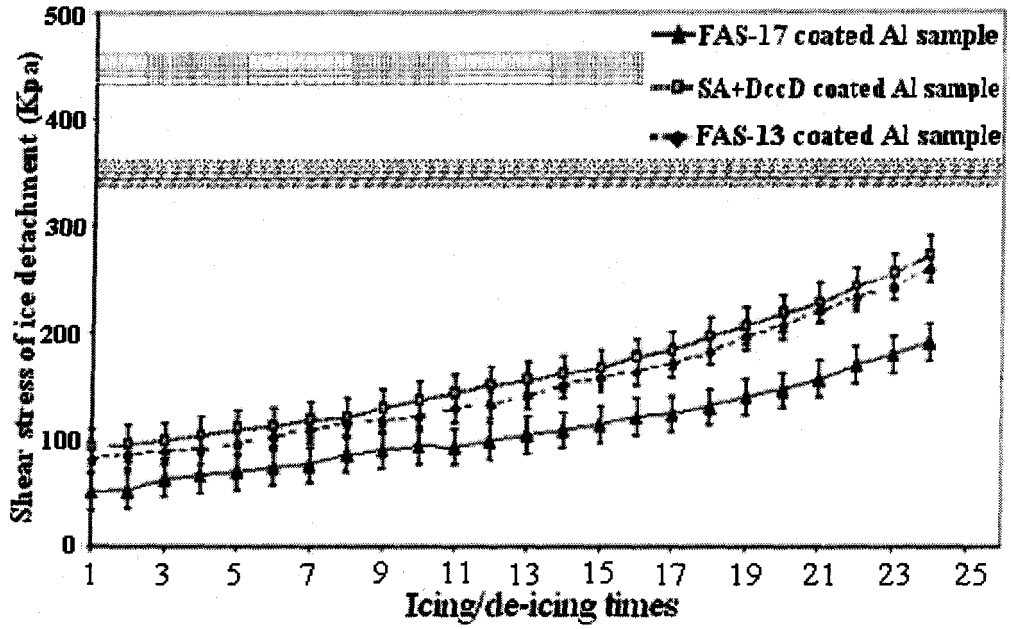

Figure 7.8. Shear stress of ice detachment *vs.* icing/de-icing cycle number for as-received, mirror-polished, FAS-17, FAS-13 and SA treated surfaces. Grey horizontal bands indicate corresponding results on non-coated as-received (445±20 kPa) and mirror-polished (350±19 kPa) Al surfaces.

All samples allow for initial IAS values at least 4 times lower as for FAS-13 and SA, and ~7 times lower as for FAS-17 than those obtained when using the as-received sample. The ice-releasing performance of the samples changed significantly, however, after 24 icing/de-icing events. A significant increase in the shear stress values may be observed after 24 icing/de-icing events. The adhesion reduction factor values (ARF) also show that ice adhesion is at least 4 (FAS-13 and SA) and ~7 (FAS-17) times lower than on the polished Al standard (Fig.7.9). The *ARF* values are seen to decrease noticeably, however, after 24 icing/de-icing events. This observation implies that the anti-icing performance of rough superhydrophobic samples is time-dependent, as some mechanical damage is likely to occur with such coatings during icing/de-icing events. The large decrease in *ARF* values may be ascribed to the partial decay of the coatings and the rough structure of etched Al surfaces caused by their contact with water and/or accumulated ice during icing/de-icing events. The rough surfaces may also be exposed to mechanical damage during icing/de-icing, namely the expansion of water during solidification.

These phenomena remains to be studied in greater detail in future studies. The results also suggest that more rigid rough surfaces should be found to serve as more stable and durable anti-icing materials.

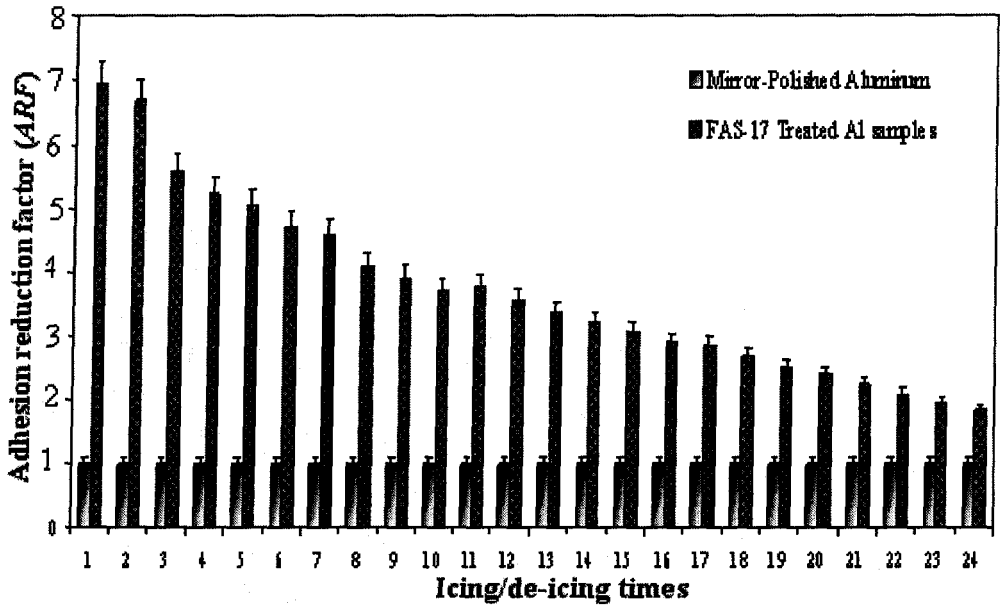

Figure 7.9. Ice adhesion reduction factor (*ARF*) as a function of icing/de-icing cycles on mirror-polished and rough Al sample coated with FAS-17.

7.3.2 Contact Angle as a Function of Icing/De-Icing Cycles for Rough Superhydrophobic Al Samples Coated with FAS-13, FAS-17 and SA

The superhydrophobic performance of ice tested FAS-13, FAS-17, and SA coated etched samples was also investigated by measuring their CA and CAH values as a function of icing/de-icing cycles. A decrease of CA values was observed in all cases Fig.7.10, which may be attributed to a loss of surface hydrophobic properties after as many as 24 icing/de-icing cycles. This observation is also consistent with the previously proposed mechanical damage of the rough structures during icing/de-icing cycles, since lower roughness of hydrophobic materials is normally associated with the smaller CA values.

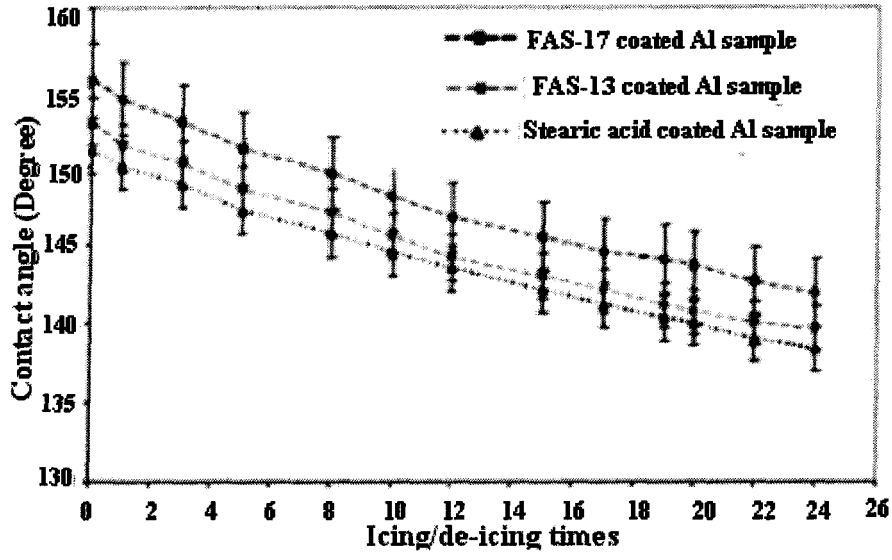

Figure 7.10. Contact angle as a function of icing/de-icing cycles of rough Al samples coated with FAS-13, FAS-17 and SA.

After each icing/de-icing event and before the succeeding cycle, the CA values of all the re-coated surfaces were also measured. This series of trials was carried out to investigate whether the loss of icephobic properties was due to the decay of low surface energy layers or to the damage of the nano-rough asperities of the coated samples, or even by both of the problems mentioned, as may be seen in the bold graphs shown in Figure 7.11.

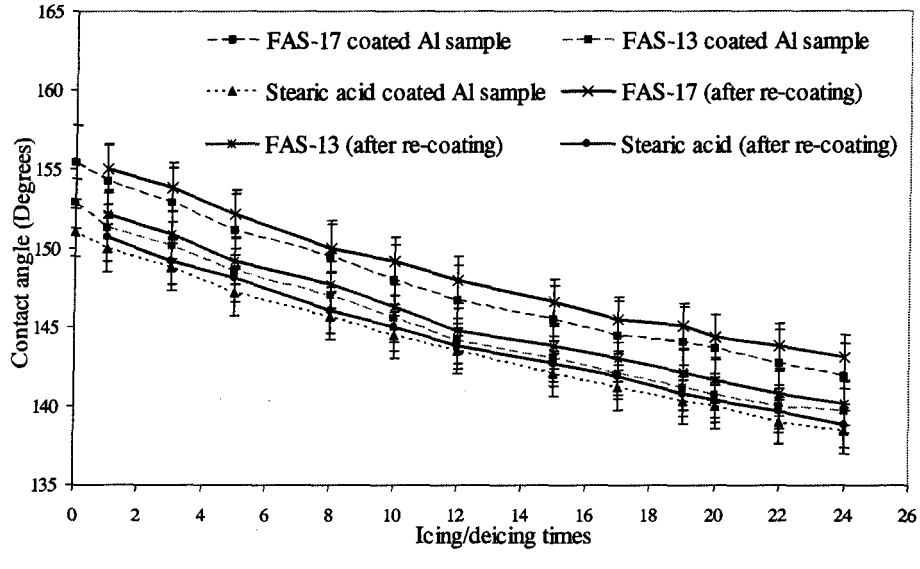

Figure 7.11. Contact angle as a function of icing/de-icing cycles for rough Al samples re-coated with FAS-13, FAS-17, and SA.

Figure 7.11 shows clearly that even after re-coating of the surfaces and before the succeeding icing/de-icing cycle, the CA values decrease slightly. It may thus be concluded that the loss of icephobicity is due both to the gradual damage caused by the nano-rough structure of the coated samples and to the removal of certain portions of the low surface energy coatings used. Another method used in characterizing the wetting characteristics of the prepared surfaces is to measure the CAH, *i.e.* the difference between advancing and receding CAs, as illustrated in Fig.7.12. As mentioned earlier, the contact angle hysteresis, or CAH, is defined as the difference between the advancing and receding CAs of water obtained on a surface during the motion of a water drop in one direction. The CAH value will reveal the ability of a water drop to stick or slide on a surface. It has been demonstrated that the CA continues to increase when the roughness factor exceeds a certain level, whereas the hysteresis starts to decrease because of transition from the Wenzel regime to the Cassie-Baxter regime [107].

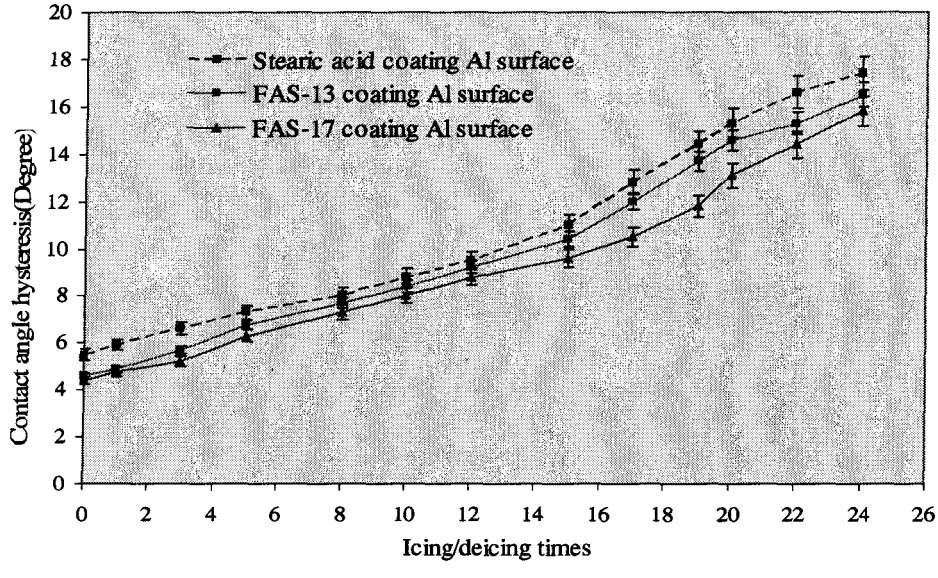

Figure 7.12. CAH as a function of icing/de-icing cycles of rough Al samples coated with FAS-13, FAS-17, and SA.

All rough Al surfaces coated with SA, FAS-13, and FAS-17 provide superhydrophobicity with the initial CA as high as ~150° and CAH as low as ~4 to 6° from which water drops roll off easily even with the slightest tilt of the sample. The cause of such a low initial hysteresis on

these surfaces may be attributed to the presence of a rough structure and coating with low free surface energy material which eventually reduces the area of contact between the drop and the rough surface.As may be seen in Fig.7.12, however, after as many as 24 icing/de-icing cycles, the CAH changed and turned to ~15-17°. As will be clear from Fig.7.12, CAH undergoes an increase as the surfaces are subjected to icing/de-icing, from ~4-6° to ~16°, although the water drops still roll off the surfaces. This behavior can be explained by gradual damage of the surface asperities during icing/de-icing, as mentioned earlier. Figure 7.13 illustrates the corresponding images of the water droplet on the same superhydrophobic sample coated with FAS-13 to measure the CAH before (a) and after (b) 24 icing/de-icing cycles.

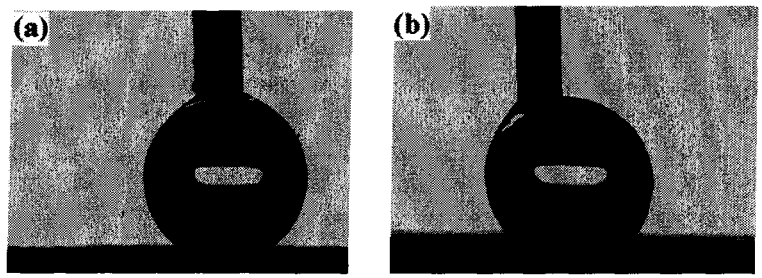

Figure 7.13. Water droplet images on superhydrophobic Al surface coated with FAS-13 (a) before, and (b) after 24 icing/de-icing cycles.

7.4 Conclusions

A series of experiments was carried out to study and then to reduce the adhesion of ice to the surface of Al samples, based on improved hydrophobic properties of both flat and rough Al surfaces passivated with the proper layers. Lower ice adhesion to those surfaces was obtained by applying low surface energy coatings, as for hydrophobic samples, as well as appropriate micro-nano roughness, as in the case of superhydrophobic samples, providing ice-repellent performance. Alkyl-terminated coatings were prepared by depositing layers of stearic acid,

ODTMS, FAS-13, and FAS-17 on flat and rough AA surfaces. The ice-releasing performance of these coatings was examined by accumulating glaze ice in a wind tunnel at subzero temperatures. All flat coated surfaces demonstrated ice adhesion strength (IAS) about ~2 times lower compared to the uncoated as-received Al surfaces. In addition, all rough finished samples allowed for IAS values of at least ~4 (FAS-13 and SA) and ~7 (FAS-17) times lower than those obtained on the un-coated as-received surfaces. The values remained mainly unchanged after as many as 12 icing/de-icing events for flat surfaces. After 24 icing/de-icing experiments, however, rough surfaces demonstrated somewhat different behavior. Ice adhesion strength was increased significantly on those surfaces by a factor of ~2 after 24 icing/de-icing cycles.

Hydrophobic properties of all flat and rough coated Al surfaces were investigated after each icing/de-icing cycle to study their stability after ice releasing. All coated samples showed a slight decrease in CA after icing/de-icing cycles. Thus, the ice-releasing performance of all the samples tested was found to be time-dependent. This observation implies that the stability and ice-releasing performance of the candidate icephobic materials should be studied with greater attention in order to further develop realistically durable and highly attractive anti-ice materials for widespread application.

CHAPTER 8

CONCLUSIONS AND RECOMMENDATIONS

8.1 Conclusions

With a view to the prevention of ice adhesion and corrosion of Al alloy surfaces, the relevant literature on the mechanisms of ice adhesion on Al surfaces, as well as corrosion phenomena, has been scrutiny reviewed. Since hydrophobicity is a key requirement leading to icephobic properties, thus low surface energy coating material is needed. Among candidate materials for the under-layer, a number of inorganic conversion coatings, such as permanganate-based coatings, together with certain organosilane-based layers were investigated, since they are environmentally friendly compared to the presently used chromate-based treatments. At the same time, several low-surface-energy materials, such as alkylsilanes, stearic acid, and fluoroalkylsilane-based layers were tested for use as the upper layers. There are a number of process parameters which directly affect the final surface structure and the reduction of ice adhesion on the surfaces. For these goals, it is necessary to control two essential properties, namely, surface roughness and low surface energy. Passivation of a surface with low surface energy materials, whether stearic acid or fluoroalkyl-silane, may also be applied to obtain a surface with hydrophobic properties. A series of studies was conducted with a view to examining the effects of roughness and other experimental conditions on the adhesion of ice and on coating durability. In this work, different organic coatings were systematically studied; these were based on alkyl groups grafted onto Al surfaces as potential ice and wet-snow repellent layers, including some chemical conversion coatings based on permanganate coatings as

potential corrosion resistance layers. Alkyl-terminated surfaces were prepared *via* wet-chemistry techniques by depositing thin films of stearic acid, octadecyltrimethoxysilane, FAS-13, and FAS-17 on both mirror-polished and etched Al alloys AA6061 and AA2024 surfaces, considering that both are widely used in many sectors of the industry concerned. Similar coatings were previously reported to bring about a twofold reduction in ice adhesion, compared to uncoated Al [2], although no systematic work has been carried out in this area since that time. Both the stability of such coatings in a water environment and their ice-releasing properties were carefully investigated. On the basis of the experimental results and their analysis the following conclusions may be drawn:

1. The stability of such prepared coated surfaces in water was tested by means of contact angle measurements, clearly showing that all coatings gradually lose their hydrophobicity after ~1000 h immersion in water; this was illustrated by a considerable decrease in the water contact angle. Although water drops did not adhere to flat surfaces, regardless of the type of coating, they did, however, decay either partially or completely after 1000 h immersion in water; water could thus reach the substrate resulting in a decrease in the water contact angle and a partial corrosion of the surfaces.

2. At the same time, ice-releasing properties of the same coated surfaces were investigated by accumulating glaze ice prepared by spraying super-cooled micrometer-sized water droplets in a wind tunnel at subzero temperatures and a wind speed of 11 m/s to simulate the conditions of natural outdoor atmospheric icing.

3. Ice adhesion strength and the adhesion reduction factor (*ARF*) were evaluated. All flat coated surfaces demonstrated shear stress of ice detachment values about ~1.5 times lower than uncoated mirror-polished Al surfaces, and ~2 times lower than those for the as-received Al sample with a rougher finish. In other words, the atmospheric ice accreted on this type of coating surface can be much more easily detached from them than from bare Al surfaces.

4. Meanwhile, the *ARF* values remained mainly unchanged after as many as 12 icing/de-icing events with no significant changes to be observed in ice adhesion strength, thereby showing great promise. The coatings in question proved to be relatively stable in subsequent icing/de-icing cycles. The slight increase in ice adhesion strength may be ascribed to a slight degradation of the coatings upon contact with water.

5. The results obtained demonstrate that the strength of ice adhesion to flat surfaces depends to a great degree on the surface finish; the smoother surfaces were the smaller adhesion of ice was observed.

6. Some chemical conversion coatings such as permanganate conversion coating (PCC) were also considered as under-layers providing good anti-corrosive protection according to SEM observations.

7. Superhydrophobic properties were also obtained by chemically etching Al surfaces with hydrochloric acid followed by the application of low surface energy coatings. The etched surfaces, when coated with low surface energy material, allowed ice to form under freezing conditions with lower accumulation rates compared to the flat coated Al surfaces; this may be attributed to the presence of nano-roughness and the application of the low surface energy coating, ultimately leading to the lower wetting behavior of water drops under freezing conditions. None of the samples showed superhydrophobicity, CA>150°, without displaying well developed micro/nano-roughness; this may be ascribed to switching the wetting regime from the Young-Laplace regime to the Cassie-Baxter regime.

8. The shear stress of ice detachment was not the same for etched Al surfaces. All rough finished samples allowed for values of ice adhesion shear stress (IAS) of at least ~4 times lower (FAS-13 and SA) and ~7 times lower (FAS-17) than those obtained on the un-coated as-received surfaces. A dependence of ice adhesion strength on roughness was observed in these cases.

9. After 24 icing/de-icing experiments, however, rough surfaces demonstrated somewhat different behavior. Ice adhesion strength was increased significantly on those surfaces by a factor of ~2 after 24 icing/de-icing cycles. This increase in IAS values is believed to be related to the mechanical damage occurring on such surfaces during icing/de-icing cycles and to the partial decay of passivation layers coming into contact with water.

10. The effects of icing on wettability parameters were also studied. Contact angle measurements were carried out on the samples as a function of icing/de-icing cycles to investigate whether or not the hydrophobic properties of the coated samples will persist following detachment of ice from the surfaces. In the case of the flat surfaces, the coatings gradually lost their hydrophobicity after nearly each icing/de-icing events, observable in the form of a considerable decrease in the water contact angle. As a result, the ice-releasing ability of such flat samples tested was found to be time-dependent. This implies that the use of rough superhydrophobic surfaces, extensively claimed in the relevant literature as anti-icing materials, are susceptible to being limited, unless alternative rough materials with much more rigid anti-icing performance can be discovered in the future.

11. All rough coated surfaces gradually lose their hydrophobic properties and show a slight decrease in the CA after 24 icing/de-icing events. Thus, once again, the ice-releasing ability of all of the samples tested was found to be time-dependent.

12. Finally, although both improved corrosion resistance and ice-repellent qualities may be obtained and combined on Al alloy surfaces, all the samples prepared demonstrated relatively fast decay of their topmost passivation layers in contact with water. This decay led to a relatively rapid degradation of the anti-icing properties; based on these observations, therefore, materials with improved stability in water should be developed. In addition, rough superhydrophobic surfaces were found to be mechanically damaged during icing/de-icing

events, implying that rough materials displaying greater rigidity should be tested in future studies as candidates for anti-ice performance.

The great advantage of the work submitted in this thesis, compared to the existing research available to date, is that the strength of ice adhesion in the prepared coatings was conducted between 12 to 24 icing/de-icing cycles; it should be noted that this has never, on record, been done before.

8.2 Recommended Works

For the purposes of this Master's thesis, the research was carried out to investigate and characterize the ice-releasing performance, durability, and corrosion protection of the coating samples. In light of the results obtained in this work, the following recommendations are presented for future work in order to improve the corrosion resistance and hydrophobic properties of the coated surfaces. Further work should be planned to prepare and characterize different coatings for Al alloys, which may also be deemed icephobic materials. It is recommended that a number of harder materials be used to coat Al surfaces, for instance, DLC instead of the organic or inorganic coatings prepared for use in this work, or otherwise to apply other types of chemicals normally used for passivation, *e.g.* OTS, in order to increase the coating durability. The performance of the same coatings from the point of view of corrosion resistance, and hydrophobic or icephobic properties in severe icing conditions, or when subjected to a number of ice accumulation and detachment events, must be considered in order to evaluate the stability and durability of the coating in real-world conditions. At the same time, in order to apply these coatings on a large and industrial scale, further and more detailed studies will be required. As mentioned earlier, the great advantage of this research work, compared to the existing research available to date, is that the strength of ice adhesion in the prepared

coatings was conducted between 12 to 24 icing/de-icing cycles. These numbers of icing/de-icing experiments has never, on record, been done before. Therefore, it can be considered and employ as a first standard system when using same and accurate ice accumulation conditions. Using methods that can calculate the shear stress directly may give more reasonable, trustable results and decreases the certitude of the result since the technique used here quantified the value of shear stress indirectly. It would be of interest if such prepared coatings extend on various types of substrate and investigate their ice-repellent properties as well as corrosion properties by adjusting all proper experimental parameters. In order to study deeply corrosion phenomena and attain a better knowledge for producing anticorrosive coatings, the necessary experimental equipment, *e.g.* potentiostat and galvanostat should be used. The water used in this study was de-ionized water with the set water conductivity of ~0.32 μs/cm at room temperature in order to eliminate free ions resulting from dissolved salts. It may be interesting to perform further experiments to study the influence of temperature and types of water on coating stability and performance. It is also proposed to find out more cost-effective and environmentally friendly chemicals used for coating of Al surfaces.

In the case of rough superhydrophobic surfaces, a modified water-immersion test procedure should be conducted. This procedure involves two steps: the first step is immersion in water and the second comprises a dry period. In other words, rough samples should be immersed in water for a period of time after taking CA measurements, then sample drying in an oven for a few minutes to evaporate, as much as possible, the water which has penetrated the rough asperities. Thereafter, this cycle of immersion in water and drying out in an oven or furnace should be repeated consecutively. These test conditions are indeed closer to those prevailing outdoors in real-life. As superhydrophobic surfaces gradually lose their initial level of ice-repellency and damaged and regarding to difference in degree of deterioration of samples' performance for different rough materials, thus, some superhydrophobic coatings with better

mechanical properties with more rigid and/or stable surface asperities can be found in the future to resist against icing/de-icing cycles more effectively. This direction requires further research and especially laying greater emphasis on the mechanical aspects of rough superhydrophobic surfaces as an important aspect of their durability. Alternatively, smooth surfaces are to be studied as potential ice-releasing surface if no quick solution with apparently more icephobic rough superhydrophobic surfaces can be found.

References

[1] M. Farzaneh, "Atmospheric Icing of Power Networks", Dordrecht, Netherlands: Springer 2008.

[2] B. Somlo and V. Gupta, ''A hydrophobic self-assembled monolayer with improved adhesion to aluminium for de-icing application'', Mech. Mater., 33 (2001) 471.

[3] V. K. Croutch and R. A. Hartley, "Adhesion of ice to coatings and the performance of ice release coatings", J. Coat.Technol., 64(1992) 41.

[4] G. Poots, "Ice and snow accretion on structures", John Willy & Sons Inc., 1996, p.1-5.

[5] R. Menini and M. Farzaneh, "Elaboration of Al_2O_3/PTFE icephobic coatings for protecting aluminium surfaces", Surf. Coat. Technol. 203 (2009) 1941.

[6] G. McClure, K. C. Johns, F. Knoll and G. Pichette, "Lessons from the ice storm of 1998", Proceeding of IWAIS 2002.

[7] D. Kuroiwa, "Icing and snow accretion", Monograph Series of Research, Institute of Applied Electricity, Japan, pp. 1-30, 1958.

[8] I. Imai and l. Chiro, "Studies on ice accretion", Researches on Snow and Ice, No. l,pp.35-44, 1953.

[9] H. Oguchi, "Icing on Electric Wires", Researches on Snow and Ice, No. 1, pp.45-49, 1953.

[10] J. Druez, P. McComber and M. Farzaneh, "Atmospheric icing on a test power line". T. Can. Soc. Mech. Eng., C.S.M.E., Vol. 24, No. 2, 2000, pp. 359-374.

[11] V. F. Petrenko and S. Qi, "Reduction of ice adhesion to stainless steel by ice electrolysis", J. Appl. Phys., 86 (1999) 10.

[12] I. A. Ryzhkin and V. F. Petrenko, "Physical Mechanisms Responsible for Ice Adhesion", J. Phys. Chem. B 101 (1997) 6267.

[13] M. Farzaneh, J. Zhang, M. Frechette, T. Sakakibara, E. Da Silva, "Effects of High Altitude and Atmospheric Icing on the Performance of Outdoor Insulators", IEEE PES Transmission and Distribution Conference, Caracas, August 2006, ID-014.

[14] C. Laforte, J. -L. Laforte, J. C. Carrier, "How a solid coating can reduce the adhesion of ice on a structure", Proceedings of the International Workshop on Atmospheric Icing of Structures (IWAIS), 2002 p. 1-5.

[15] http://water.epa.gov/scitech/wastetech/upload/2002_06_28_mtb_airplnde.pdf: Storm Water Technology Fact Sheet Airplane De-icing Fluid Recovery Systems, EPA 1999, 832-F-99-043.

[16] B. Y. Yang and R. Montgomery, "De-icers derived from corn steep water", Bioresour. Technol., 90 (2003) 265.

[17] A. Nakajima, K. Hashimoto and T. Watanabe, "Invited review, recent studies on superhydrophobic films'', Monatsh. Chem., 132 (2001) 31.

[18] M. Javan-Mashmool, C. Volat, and M. Farzaneh, "A new method for measuring ice adhesion strength at an ice/substrate interface", Hydrol. Process., 20 (2006) 645.

[19] A. Franquet, C. Le Pen, H. Terryn, et al., "Effect of bath concentration and curing time on the structure of nonfunctional thin organosilane layers on aluminium", Electrochim. Acta, 48 (2003) 1245.

[20] T. C. Yip, "Estimating icing amounts caused by freezing precipitation in Canada", Atmospheric Research, 36 (1995) 221.

[21] C. Ryerson, "Ice protection of offshore platforms", Cold Reg. Sci. Technol., 65 (2011) 97.

[22] S. Fikke, G. Ronsten, A. Heimo, S. Kunz, M. Ostrozlik, P.-E. Persson, J. Sabata, B. Wareing, B. Wichura, J. Chum, T. Laakso, K. Säntti, L. Makkonen, "Atmospheric icing on structures measurements and data collection on icing: State of the Art", COST-727, Publication of Meteo swiss, 2006.

[23] M. Farzaneh, "Insulator Icing Test Methods and Procedures", IEEE T. Power Delivery, 18(2003)1503.

[24] M. Farzaneh, "Selection of station insulators with respect to ice or snow–part I: Technical context and environmental exposure", IEEE T. Power Delivery, 20 (2005)264.

[25] M. Farzaneh, "Selection of station insulators with respect to ice or snow–part II: Methods of selection and options for mitigation", IEEE T. Power Delivery, 20(2005)271.

[26] M. Farzaneh, "Selection of line insulators with respect to ice and snow –Part I: Context and stresses", IEEE T. Power Delivery, 22(2007) 2289.

[27] M. Farzaneh, "Selection of line insulators with respect to ice and snow – Part II: Selection methods and mitigation options", IEEE T. Power Delivery, 22 (2007) 2297.

[28] https://www.rms.com/Publications/1998-Ice-Storm-Retrospective.pdf: The 1998 Ice Storm: 10-Years Retrospective.

[29] Atmospheric Icing on Structures, COST-727 Action. ISO12494, ISO/TC 98/SC3, 2000-07-20.

[30] J. Levine, "Statistical Explanation of Spontaneous Freezing of Water Droplets", NASA Center: Glenn Research Center, Report NACA-TN-2234, 1950.

[31] http://www.britannica.eom/EBchecked/topic/218741/freezing-nucleus: Freezing Nucleus in Britannica Online Encyclopedia.

[32] M. Palanisamy, K. Thangaraj, R. Gobinathan, and P. Ramasamy, "X-Ray Diffraction and Ice Nucleation Studies of Agl-AgBr-Cul System", J. Mater. Sci., 21(1986)1075-1079.

[33] N. Dalili, A. Edrisy, R. Carriveau, "A review of surface engineering issues critical to wind turbine performance", Renewable and Sustainable Energy Reviews 13 (2009) 428.

[34] R. Cattin, S. Kunz, A. Heimo, R. Oechslin, M. Russi, "An improved approach for the determination of in-cloud icing at wind turbine sites", Federal Office of Meteorology and Climatology Meteo-Swiss COST Action 727.

[35] D. Kuroiwa, "Icing and Snow Accretion on Electric Wires", CRREL Res. Report 123,1965.

[36] http://amsglossary.allenpress.com/glossary/search7icNglazel: Glaze in the Glossary of Meteorology.

[37] F. Kiessling, P. Nefzger, J. F. Nolasco, U. Kaintzyk, "Overhead Power Lines: Planning, Design, Construction", Springer 2003.

[38] C. Ryerson, "Assessment of Superstructure Ice Protection as Applied to Offshore Oil Operations Safety", ERDC/CRRELTR-08-14, September 2008.

[39] http://amsglossary.allenpress.com/glossary/search7icNrime-icel: Rime Ice in the Glossary of Meteorology.

[40] C. Ryerson and K. Claffey, "Efficacy of ice detector hoarfrost observations", Proceedings of the Fourth Annual Mt. Washington Observatory Symposium Focus 2000: Wind, Ice, and Fog, North Conway, NH, 1995, 45-55.

[41] C. Ryerson, "Assessment of Superstructure Ice Protection as Applied to Offshore Oil Operations Safety: Ice Protection Technologies, Safety Enhancements, and Development Needs", U.S. Army Cold Regions Research and Engineering Laboratory, 2009, p. 342.

[42] T. Haavasoja, V. Haavisto, M. J. Turunen, P. Nylander, and Y. Pilli-Sihvola, "A field trial of vehicle grip compared to RWS data", Vaisala News, 159 (2002) 28–30.

[43] M. Landy and A. Freiberger, "Studies of Ice Adhesion, I: Adhesion of Ice to Plastics", J. Colloid Interface Sci., 25(1967) 231 - 244.

[44] V. F. Petrenko, R. W. Whitworth, "Physics of Ice", Oxford university press, Oxford, 1999.

[45] U. Bovensiepen, "Ultrafast Electron Transfer, Localization and Solvation at Ice-Metal Interfaces: Correlation of Structure and Dynamics", Prog. Surf. Sci., 78 (2005) 87-100.

[46] I. A. Ryzhkin and V. F. Petrenko, "Proton Ordering in Ice at an Ice-Metal Interface", J. Exp. Theor. Phys., 101(2005) 317 - 321.

[47] L. A. Wilen, J. S. Wettlaufer, M. Elbaum and M. Schick, "Dispersion-force effects in interfacial premelting of ice", Phys. Rev. B, 52 (1995) 12426.

[48] G. Salomon, "Adhesion and adhesives", Amsterdam. Elsevier, 1 (1965) 1-140.

[49] V. F. Petrenko and S. Peng, "Reduction of ice adhesion to metal by using self-assembling monolayers (SAMs)", Can. J. Phys., 81 (2003) 387.

[50] J. L. Laforte,M. A. Allaire and J. Laflamme, " State-of-the-art on power line de-icing", Atm. Res., 46 (1998) 143.

[51] N. K. Adam, Principles of Water-Repellency, in Water-Proofing and Water-Repellency, Elsevier Publishing Co., Amsterdam, 1963, p. 17.

[52] W. A. Zisman, "Relation of the Equilibrium Contact Angle to Liquid and Solid Constitution", U. S. Naval Research Laboratory Washington, D. C., Chapter 1, p 1-51.

[53] D. Eley, "Thermodynamic adhesion, concluding remarks In Adhesion", London Oxford University Press, 1961.

[54] J. Gregg, "The surface chemistry of solids", 2nd ed., Reinhold Publishing Corp, New York, 1961.

[55] K. R. Wilson et al., "Surface Relaxation in Liquid Water and Methanol Studied by X-Ray Absorption Spectroscopy", J. Chem. Phys., 17 (2002) 7738 - 7744.

[56] X. Wang, "The Calculation of the Surface Energy of High-Index Surfaces in Metals at Zero Temperature", Surf. Sci., 551 (2004) 179 - 188.

[57] J. M. Zhang, F. Ma, and K. W. Xu, "Calculation of the Surface Energy of FCC Metals with Modified Embedded-Atom Method", Chinese Phys., 13 (2004) 1082- 1090.

[58] K. F. Wojciechowski, "Surface Energy of Metals: Theory and Experiment", Surf. Sci., 437 (1999) 285 - 288.

[59] W. I. Dunning, "Thermodynamics and imperfections of solid surfaces in adhesion", London oxford university press, 1961.

[60] A. W. Adamson, "Physical chemistry of surfaces", New York inter-science, second edition, 1967.

[61] Sayward JM. 1979, "Seeking low ice adhesion", Special Report AD-A071-040, US Army Regions Research and Engineering Laboratory, Hanover, NH.

[62] G. R. Desiraju, "Hydrogen Bridges in Crystal Engineering: Interactions without Borders", Ace. Chem. Res., 35(2002) 565 - 573.

[63] M. R. Kasaai and M. Farzaneh, "A Critical Evaluation of the Existing Methods to Determine Ice Adhesion Strength", in the 23rd International Conference on Offshore Mechanics and Arctic Engineering, Vancouver, Canada, 2004, p. 51264.

[64] J. Ahn, L. K. Mittal, and R. H. McQueen, "Hardness and Adhesion of Filmed Structures as Determined by the Scratch Techniques", Thick Films and Bulk Coatings, L. K. Mittal, Ed.: American Society for Testing and Materials, 1978, pp. 134 -157.

[65] P. Archer and V. Gupta, "Measurement and Control of Ice Adhesion to Aluminium 6061 Alloy", J. Mech. Phys. Solids, 46 (1998)1745 -1771.

[66] S. Krongelb, "Electromagnetic Tensile Adhesion Tests Methods", in Adhesion Measurements of Thin Films, Thick Films and Bulk Coatings, L. K. Mittal, Ed.: American Society for Testing and Materials, 1978, 640 (1978)107 - 121.

[67] M. R. Kasaai and M. Farzaneh, "Analytical Evaluation of Existing Mechanisms of Ice Adhesion on Power Network Equipment", in The 23rd International Conference on Offshore Mechanics and Arctic Engineering, Vancouver, Canada, 2004, p. 51267.

[68] J. W. McBain and W. B. Lee, "Third and Final Report of the Adhesives Research Committee", J. Phys. Chem., 37 (1933) 826.

[69] D. L. Loughborough and E. G. Hass, "Reduction of the Adhesion of Ice to De-icer Surfaces", J. Aero. Sci., 13 (1946) 126.

[70] C. L. Phan, P. McComber, and A. Mansianx, "Adhesion of Rime and Glaze on Conductors Protected by Various Materials", Trans. CSME, 4 (1976) 204.

[71] J. Druez, C. L. Phan, J. L. Laforte, and D. D. Nguyen, "The Adhesion of Glaze and Rime on Aluminium Electric Conductors", Trans. CSME, 5 (1979) 215.

[72] J. L. Laforte, C. L. Phan, B. Felin, and R. Martin, "Adhesion of Ice on Aluminium Conductor and Crystal Size in the Surface Layer", CRREL Special Report, pp. 83-91, 1983.

[73] J. W. Beams, J. B. Breazeale, and W. L. Bart, "Mechanical Strength of Thin Film of Metals", Phys. Rev., 100 (1983) 241.

[74] L. E. Raraty, D. Tabor, "The Adhesion and Strength properties of Ice", Proc. R. Soc. Lond. A, 245 (1958) 184.

[75] J. R. Stallabrass and R. D. Price, "On the Adhesion of Ice to Various Materials", NRC Report LR-350, 1962.

[76] K. Itagaki, "Adhesion of Ice to Polymers and Other Surfaces", in Physicochemical Aspects of Polymer Surfaces, K. L. Mittal, Ed.: Plenum Press, 1983, p. 241.

[77] L. Cao, A.K. Jones, V.K. Sikka, J. Wu, and D. Gao, "Anti-icing superhydrophobic coatings", Langmuir,25 (2009) 12444.

[78] D. Sarkar and M. Farzaneh, "Superhydrophobic coatings with reduced ice adhesion". Journal of Adhesion Science and Technology, 23 (2009)1215.

[79] Min He; Jingxia Wang; Huiling Li; Xiaoling Jin; Jianjun Wang; Biqian Liu; Yanlin Song, "Superhydrophobic film retards frost formation", Soft Matter, 6 (2010) 2396 – 2399.

[80] A.W. Adamson, F.P. Shirley, K.T. Kunichika, "Contact angles on molecular solids", J. Colloid Interface Sci., 34 (1970) 461.

[81] S. Mantovani and S. Valen, "Mechanical behavior at ice metal interfaces", Philos. Mag. A., 37 (1978) 17.

[82] J.R. Huntsberger, "The relationship between wetting and adhesion in advances Chemistry", J. Am. Chem. Soc, Washington DC, 11 (1964) 180.

[83] X. Zhang, Feng Shi, Jia Niu, Yugui Jiang and Zhiqiang Wang, "Superhydrophobic surfaces: from structural control to functional Application", J. Mater. Chem, 18 (2008) 621.

[84] S. T. Wang, Y. L. Sun and L. Jiang, J. Photochem. Photobiol., C, 8 (2007) 18.

[85] J. T. Davies and E. K. Rideal, "Interfacial phenomena", Academic Press, New York, 1961.

[86] A.C Zettlemoyer, "Hydrophobic surfaces", J. Colloid Interface Sci., 28 (1968) 343.

[87] L. Feng, S. Li, Y. Li, H. Li, L. Zhang, J. Zhai, Y. Song, B. Liu, L. Jiang and D. Zhu, Adv. Mater., 14 (2002)1857.

[88] L. C. Gao and T. J. McCarthy, J. Am. Chem. Soc., 128 (2006) 9052.

[89] D. Richard, C. Clanet and D. Quéré, Nature, 417 (2002) 811.

[90] D. Richard and D. Quéré, Europhys. Lett., 50 (2000) 769.

[91] T. Nishino, M. Meguro, K. Nakamae, M. Matsushita, and Y. Ueda, "The Lowest Surface Free Energy Based on -CF_3 Alignment", Langmuir, 15 (1999) 4321.

[92] E. F. Hare, E. G. Shafrin, and W. A. Zisman, "Properties of Films of Adsorbed Fluorinated Acids", J. Phys. Chem., 58 (1954) 236 - 239.

[93] S. A. Kulinich and M. Farzaneh, "Hydrophobic properties of surfaces coated with fluoroalkylsiloxane and alkylsiloxane monolayers", Surf. Sci., 573 (2004) 379.

[94] W. J. Dohaney and J. D. Innes, "ice-free pavement-evaluation of verglimit as a de-icing agent", Mater. Performance., 3 (1981) 39.

[95] J. N. Israelachvili, "Intermolecular and Surface Forces", 2nd ed.; Academic Press: London, 1991, Chapter 2.

[96] D. J. Crisp, "Waterproofing mechanisms in animals and plants", in: water-proofing and water-repellency, In J. L. Molliet [ed.], 1963, p. 416.

[97] M. Ma and R. M. Hill, Curr. Opin. Colloid Interface Sci., 11 (2006) 193.

[98] J. A. Jaber and J. B. Schlenoff, Curr. Opin. Colloid Interface Sci., 11 (2006) 324.

[99] D. Quéré, "Non-sticking drops", Rep. Prog. Phys. 68 (2005) 2495.

[100] L. Feng and L. Jiang, Biomimic and Smart Nano-Interface Materials, Chemical Industry Press, Beijing, 2007.

[101] X.-M. Li, D. Reinhoudt and M. Crego-Calama, Chem. Soc. Rev., 36 (2007)1350.

[102] H. Ollivier, Ann. Chim. Phys., 10 (1907) 229.

[103] J. J. Bikerman, in Surface Chemistry, 2nd edn, Academic Press, New York, 353 (1958) 362–364.

[104] W. H. Coghill and C. O. Anderson, U. S. Bur. Mines Tech. Pap., 262 (1923) 47.

[105] N. K. Adam, Physics and Chemistry of Surfaces, Clarendon Press, Oxford, 1930, p. 180–181.

[106] N. K. Adam, Physics and Chemistry of Surfaces, 3rd edn, Humphrey Milford, Oxford University Press, London, 1941, p. 186.

[107] R. N. Wenzel, "Resistance of Solid Surfaces to Wetting by Water", Ind. Eng. Chem. 28 (1936) 988.

[108] A. Cassie and S. Baxter, "Wettability of porous surfaces", Trans. Faraday Soc., 40 (1944) 546.

[109] H. J. Busscher, I. Stokroos, J. G. Golverdingen and J. M. Schakenraad, Cells Mater., 1 (1991) 243.

[110] F. G. Reick, Substrate coated with superhydrophobic layers, US Pat., 1976, US 3931428.

[111] Y. Chong and N. Watanabe, J. Fluorine Chem., 54 (1991), T43.

[112] K. Ogawa, M. Soga, Y. Takada and I. Nakayama, Jpn. J. Appl. Phys., Part 2, 32 (1993), L614.

[113] F. E. Bartell and J. W. Shepard, J. Phys. Chem., 57 (1953) 211.

[114] A. Cassie and S. Baxter, Nature, 155 (1945) 21.

[115] M. W. Holdgate, J. Exp. Biol., 32 (1955) 591.

[116] C. Neinhuis and W. Barthlott, Ann. Bot., 79 (1997) 667.

[117] W. Barthlott and C. Neinhuis, Planta, 202 (1997)1.

[118] T. S. Lin, C. F. Wu, C. T. Hsieh, "Enhancement of water-repellent performance on functional coating by using the Taguchi method", Surf. Coat. Technol, 200 (2006) 5253.

[119] R. Parker and C. R. Lawrence, Nature, 414 (2001) 33.

[120] S. Shibuichi, T. Onda, N. Satoh and K. Tsujii, "Super water-repellent surfaces resulting from fractal structure", J. Phys. Chem, 100 (1996) 19512.

[121] K. Tadanaga, N. Katata, and T. Minami, "Super-water-repellent Al_2O_3 coating films with high transparency", J. Am. Ceram. Soc., 80 (1997) 1040.

[122] A. Lafuma, and D. Quéré, "Superhydrophobic states", Nat. Mater., 2 (2003) 457.

[123] D. Oner and T. J. McCarthy, "Ultrahydrophobic surfaces. Effects of topography length scales on wettability", Langmuir 16 (2000) 7777-7782.

[124] M. Miwa, A. Nakajima, A. Fujishima, K. Hashimoto and T. Watanabe, "Effects of the surface roughness on sliding angles of water droplets on superhydrophobic surfaces", Langmuir 16 (2000) 5754-5760.

[125] T. Onda, S. Shibuichi, N. Satoh and K. Tsujii, Langmuir, 12 (1996) 2125.

[126] J. Y. Shiu, C. W. Kuo, P. Chen and C. Y. Mou, Chem. Mater., 16 (2004) 561.

[127] A. Pozzato, S. D. Zilio, G. Fois, D. Vendramin, G. Mistura, M. Belotti, Y. Chen and M. Natali, Microelectron. Eng., 83 (2006) 884.

[128] T. Baldacchini, J. E. Carey, M. Zhou and E. Mazur, Langmuir, 22 (2006) 4917.

[129] B. Qian and Z. Shen, Langmuir, 21 (2005) 9007.

[130] S. Lau, J. Bico, K. B. K. Teo, M. Chhowalla, G. A. J. Amaratunga, W. I. Milne, G. H. Mckinley and K. K. Gleason, Nano Lett., 3 (2003) 1701.

[131] Y. Wu, H. Sugimura, Y. Inoue and O. Takai, Chem. Vap. Deposition, 8 (2002) 47.

[132] Y. Wu, M. Bekke, Y. Inoue, H. Sugimura, H. Kitaguchie, C. Liu and O. Takai, Thin Solid Films, 457 (2004) 122.

[133] H. Tavana, A. Amirfazli and A. W. Neumann, Langmuir, 22 (2006) 5556.

[134] B. D. Washo, Org. Coat. Appl. Polym. Sci. Proc., 47 (1982) 69.

[135] L. Jiang, Y. Zhao and J. Zhai, Angew. Chem., Int. Ed., 43 (2003) 4338.

[136] A. Nakajima, A. Fujishima, K. Hashimoto and T. Watanabe, Adv. Mater., 11 (1999) 1365.

[137] F. Shi, X. Chen, L. Wang, J. Niu, J. Yu, Z. Q. Wang and X. Zhang, Chem. Mater., 17 (2005) 6177.

[138] X. Zhang, F. Shi, X. Yu, H. Liu, Y. Fu, Z. Q. Wang, L. Jiang and X. Y. Li, J. Am. Chem. Soc., 126 (2004) 3064.

[139] S. Wang, L. Feng and L. Jiang, Adv. Mater., 18 (2006) 767.

[140] J. Sagiv, J. Am. Chem. Soc., 92 (1980) 92.

[141] F. Shi, X. Chen, L. Wang, J. Niu, J. Yu, Z. Q. Wang, Chem. Mater., 17 (2005) 6177.

[142] E. Hosono, S. Fujihara, I. Honma and H. Zhou, J. Am. Chem. Soc., 127 (2005) 13458.

[143] S. Wang, L. Feng, H. Liu, T. Sun, X. Zhang, L. Jiang, ChemPhysChem, 6 (2005) 1475.

[144] D. H. Wang, Y. H. Ni, Q. Huo, et al., "Self-assembled monolayer and multilayer thin films on Al 2024-T3 substrates and their corrosion resistance study", Thin Solid Films, 471 (2005), 177.

[145] X.W. Yu, G.Q. Li, "XPS study of cerium conversion coating on the anodized 2024 aluminium alloy", J. Alloy Compd., 364 (2004) 193-198.

[146] M. Iannuzzi, T. Young, G.S. Frankel, "Aluminium alloy corrosion inhibition by vanadates", J. Electrochem. Soc. 153 (2006) B533.

[147] M. Iannuzzi, G.S. Frankel, "Mechanisms of corrosion inhibition of AA2024-T3 by vanadates", Corros. Sci. 49 (2007) 2371.

[148] P. Campestrini, H. Terryn, A. Hovestad, J.H.W. de Wit, "Formation of a cerium-based conversion coating on AA2024: relationship with the microstructure", Surf. Coat. Technol. 176 (2004) 365-381.

[149] A.E. Hughes, J. Gorman, T.G. Harvey, D. McCulloch, S.K. Toh, "SEM and RBS characterization of a cobalt-based conversion coating process on AA2024-T3 and AA7075-T6", Surf. Interface Anal., 36 (2004) 1585.

[150] J. Hu, X.H. Zhao, S.W. Tang, W.C. Ren, Z.Y. Zhang, "Corrosion resistance of cerium-based conversion coatings on alumina borate whisker reinforced AA6061 composite", Appl. Surf. Sci., 253 (2007) 8879.

[151] A.S. Hamdy, D.P. Butt, "Novel anti-corrosion nano-sized vanadia-based thin films prepared by sol-gel method for aluminium alloys", J. Mater. Process. Tech., 181 (2007) 76.

[152] I. Danilidis, J.M. Sykes, J.A. Hunter, G.M. Scamans, "Manganese based conversion treatment", Surf. Eng., 15 (1999) 401-405.

[153] I. Danilidis, J. Hunter, G.M. Scamans, J.M. Sykes, "Effects of inorganic additions on the performance of manganese-based conversion treatments", Corros. Sci., 49 (2007) 1557-1569.

[154] I. Danilidis, A.J. Davenport, J.M. Sykes, "Characterization by X-ray absorption near-edge spectroscopy of $KMnO_4$-based no-rinse conversion coatings on Al and Al alloys", Corros. Sci., 49 (2007) 1981.

[155] M.A. Smit, J.A. Hunter, J.D.B. Sharman, G.M. Scamans, J.M. Sykes, "Effect of organic additives on the performance of titanium-based conversion coatings", Corros. Sci., 45 (2003) 1903-1920.

[156] A.K. Mishra, R. Balasubramaniam, "Corrosion inhibition of aluminium alloy 2014 by rare earth chlorides", Corros. Sci., 49 (2007) 1027.

[157] F. Andreatta, A. Turco, I. de Graeve, H. Terryn, J.H.W. de Wit, L. Fedrizzi, "SKPFM and SEM study of the deposition mechanism of Zr/Ti based pre-treatment on AA6016 aluminium alloy", Surf. Coat. Technol., 201 (2007) 7668.

[158] J.H. Nordlien, J.C. Walmsley, H. sterberg, K. Nisancioglu, "Formation of a zirconium-titanium based conversion layer on AA 6060 aluminium", Surf. Coat. Technol., 153 (2002) 72-78.

[159] R. G. Buchheit, R. P. Grant, P. F. Hlava, et al, " Local dissolution phenomena associated with S phase (AlCuMg) particles in aluminium alloy 2024-T32", J. Electrochem. Soc., 144 (1997) 2621.

[160] S. A. Kulinich, M. Farzaneh, XW. Du, "Growth of corrosion-resistant manganese oxide coatings on an aluminium alloy", Inorg. Mater. 43 (2007) 956.

[161] C.A. Smith, "The corrosion story", Part 3, "Zinc, lead and aluminium", Anti-Corrosion, 24 (1977)13–15.

[162] J.M. Bryan, "Mechanism of the corrosion of aluminium", Chemistry&Industry, 1948, p. 135–136.

[163] R.T. Foley, T. H. Nguyen, "The chemical nature of aluminium corrosion V. Energy transfer in aluminium dissolution", J. Electrochem. Soc., 129 (1982) 464.

[164] A. Frignani, F. Zucchi, G.Trabanelli,"Protective action towards aluminium corrosion by silanes with a long aliphatic chain Growth of corrosion-resistant manganese oxide coatings on an aluminium alloy ", Corros. Sci., 48 (2006) 2258.

[165] S. Meth, CN. Sukenik, "Siloxane-anchored thin films on silicon dioxide-modified stainless steel", Thin Solid Films, 425 (2003) 49.

[166] A. Franquet, H. Terryn, C. Le Pen, J. Vereecken, "Characterization of protection behaviour of aluminium alloys by silane coatings", Eurocorr., (2001).

[167] A. Franquet, J. De Laet, T. Schram, et al., "Determination of the thickness of thin silane films on aluminium surfaces by means of spectroscopic ellipsometry", Thin Solid Films, 384 (2001) 37.

[168] D. Wang, Y. Ni, Q. Huo, D.E. Tallman, Thin Solid Films 471 (2005) 177.

[169] W. Thompson, J. pemberton, "Characterization of octadecylsilane and stearic-acid layers on Al_2O_3 surfaces by Raman-Spectroscopy", langmuir, 11 (1995) 1720.

[170] J.W. Bibber, "Chromate-free conversion coatings for aluminium", Plat. Surf. Finish., 90 (2003) 40.

[171] A. E. Hughes, R.J. Taylor and B. R. Hinton, "Chromate Conversion Coatings on 2024 Al Alloy", Surf. Interface Anal., 25 (1997) 223.

[172] F. Delaunois, V. Poulain, J. P. Petitjean, "The trivalent chromium pretreatment applied to Aluminium 1050", Mater. Sci. Forum, 242 (1997) 213.

[173] M. Callies, Y. Chen, F. Marty, A. Pépin, and D. Quéré, "Microfabricated Textured Surfaces for Superhydrophobicity Investigations", Microelectron. Eng., 78 (2005) 100.

[174] "User Manual for drop shape analyzer", Kruss GmbH, DSA 100, Vl.9-03.

[175] M. Mashmool, "Theoretical and Experimental Investigations for Measuring Interfacial Bonding Strength between Ice and SubstrateNanostructured Thin Films for Icephobic Applications", PhD thesis in Engineering, UQAC, November 2005.

[176] L.E. Kollar and M. Farzaneh, "Wind-Tunnel Investigation of Icing of an Inclined Cylinder", Int. J. Heat Mass Trans., 53 (2010) 849.

[177] L. Kollar and M. Farzaneh, "Spray Characteristics of Artificial Aerosol Clouds in a Low-Speed Icing Wind Tunnel", Atomization Spray, 19 (2009) 389.

[178] L. Kollar, M. Farzaneh and A. Karev, "Modeling Droplet-Size Distribution near a Nozzle Outlet in an Icing Wind Tunnel", Atomization Spray, 16(2006) 673.

[179] A.R. Karev, M. Farzaneh and L.E. Kollar, "Measuring Temperature of the Ice Surface During its Formation by Using Infrared Instrumentation". Int. J. Heat Mass Trans., 50 (2007) 566.

[180] A. R. Karev and M. Farzaneh, "Evolution of Droplet Size Distribution in an Icing Wind Tunnel", Comptes rendus de la 10th International Workshop on Atmospheric Icing of Structures, IWAIS 2002, Brno, Czech Republic, Juin 2002, 7-3.

[181] M. Kermani, "Ice Shedding from Cables and Conductors - A Cracking Model of Atmospheric Ice", Ph.D. thesis, University of Quebec at Chicoutimi (UQAC), December 2007.

[182] C. Laforte, A. Beisswenger, "Icephobic Material Centrifuge Adhesion Test", Proceedings of the International Workshop on Atmospheric Icing of Structures (IWAIS XI), Montréal, 2005, p. 357.

[183] A. Safaee, "Nanostructured metal surfaces and their passivation for superhydrophobic and antiicing applications", PhD thesis in Engineering, UQAC, December 2008.

[184] C. Laforte, A. Beisswenger, Proceedings of the International Workshop on atmospheric Icing of Structures (IWAIS XI), Montréal, June 2005, pp 357.

[185] X. T. Zhang, O. Stao and A. Fujishima, "Water Ultrarepellency Induced by Nanocolumnar ZnO Surface", Langmuir 20 (2004) 6065.

[186] S. Noormohammed, "Nanostructured Thin Films for Icephobic Applications", PhD thesis in Engineering, UQAC, April 2009.

[187] D. Kim, S. Jeong, and J. Moon, "Synthesis of Silver Nanoparticles using the Polyol Process and the Influence of Precursor Injection", Nanotechnology, 17 (2006) 4019.